ABSTRACT

Title of Document: PROGNOSTICS AND HEALTH MANAGEMENT OF ELECTRONICS BY UTILIZING ENVIRONMENTAL AND USAGE LOADS

Nikhil M. Vichare, Doctor of Philosophy (Ph.D.), 2006

Directed By: Chair Professor and Director, Michael G. Pecht, Department of Mechanical Engineering

Prognostics and health management (PHM) is a method that permits the reliability of a system to be evaluated in its actual application conditions. Thus by determining the advent of failure, procedures can be developed to mitigate, manage and maintain the system. Since, electronic systems control most systems today and their reliability is usually critical for system reliability, PHM techniques are needed for electronics.

To enable prognostics, a methodology was developed to extract load-parameters required for damage assessment from irregular time-load data. As a part of the methodology an algorithm that extracts cyclic range and means, ramp-rates, dwell-times, dwell-loads and correlation between load parameters was developed. The algorithm enables significant reduction of the time-load data without compromising features that are essential for damage estimation. The load-parameters

are stored in bins with a-priori calculated (optimal) bin-width. The binned data is then used with Gaussian kernel function for density estimation of the load-parameter for use in damage assessment and prognostics. The method was shown to accurately extract the desired load-parameters and enable condensed storage of load histories, thus improving resource efficiency of the sensor nodes.

An approach was developed to assess the impact of uncertainties in measurement, model-input, and damage-models on prognostics. The approach utilizes sensitivity analysis to identify the dominant input variables that influence the model-output, and uses the distribution of measured load-parameters and input variables in a Monte-Carlo simulation to provide a distribution of accumulated damage. Using regression analysis of the accumulated damage distributions, the remaining life is then predicted with confidence intervals. The proposed method was demonstrated using an experimental setup for predicting interconnect failures on electronic board subjected to field conditions.

A failure precursor based approach was developed for remaining life prognostics by analyzing resistance data in conjunction with usage temperature loads. Using the data from the PHM experiment, a model was developed to estimate the resistance based on measured temperature values. The difference between actual and estimated resistance value in time-domain were analyzed to predict the onset and progress of interconnect degradation. Remaining life was predicted by trending

several features including mean-peaks, kurtosis, and 95% cumulative-values of the resistance-drift distributions.

PROGNOSTICS AND HEALTH MANAGEMENT OF ELECTRONICS BY UTILIZING ENVIRONMENTAL AND USAGE LOADS

By

Nikhil M. Vichare

Dissertation submitted to the Faculty of the Graduate School of the
University of Maryland, College Park, in partial fulfillment
of the requirements for the degree of
Doctor of Philosophy
2006

Advisory Committee:
Professor Michael G. Pecht, Chair
Professor Abhijit Dasgupta
Professor Bilal Ayyub
Professor Donald Barker
Associate Professor F. Patrick McCluskey

Acknowledgements

With a deep sense of gratitude, I wish to express my sincere thanks to my advisor Prof. Michael Pecht for allowing me to work on this interesting topic and continuously challenging me to set my benchmark higher.

I thank Dr. Peter Rodgers for the technical discussions, encouragement, and for reviewing my work. I am grateful to Prof. Bilal Ayyub for the discussions on uncertainty modeling.

A lot of good suggestions were provided on my dissertation by Prof. Donald Barker, Prof. Abhijit Dasgupta, and Prof. Patrick McCluskey and I am grateful to all of them. I also thank Dr. Valerie Eveloy for thoroughly reviewing my papers. Dr. Diganta Das and Dr. Michael Azarian, thank you for the numerous suggestions on my presentations. Your comments have helped me a lot. I also thank Dr. Michael Osterman for his help on my CALCE consortium research projects.

I am thankful to all the participants in the morning group meetings, Sanjay Tiku, Anupam Choubey, Brian Tuchband, Jie Gu, Reza Keimasi, Yan Liu, Dan Donahoe, Dr. Keith Rogers, Sony Mathew, Haiyu Qi, Bhanu Sood, Anshul Shrivastava, Dr. Sanka Ganesan, Dr. Ji Wu, Satya Ganesan, Yuliang Deng, Shirsho Sengupta, Bo Song, Sheng Zhan – you guys forced me do my best by asking tough questions.

Very special thanks for my girl-friend Yuki Fukuda for always supporting and encouraging me. I am indebted to my parents for standing by all my decisions I can never thank you enough.

Table of Contents

Acknowledgements ii
Table of Contents iii
List of Tables v
List of Figures vi
Chapter 1: Prognostics and Health Management 1
1.0 Introduction 1
1.1 Reliability and Prognostics 1
1.2 Motivation for Electronic Prognostics 3
1.3 Objectives of Thesis 5
1.4 Overview of Thesis 6
Chapter 2: Literature Review 9
2.0 Introduction 9
2.1 Built-In Test 10
2.2 Fuses and Canaries 13
2.3 Monitoring Precursors to Failure 17
2.4 Monitoring Environmental and Usage Loads 27
2.5 PHM Integration 33
Chapter 3: Prognostics Using Environmental and Usage Loads 36
3.0 Introduction 36
3.1 Approach 36
3.2 Implementation Setup 39
3.3 Summary 44
Chapter 4: Methods for In-situ Monitoring 45
4.0 Introduction 45
4.1 In-situ Monitoring of Environmental and Usage Loads 46
4.1.1 Selection of Load Parameters for Monitoring 46
4.1.2. Selection of Monitoring Equipment 47
4.1.4 Data Preprocessing for Model Input 59
4.2 In-situ Monitoring Case Study of Notebook Computer 61
4.3 Conclusions 70
Chapter 5: Methodology for Extracting Load Parameters from Time-Load Signals 72
5.0 Introduction 72
5.1 Review of Existing Load Parameter Extraction Methods 72
5.2 Limitations of Existing Methods 74
5.2.1 Extracting ramp rates and dwell information 75
5.2.2 Concerns with data reduction 76
5.2.3 Correlation of load parameters 77
5.3 Methodology for Load Extraction 77
5.4 Demonstration 82
5.5 Method for Binning and Density Estimation 87
5.5.1 Optimal Binning and Density Estimation 87
5.5.2 Implementation Approach for PHM 90

5.5.3 Results 91
5.6 Conclusions 95
Chapter 6: Prognostics Approach Considering Uncertainties 97
6.0 Introduction 97
6.1 Background 97
6.2 Overview of Methodology 99
6.3 Case Study 109
6.3.1 Decision Variables 110
6.3.2 Model Parameters 112
6.3.3 Random Sampling 113
6.3.4 Model Uncertainty 114
6.3.5 Remaining Life Prognostics 115
6.3.6 Damage Histories for Prognostics 116
6.4 Conclusion 119
Chapter 7: Failure Precursors Based on Resistance Analysis 121
7.0 Introduction 121
7.1 Approach 125
7.1.1 Temperature – Resistance Model 126
7.1.2 Features Investigated 128
7.2 Results 129
7.3 Conclusions 135
Chapter 8: Contributions 136
Appendix I 139
Appendix II 140
Appendix III 143
Bibliography 144

List of Tables

Table 1. Potential failure precursors for electronics 18
Table 2. Monitoring parameters based on reliability concerns in hard drives..... 23
Table 3. Examples of life-cycle loads..... 27
Table 4. Failure mechanisms, relevant loads, and models in electronics 39
Table 5. Assessing product environmental and usage conditions..... 58
Table 6. Environmental, usage and performance parameters for PHM of notebook computers..... 69
Table 7. Review of existing load parameter extraction methods..... 73
Table 8. Estimate of parameters used for the bin width calculation..... 92
Table 9. Format of load distribution obtained in Gaussian kernel format..... 105
Table 10. Sensitivity analysis of model-input parameters..... 113
Table 11. Remaining life distributions for BGA 225 116
Table 12. Remaining life prognostics in terms of missions..... 119
Table 13. Values of coefficients used in regression model 127
Table 14. Features investigated for determining consistent precursor 128

List of Figures

Figure 1. Framework for prognostics and health management..... 3
Figure 2. Advance warning of failure using canary structures 16
Figure 3. SUN's approach to PHM 25
Figure 4. CALCE life consumption monitoring methodology 28
Figure 5. Prognostic approach using environmental and usage loads 38
Figure 6. Experimental setup for PHM implementation on electronic board..... 41
Figure 7. Illustration of temperature measured on the board for first 20 days 42
Figure 8. Conceptual schematic of integrated sensor system 48
Figure 9. Example of percentage data reduction and error in damage accumulation. 56
Figure 10. Comparison of histograms of filtered and non-filtered load cycles 56
Figure 11. histogram of mean loads associated with the filtered cycles..... 57
Figure 12. Location of RTD temperature sensor on CPU heat sink base 62
Figure 13. Measured temperature profiles of CPU heat sink, hard disk drive, and external ambient air..... 63
Figure 14. Measured CPU usage and CPU heat sink absolute temperature. Event A: notebook is powered on. Events B to C: numerical simulation is executed. Event D: Notebook is powered off..... 64
Figure 15. . Cooling fan operation in time periods A-B and C-D 64
Figure 16. Distributions of measured absolute temperature for the CPU heat sink and hard disk drive..... 66
Figure 17. Occurrence of CPU heat sink and hard disk drive temperature cycles as a function of cycle magnitude..... 66
Figure 18. Distribution of measured temperature cycle ramp rates for the CPU heat sink and hard disk drive. R refers to temperature cycle ramp rate 67
Figure 19. Geometric definition of a cycle 73
Figure 20. Data reduction methods can potentially eliminate dwell regions..... 77
Figure 21. Results of MA filter with different smoothening parameter based sampling frequency..... 79
Figure 22. Threshold level increases as value of power in damage law (n) decreases80
Figure 23. (a) Reduces noise using moving average filter (b) Eliminates monotonic data patterns and merges small ranges into overall data streams (c) Identifies dwells temperatures and time using ramp-rate and range (d) Scans the time-temperature data to extract cyclic load parameters..... 82
Figure 24. Histogram of cyclic range 84
Figure 25. Histogram of cyclic mean temperatures 84
Figure 26. Histogram of ramp-rates..... 85
Figure 27. Histogram of temperature dwell times 85
Figure 28. Correlation between dwell time and temperature..... 86
Figure 29. Correlation between delta T and mean temperatures 86
Figure 30. Correlation between delta T and ramp-rate 86
Figure 31. Approach for binning and density estimation of monitored load parameters 91
Figure 32. Comparison of density estimates for T_{mean} values of day 6..... 94

Figure 33. Comparison of distributions obtained from estimated versus actual parameters 95
Figure 34. CALCE Life consumption monitoring methodology 98
Figure 35. Prognostic health monitoring methodology considering uncertainty 101
Figure 36. Accumulated damage distribution for the monitoring period being assessed 108
Figure 37. Sources of uncertainty in damage estimation and prognostics for BGA225 111
Figure 38. Error in damage accumulation due to reversal elimination and signal interruption 112
Figure 39. Monte-Carlo simulation for damage assessment 114
Figure 40. Monte Carlo results and stopping criteria 115
Figure 41. Distribution of calibration parameter for model uncertainty 115
Figure 42. Accumulated damage distributions with time for BGA 225 116
Figure 43. Distributions of accumulated damage over time 117
Figure 44. Condensed storage of load histories based on missions 118
Figure 45. No indication of degradation before the occurrence of the first spike 123
Figure 46. Change in resistance with temperature 124
Figure 47. Approach for precursor identification and tracking using resistance drift values 125
Figure 48. Second order polynomial fit between temperature and resistance 127
Figure 49. Details of prediction model 127
Figure 50. Trending mean values of resistance drift 129
Figure 51. Trending mean-peak values of resistance drift 130
Figure 52. Trending values of standard deviation of resistance drift 131
Figure 53. Trending values of 95% cumulative distribution values of resistance drift 132
Figure 54. Trending values of 95% cumulative distribution peaks of resistance drift 132
Figure 55. Trending skewness values of resistance drift 133
Figure 56. Trending kurtosis values of resistance drift 133
Figure 57. Trending skewness peak values of resistance drift 134
Figure 58. Failure prediction using two features 135

Chapter 1: Prognostics and Health Management

1.0 Introduction

There has been a growing interest in monitoring the ongoing "health" of products and systems in order to predict failures and provide warning to avoid catastrophic failure. Here, health is defined as the extent of degradation or deviation from an expected normal condition. "Prognostics" is the prediction of future state of health based on current and historic health conditions [1]. While the application of health monitoring and diagnostics is well established for assessment of mechanical systems, this is not the case for electronic systems. However, electronic systems are integral to the functionality of most systems today, and their reliability is often critical for system reliability [1] [2]. This dissertation is about developing techniques to enable the prognostics of electronic systems.

1.1 Reliability and Prognostics

Reliability is the ability of a product or system to perform as intended (i.e., without failure and within specified performance limits) for a specified time, in its life - cycle environment. Commonly-used electronics reliability prediction methods generally do not accurately account for the life cycle environment of electronic equipment. This arises from fundamental flaws in the reliability assessment methodologies used [3], and uncertainties in the product life cycle loads [4]. In fact, traditional reliability prediction methods based on the use of handbooks have been

shown to be misleading and provide erroneous life predictions [3] [4], a fact that led the U. S. military to abandon their electronics reliability prediction methods [4]. Although the use of stress and damage models permits a more accurate account of the physics-of-failure [5], their application to long-term reliability predictions based on extrapolated short-term life testing data or field data, is typically constrained by insufficient knowledge of the actual operating and environmental application conditions of the product.

Prognostics and health monitoring techniques combine sensing, recording, and interpretation of environmental, operational, and performance-related parameters that are indicative of a system's health. Product health monitoring can be implemented through the use of various techniques to sense and interpret the parameters indicative of: i) Performance degradation, such as deviation of operating parameters from their expected values; ii) Physical or electrical degradation, such as material cracking, corrosion, interfacial delamination, increase in electrical resistance or threshold voltage; or iii) Changes in a life cycle environment, such as usage duration and frequency, ambient temperature and humidity, vibration, and shock. Based on the product's health, determined from the monitored life cycle conditions, maintenance procedures can be developed. Health monitoring therefore permits new products to be concurrently designed for a life cycle environment known through monitoring [1] [2]. The framework for prognostics is shown in **Figure 1**. Sensor data from various levels in an electronic product or system will be monitored in-situ and analyzed using prognostic algorithms. Different implementation approaches can be adopted

individually or in combination. These approaches will be discussed in detail in the next chapter. Ultimately, the objective is to predict the advent of failure in terms of a distribution of remaining life, level of degradation, probability of mission survival etc.

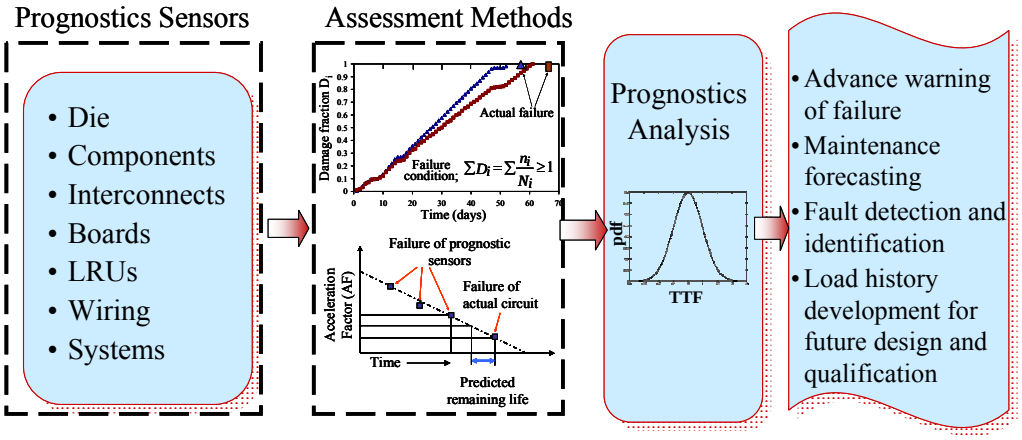

Figure 1. Framework for prognostics and health management

1.2 Motivation for Electronic Prognostics

Safety critical mechanical systems and structures, such as propulsion engines, aircraft structures, bridges, buildings, roads, pressure vessels, rotary equipment, and gears, have been known to benefit from advanced sensor systems and models, developed specifically for in-situ fault diagnosis and prognosis (often called health and usage monitoring or condition monitoring) [6], [7], [8], [9], [10], [11]. Thus, for mechanical systems, there is a considerable body of knowledge on health monitoring.

Today, most products and systems contain significant electronics content to provide the needed functionality and performance. However, the application of PHM concepts to electronics is rare. If one can assess the extent of deviation or degradation from an expected normal operating condition for the electronics, this data can be used

to meet several powerful goals, which includes: 1) advanced warning of failures; 2) minimizing unscheduled maintenance, extending maintenance cycles, and maintaining effectiveness through timely repair actions; 3) reducing life cycle cost of equipment by decreasing inspection costs, downtime, and inventory; and 4) improving qualification and assisting in the design and logistical support of fielded and future systems. In other words, because electronics are playing an increasingly large role in providing operational capabilities for today's systems, prognostic techniques are needed.

In recent years, PHM has emerged as one of the key enablers for achieving efficient system-level maintenance and lowering life-cycle costs. In November 2002, the U.S. Deputy Under Secretary of Defense for Logistics and Materiel Readiness released a policy called condition-based maintenance plus (CBM+) [12]. CBM+ represents an effort to shift unscheduled corrective equipment maintenance of new and legacy systems to preventive and predictive approaches that schedule maintenance based upon the evidence of need.

The importance of PHM implementation was explicitly stated in the DoD 5000.2 policy document on defense acquisition, which states that "program managers shall optimize operational readiness through affordable, integrated, embedded diagnostics and prognostics, and embedded training and testing, serialized item management, automatic identification technology (AIT), and iterative technology refreshment" [13]. Thus, PHM has become a requirement for any system sold to the

DOD. A 2005 survey of eleven CBM programs highlighted "electronics prognostics" as one of the most needed maintenance-related features or applications, without regard for cost [14], a view also shared by the avionics industry [15].

1.3 Objectives of Thesis

PHM concepts have been rarely applied to electronics, despite the fact that most mechanical systems contain significant electronics content that are often the first to fail [16] [17] [18]. This may be due to the fact that wear and damage in electronics is comparatively more difficult to detect and inspect due to geometric scale of electronic parts being of the order of micro- to nano-scale, and their complex architecture. In addition, faults in electronic parts may not necessarily lead to failure or loss of designated electrical performance or functionality, making it difficult to quantify product degradation and the progression from faults to final failure. Consequently, it is generally difficult to implement prognostic or diagnostic systems in electronics, that can directly monitor the faults or conditions in which fault occurs. In addition, there is a significant shortage of knowledge about failure precursors in electronics.

The broad objective of this work is to develop techniques to enable electronic prognostics. Two specific research areas have been identified. i) Development of a methodology to extract load parameters required for damage assessment from large irregular time-load history. ii) Develop and demonstrate a prognostic approach for predicting the remaining life of electronic board in its application environment.

1.4 Overview of Thesis

The different approaches to prognostics, the state-of-art and the state-of-research in electronics PHM is reviewed in chapter 2. Three current approaches include, use of fuses and canary devices, monitoring and reasoning of failure precursors, and modeling accumulated damage based on measured life-cycle loads. Examples are provided for these different approaches, and the implementation challenges are discussed. Chapter 3 presents the approach that combines environmental and usage loads, data simplification techniques, and damage models to provide in-situ damage assessment and prognostics. The experimental setup for demonstrating the PHM techniques is discussed.

Environmental and usage load profiles need to be efficiently and accurately captured in the application environment, and utilized in real time or near real time health assessment and prognostics. Chapter 4 outlines generic strategies both for load monitoring and conversion of the sensor data into a format that can be used in physics-of-failure models, for both damage estimation and remaining life prediction due to specific failure mechanisms. The selection of appropriate parameters to monitor, design of an effective monitoring plan, and selection of appropriate monitoring equipment are discussed. Methods to process the raw sensor data during in-situ monitoring for reducing the memory requirements and power consumption of the monitoring device are suggested. The strategies presented are generically applicable to electronic health monitoring processes and are illustrated using a case-study of in-situ monitoring of a note-book computer.

Chapter 5 presents a novel method for processing the in-situ monitored load data to enable prognostic assessment of electronic products and systems. The proposed method processes the time-domain sensor data to extract load parameters including cyclic ranges, mean load, ramp-rates, and dwell times. The load parameters and their correlations are then used in conjunction with damage models for assessing and predicting the health due to commonly observed failure mechanisms in electronics. Methods for optimal binning and density estimation of load parameter are outlined.

Remaining life predictions are made by assessing the accumulated damage due to measured environmental and usage exposure. However, often the effect of uncertainty and variability in the measurement and procedures used for making predictions is neglected. In chapter 6, a generic method is developed for remaining life prognostics that accounts for the measurement, model-input, and model uncertainties. The method is demonstrated to predict the remaining life distributions of solder interconnects subjected to field temperature conditions. The details of the proposed method and the implementation case-study are presented.

Chapter 7 presents a different approach for prognostics using the same setup described in chapter 3. Instead of assessing the accumulated damage due to temperature cycles, the performance of the electronic board is directly monitored and analyzed to provide an advance warning of failure and estimate remaining life. The

challenges in monitoring the performance, the methodology adopted for analysis of failure precursors and the results are presented. The contributions of this research are listed in chapter 8.

Chapter 2: Literature Review

2.0 Introduction

Most products and systems contain some electronics to provide functionality and performance. These electronics are often the first item of the product or system to fail [16] [17] [18]. Assessing the extent of deviation or degradation from an expected normal operating condition (i.e., health) for electronics provides data that can be used to meet several critical goals, which include (1) advance warning of failures; (2) minimizing unscheduled maintenance, extending maintenance cycles, and maintaining effectiveness through timely repair actions; (3) reducing the life-cycle cost of equipment by decreasing inspection costs, downtime, and inventory; and (4) improving qualification and assisting in the design and logistical support of fielded and future systems.

In this section the state-of-practice and the current state-of-research in the area of electronics prognostics and health management. Three current approaches include, use of fuses and canary devices, monitoring and reasoning of failure precursors, and modeling accumulated damage based on measured life-cycle loads. Examples are provided for these different approaches, and the implementation challenges are discussed. A brief discussion is included on Built-in test (BIT) the traditional diagnostic tool for electronics.

2.1 Built-In Test

The first efforts in diagnostic health monitoring of electronics involved the use of built-in test (BIT). Built-in test is defined as an on-board hardware-software diagnostic means to identify and locate faults, and includes error detection and correction circuits, totally self-checking circuits, and self-verification circuits [19]. The equipment manufacturer sometimes provides BIT circuitry and software to allow the user to verify system functionality by providing access to internal nodes for comparison with known voltages or data patterns. BIT can also be used to debug, troubleshoot, and perform preventive maintenance.

Various levels of BIT include (1) circuit-level BIT (also referred as BIST - built-in self-test) for fault logging and diagnostics of individual circuits; (2) module- or assembly-level BIT that supports one or more circuit card assemblies, such as line-replaceable units and (3) system-level BIT that performs diagnostics and operational testing of entire electronic systems. Among the earliest equipment available with BIT was the HP-3325A (1980) synthesizer function generator. BIT has since been used in diverse applications, including oceanographic systems, multichip modules, large-scale integrated circuits, power supply systems, avionics, and even passenger entertainment systems for the Boeing 767 and 777 [20].

Two types of BIT concepts are employed in electronic systems--interruptive BIT (I-BIT) and continuous BIT (C-BIT). The concept behind I-BIT is that normal equipment operation is suspended during BIT operation. Such BITS are typically initiated by the operator or occur during the power-up process. The concept behind C-

BIT is that equipment is monitored continuously and automatically without affecting normal operation. Periodic BIT (P-BIT) is an I-BIT system that interrupts normal operation periodically in order to carry out a pseudocontinuous monitoring function. BIT concepts are still being developed to reduce the occurrence of spurious failure indications.

The nature of BIT depends on the nature of the equipment that it monitors. System-wide BIT may be centralized, controlling all BIT functions, or may comprise a number of BIT centers (often at the level of line-replaceable units) that communicate with each other and with a master processing unit that processes the results. A centralized BIT will often require dedicated hardware. BIT can also be incorporated and processed at the level of line-replaceable units to test the functionality of key circuits within a unit or on individual circuit cards. The advantage of BIT at this level is to help identify problems closer to the root cause, thus allowing cost-effective assembly and maintenance [20].

For example, a board-level BIT implemented by Motorola (MBIT), consisted of a diagnostic hardware and software package designed to verify the correct operation of board-mounted logical devices [21]. All tests could be executed at boot-up and selected tests ran continuously in the background of user applications. An application programming interface (API) was included to provide access to test results and to control the operation of device tests. The board-level MBIT consisted of hardware diagnostics and an API to control operation of the test driver suite.

Examples of tested devices are the processor, L2 cache, VMEbus ASIC, ECC RAM, serial EPROM, Flash, NVRAM and real-time clock. Internal operation tests included checking register stuck-at conditions, register manipulations, and device setup instructions. The system-level MBIT, connects to all board-level versions to enable system-wide testing [21].

One of the early efforts in using monitored BIT and operational loads for maintenance analysis was the development of the time stress measurement device (TSMD). Broadwater, et al., [22] [23] proposed the use of a microprocessor-based TSMD that can serve as a single-chip built-in-test (BIT) and maintain logs between users and depot repair facilities. The primary objective of the TSMD was to store sub-system fault testing and environmental stress data. Thus, when a sub-system failure occurred, the TSMD would record the time stamp, the BIT fault code and the system mode. This data could be analyzed with the environmental stress data measured before, during, and after the fault event, and then used to constitute a fault signature for future diagnosis. However, this study identified intermittent failures and fault isolation ambiguity in electronic systems as a major obstacle in achieving the complete benefits of TSMD. Fault isolation ambiguity occurs in systems where the BIT is unable to discriminate failures between the BIT computer, various LRU's, and system interconnections.

Despite the apparent sophistication of BIT, there has been some concern that the requirement for BIT and the actual capabilities of BIT are not easy to match. For

example, airline experience with modern avionics systems has indicated that spurious fault detection is unacceptably high. In 1996, Johnson [24] reported that the Lufthansa Airbus A 320 had a daily average of two thousand error logs on its BIT. About seventy of these corresponded with faults reported by pilots, while another seventy or so pilot reports of faults had no corresponding BIT log. Of the seventeen line-replaceable units replaced daily, typically only two were found to have faults that correlated with the fault indicated by the reports. Several studies [20] [25] [26] [27] conducted on the use of BIT for fault identification and diagnostics showed that BIT can be prone to false alarms and can result in unnecessary costly replacement, re-qualification, delayed shipping, and loss of system availability. However, there is also reason to believe that many of the failures were "real", but intermittent in nature [28].

The persistence of such issues over the years is perhaps due to the fact that the use of BIT has been restricted to low-volume systems. Thus, BIT has generally not been designed to provide prognostics or remaining useful life due to accumulated damage or progression of faults. It has served primarily as a diagnostic tool.

2.2 Fuses and Canaries

Expendable devices such as fuses and canaries have been a traditional method of protection for structures and electrical power systems. Fuses and circuit breakers are examples of elements used in electronic products to sense excessive current drain and to disconnect power from the concerned part. Fuses within circuits safeguard parts against voltage transients or excessive power dissipation, and protect power

supplies from shorted parts. For example, thermostats can be used to sense critical temperature limiting conditions, and to shut down the product, or a part of the system, until the temperature returns to normal. In some products, self-checking circuitry can also be incorporated to sense abnormal conditions and to make adjustments to restore normal conditions, or to activate switching means to compensate for the malfunction [29].

The word "canary" is derived from one of coal mining's earliest systems for warning of the presence of hazardous gas using the canary bird. Because the canary is more sensitive to hazardous gases than humans, the death or sickening of the canary was an indication to the miners to get out of the shaft. The canary thus provided an effective early warning of catastrophic failure by providing advance warning that was easy to interpret. The same approach, using canaries, has been employed in prognostic health monitoring (PHM).

Canary devices mounted on the actual product can also be used to provide advance warning of failure due to specific wearout failure mechanisms. Mishra, et al., [30] studied the applicability of semiconductor-level health monitors by using pre-calibrated cells (circuits) located on the same chip with the actual circuitry. The prognostics cell approach has been commercialized by Ridgetop Group (known as Sentinel SemiconductorTM technology) to provide an early-warning sentinel for upcoming device failures [31]. The prognostic cells are available for 0.35, 0.25, and 0.18 micron CMOS processes; the power consumption is approximately 600

microwatts. The cell size is typically 800 μm2 at the 0.25 micron process size. Currently, prognostic cells are available for semiconductor failure mechanisms such as electrostatic discharge (ESD), hot carrier, metal migration, dielectric breakdown, and radiation effects.

The time to failure of these prognostic cells can be pre-calibrated with respect to the time to failure of the actual product. Because of their location, these cells contain and experience substantially similar dependencies as does the actual product. These stresses that contribute to degradation of the circuit include voltage, current, temperature, humidity, and radiation. Since the operational stresses are the same, the damage rate is expected to be the same for both the circuits. However, the prognostic cell is designed to fail faster through increased stress on the cell structure by means of scaling.

Scaling can be achieved by controlled increase of the current density inside the cells. With the same amount of current passing through both circuits, if the cross-sectional area of the current-carrying paths in the cells is decreased, a higher current density is achieved. Further control in current density can be achieved by increasing the voltage level applied to the cells. A combination of both of these techniques can also be used. Higher current density leads to higher internal (joule) heating, causing greater stress on the cells. When a current of higher density passes through the cells, they are expected to fail faster than the actual circuit [30].

Figure 2 shows the failure distribution of the actual product and the canary health monitors. Under the same environmental and operational loading conditions, the canary health monitors wearout faster to indicate the impending failure of the actual product. Canaries can be calibrated to provide sufficient advance warning of failure (prognostic distance) to enable appropriate maintenance and replacement activities. This point can be adjusted to some other early indication level. Multiple trigger points can also be provided, using multiple cells evenly spaced over the bathtub curve.

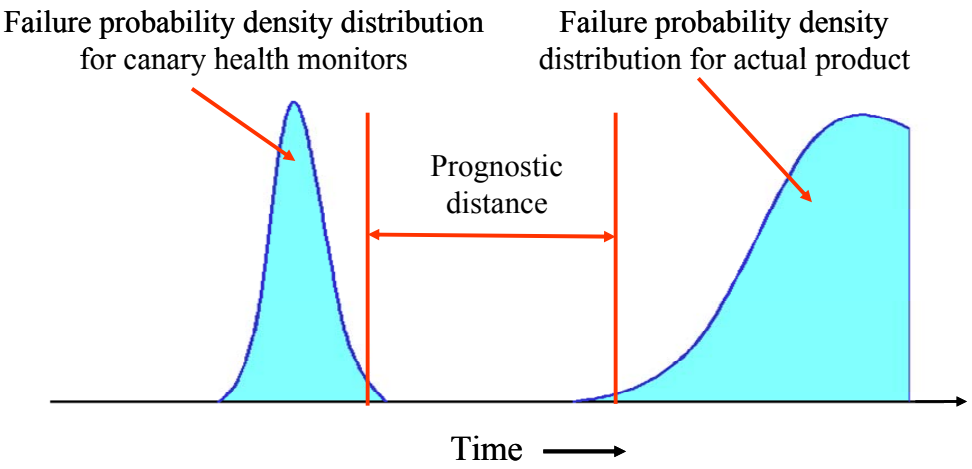

Figure 2. Advance warning of failure using canary structures

The extension of this approach to board-level failures was proposed by Anderson, et al., [32], who created canary components (located on the same printed circuit board) that include the same mechanisms that lead to failure in actual components. Anderson et al., identified two prospective failure mechanisms: (1) low cycle fatigue of solder joints, assessed by monitoring solder joints on and within the canary package; and (2) corrosion monitoring using circuits that will be susceptible to corrosion. The environmental degradation of these canaries was assessed using

accelerated testing, and degradation levels are calibrated and correlated to actual failure levels of the main system. The corrosion test device included an electrical circuitry susceptible to various corrosion-induced mechanisms. Impedance Spectroscopy was proposed for identifying changes in the circuits by measuring the magnitude and phase angle of impedance as a function of frequency. The change in impedance characteristics would be correlated to indicate specific degradation mechanisms.

There remain unanswered questions with the use of fuses and canaries. For example, if a canary monitoring a circuit is replaced, what is the impact when the product is re-energized? What protective architectures are appropriate for post-repair operations? What maintenance guidance must be documented and followed when fail-safe protective architectures have or have not been included? This approach is difficult to implement in legacy systems, because it may require re-qualification of the entire system with the canary module. Also, the integration of fuses and canaries with the host electronic systems could be an issue with respect to real estate on semiconductors and boards. Finally, the company has to ensure that the additional cost of implementing PHM can be recovered through increased operational and maintenance efficiencies.

2.3 Monitoring Precursors to Failure

A failure precursor is an event that signifies impending failure. A precursor indication is usually a change in a measurable variable that can be associated with subsequent failure. For example, a shift in the output voltage of a power supply would

suggest impending failure due to damaged feedback regulator and opto-isolator circuitry. Failures can then be predicted by using a causal relationship between a measured variable that can be correlated with subsequent failure.

A first step in PHM is to select the life-cycle parameters to be monitored. Parameters can be identified based on factors that are crucial for safety, that are likely to cause catastrophic failures, that are essential for mission completeness, or that can result in long downtimes. Selection can also be based on knowledge of the critical parameters established by past experience and field failure data on similar products and on qualification testing. More systematic methods, such as failure mode mechanisms and effects analysis (FMMEA) [33], can be used to determine parameters that need to be monitored.

Born and Boenning, [34] and Pecht et al., [35] proposed several measurable parameters that can be used as failure precursors for electronic switching power supplies, cables and connectors, CMOS integrated circuits, and voltage-controlled high-frequency oscillators (see Table 1). Testing was conducted to demonstrate the potential of select parameters to be viable for detection of incipient failures in electronic systems.

Table 1. Potential failure precursors for electronics

Electronic Subsystem	Failure Precursor Parameter
Switching power supply	• DC output (voltage and current levels) • Ripple • Pulse width duty cycle

	• Efficiency • Feedback (voltage and current levels) • Leakage current • RF noise
Cables and connectors	• Impedance changes • Physical damage • High-energy dielectric breakdown
CMOS IC	• Supply leakage current • Supply current variation • Operating signature • Current noise • Logic level variations
Voltage controlled oscillators	• Output frequency • Power loss • Efficiency • Phase distortion • Noise
FET	• Gate leakage current/resistance • Drain-source leakage current/resistance
Ceramic chip capacitors	• Leakage current/resistance • Dissipation factor • RF noise
General purpose diodes	• Reverse leakage current • Forward voltage drop • Thermal resistance • Power dissipation • RF noise
Electrolytic capacitors	• Leakage current/resistance • Dissipation factor • RF noise
RF power amplifier	• Voltage standing wave ratio (VSWR)

	• Power dissipation • Leakage current

Supply current monitoring is routinely performed for testing of CMOS ICs. This method is based upon the notion that defective circuits produce an abnormal or at least significantly different amount of current than the current produced by fault-free circuits. This excess current can be sensed to detect faults. The power supply current (Idd) can be defined by two elements: the Iddq-quiescent current and the Iddt-transient or dynamic current. Iddq is the leakage current drawn by the CMOS circuit when it is in a stable (quiescent) state. Iddt is the supply current produced by circuits under test (CUT) during a transition period after the input has been applied. Iddq has been reported to have the potential for detecting defects such as bridging, opens, and parasitic transistor defects. Operational and environmental stresses such as temperature, voltage, and radiation can quickly degrade previously undetected faults and increase the leakage current (Iddq). There is extensive literature on Iddq testing, but only little has been done on using Iddq for in-situ PHM. Monitoring Iddq has been more popular than monitoring Iddt [36] [37] [38].

Smith and Campbell, [36] developed a quiescent current monitor (QCM) that can detect elevated Iddq current in real time during operation. The QCM performed leakage current measurements on every transition of the system clock to get maximum coverage of the IC in real time. Pecuh, et al., [37] and Xue and Walker, [38] proposed a low-power built-in current monitor for CMOS devices. In the Pecuh, et al., study, the current monitor was developed and tested on a series of inverters for

simulating open and short faults. Both fault types were successfully detected and operational speeds of up to 100 MHz were achieved with negligible effect on the performance of the circuit under test. The current sensor developed by Xue and Walker enabled Iddq monitoring at a resolution level of 10 pA. The system translated the current level into a digital signal with scan chain readout. This concept was verified by fabrication on a test chip.

It has been proposed by GMA Industries [39] [40] [41] to embed molecular test equipment (MTE) within ICs to enable them to continuously test themselves during normal operation and to provide a visual indication that they have failed. The molecular test equipment could be fabricated and embedded within the individual integrated circuit in the chip substrate. The molecular-sized sensor "sea of needles" could be used to measure voltage, current, and other electrical parameters, as well as sense changes in the chemical structure of integrated circuits that are indicative of pending or actual circuit failure. This research focuses on the development of specialized doping techniques for carbon nanotubes to form the basic structure comprising the sensors. The integration of these sensors within conventional IC circuit devices, as well as the use of molecular wires for the interconnection of sensor networks, is an important factor in this research. However, no product or prototype has been developed to date.

Kanniche and Mamat-Ibrahim, [42] developed an algorithm for health monitoring of pulse width modulation - voltage source inverters. The algorithm was

designed to detect and identify transistor open circuit faults and intermittent misfiring faults occurring in electronic drives. The mathematical foundations of the algorithm were based on discrete wavelet transform (DWT) and fuzzy logic (FL). Current waveforms were monitored and continuously analyzed using DWT to identify faults that may occur due to constant stress, voltage swings, rapid speed variations, frequent stop/start-ups, and constant overloads. After fault detection, "if-then" fuzzy rules were used for VLSI fault diagnosis to pinpoint the fault device. The algorithm was demonstrated to detect certain intermittent faults under laboratory experimental conditions.

Lall, et al. [43] [44] have developed a damage pre-cursor based residual life computation approach for various package elements to prognosticate electronic systems prior to the appearance of any macro-indicators of damage. In order to implement the system-health monitoring, precursor variables have been identified for various package elements and failure mechanisms. Model-algorithms have been developed to correlate precursors with impending failure for computation of residual life. Package elements investigated include, first-level interconnects, dielectrics, chip interconnects, underfills and semiconductors. Examples of damage proxies include, phase growth rate of solder interconnects, intermetallics, normal stress at chip interface, and interfacial shear stress. Lall et al., suggest that the pre-cursor based damage computation approach eliminates the need for knowledge of prior or posterior operational stresses and enables the management of system reliability of deployed non-pristine materials under unknown loading conditions. The approach can be used

on re-deployed parts, sub-systems and systems, since it does not depend on availability of prior stress histories.

Self-monitoring analysis and reporting technology (SMART) currently employed in select computing equipment for hard disk drives (HDD) is another example of precursor monitoring [45] [46]. HDD operating parameters, including the flying height of the head, error counts, variations in spin time, temperature, and data transfer rates, are monitored to provide advance warning of failures (see Table 2). This is achieved through an interface between the computer's start-up program (BIOS) and the hard disk drive.

Table 2. Monitoring parameters based on reliability concerns in hard drives

Reliability Issues	Parameters Monitored
• Heads/head assembly - crack on head - head contamination or resonance - bad connection to electronics module • Motors/bearings - motor failure - worn bearing - excessive run-out - no spin • Electronic module - circuit/chip failure - interconnection/solder joint failure	• Head flying height: A downward trend in flying height will often precede a head crash. • Error Checking and Correction (ECC) use and error counts: The number of errors encountered by the drive, even if corrected internally, often signals problems developing with the drive. • Spin-up time: Changes in spin-up time can reflect problems with the spindle motor. • Temperature: Increases in drive temperature often signal spindle

- bad connection to drive or bus • Media - scratch/defects - retries - bad servo - ECC corrections	motor problems. • Data throughput: Reduction in the transfer rate of data can signal various internal problems.

Systems for early fault detection and failure prediction are being developed using variables such as current, voltage, and temperature, continuously monitored at various locations inside the system. Sun Microsystems refers to this approach as continuous system telemetry harnesses [47]. Along with sensor information, soft performance parameters such as loads, throughputs, queue lengths, and bit error rates are tracked. Prior to PHM implementation, characterization is conducted by monitoring the signals (of different variables) to learn a multivariate state estimation technique (MSET) model. Once the model is established using this data, it is used to predict the signal of a particular variable based on learned correlations among all variables [48]. Based on the expected variability in the value of a particular variable during application, a sequential probability ratio test (SPRT) is constructed. During actual monitoring the SPRT will be used to detect the deviations of the actual signal from the expected signal based on distributions (and not on single threshold value) [49] [50].

During implementation, the performance variables are continuously monitored using sensors already existing in Sun's servers and recorded in a circular file structure. The file retains data collected at high sampling rates for seventy-two hours

and data collected at a lower sampling rate for thirty days. For each signal being monitored, an expected signal is generated using the MSET model. This signal is generated in real time based on learned correlations during characterization (see **Figure 3**). A new signal of residuals is generated, which is the arithmetic difference of the actual and expected time-series signal values. These differences are used as input to the SPRT model, which continuously analyses the deviations and provides an alarm if the deviations are of concern [48]. The monitored data is analyzed to (1) provide alarms based on leading indicators of failure, and (2) enable use of monitored signals for fault diagnosis, root cause analysis of no-fault-founds (NFF), and analysis of faults due to software aging [47] [51].

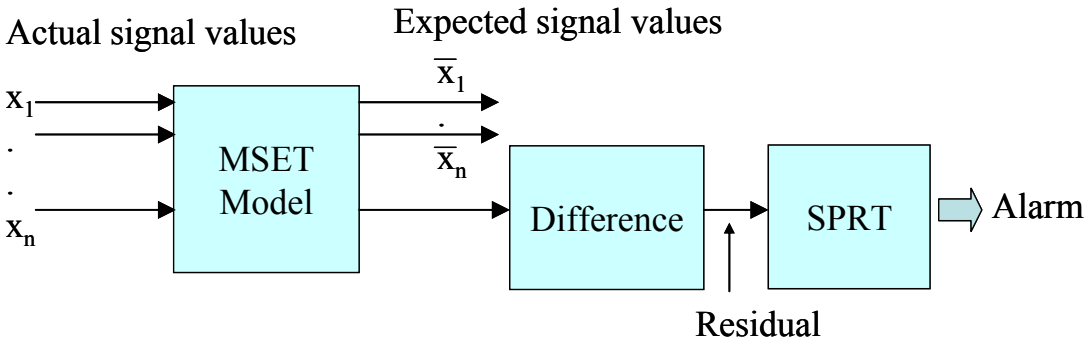

Figure 3. SUN's approach to PHM

Brown, et al., [52] demonstrated that the remaining useful life of a commercial global positioning system (GPS) system can be predicted by using precursor to failure approach. The failure modes for GPS included precision failure due to an increase in position error and solution failure due to increased outage probability. These failure progressions were monitored in-situ by recording system-level features reported using the national marine electronics association (NMEA)

protocol 0183. The GPS was characterized to collect the principal feature value for a range of operating conditions. The approach was validated by conducting accelerated thermal cycling of the GPS with the offset of the principal feature value measured in-situ. Based on experimental results, parametric models were developed to correlate the offset in the principal feature value with solution failure. During the experiment the BIT provided no indication of an impending solution failure [52].

In general to implement a precursor reasoning-based PHM system, it is necessary to identify the precursor variables for monitoring, and then develop a reasoning algorithm to correlate the change in the precursor variable with the impending failure. This characterization is typically performed by measuring the precursor variable under an expected or accelerated usage profile. Based on the characterization, a model is developed - typically a parametric curve-fit, neural-network, Bayesian network, or a time-series trending of a precursor signal. This approach assumes that there is one or more expected usage profiles that are predictable and can be simulated in a laboratory setup. In some products the usage profiles are predictable, but this is not always true.

For a fielded product with highly varying usage profiles, an unexpected change in the usage profile could result in a different (non-characterized) change in the precursor signal. If the precursor reasoning model is not characterized to factor in the uncertainty in life-cycle usage and environmental profiles, it may provide false alarms. Additionally, it may not always be possible to characterize the precursor

signals under all possible usage scenarios (assuming they are known and can be simulated). Thus, the characterization and model development process can often be time-consuming and costly and may not work.

2.4 Monitoring Environmental and Usage Loads

The life-cycle environment of a product consists of manufacturing, storage, handling, operating and non-operating conditions. The life-cycle loads (Table 3), either individually or in various combinations, may lead to performance or physical degradation of the product and reduce its service life [53]. The extent and rate of product degradation depends upon the magnitude and duration of exposure (usage rate, frequency, and severity) to such loads. If one can measure these loads in-situ, the load profiles can be used in conjunction with damage models to assess the degradation due to cumulative load exposures.

Table 3. Examples of life-cycle loads

Load	Load Conditions
Thermal	Steady-state temperature, temperature ranges, temperature cycles, temperature gradients, ramp rates, heat dissipation
Mechanical	Pressure magnitude, pressure gradient, vibration, shock load, acoustic level, strain, stress
Chemical	Aggressive versus inert environment, humidity level, contamination, ozone, pollution, fuel spills
Physical	Radiation, electromagnetic interference, altitude
Electrical	Current, voltage, power

The assessment of the impact of life-cycle usage and environmental loads on electronic structures and components was studied by Ramakrishnan and Pecht [53]. This study introduced the life consumption monitoring (LCM) methodology (**Figure 4**), which combined in-situ measured loads with physics-based stress and damage models for assessing the life consumed.

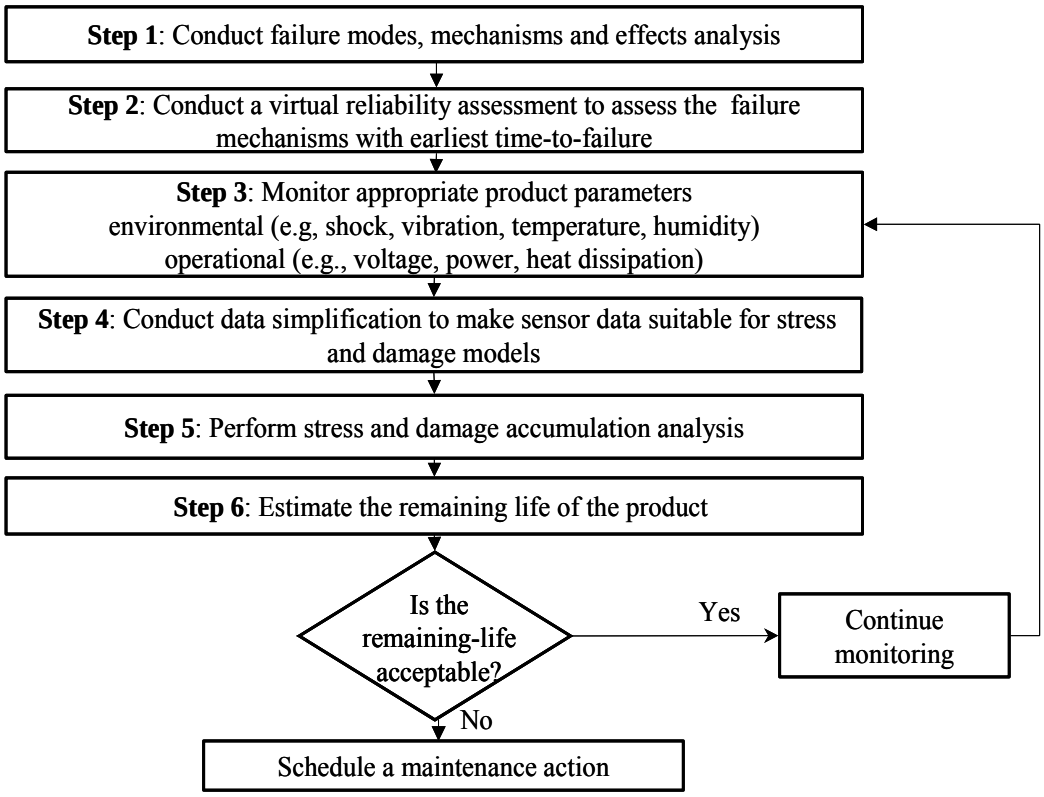

Figure 4. CALCE life consumption monitoring methodology

The application of the LCM methodology to electronics PHM was illustrated with two case studies [53] [54]. The test vehicle consisted of an electronic component-board assembly placed under the hood of an automobile and subjected to normal driving conditions in the Washington, DC, area. The test board incorporated eight surface-mount leadless inductors soldered onto an FR-4 substrate using eutectic tin-lead solder. Solder joint fatigue was identified as the dominant failure

mechanism. Temperature and vibrations were measured in-situ on the board in the application environment. Using the monitored environmental data, stress and damage models were developed and used to estimate consumed life. The LCM methodology accurately predicted remaining life.

Mathew, et al., [55] applied the LCM methodology in conducting a prognostic remaining-life assessment of circuit cards inside a space shuttle solid rocket booster (SRB). Vibration time history recorded on the SRB from the pre-launch stage to splashdown were used in conjunction with physics-based models to assess the damage caused due to vibration and shock loads. Using the entire life-cycle loading profile of the SRBs, the remaining life of the components and structures on the circuit cards were predicted. It was determined that an electrical failure was not expected within another forty missions. However, vibration and shock analysis exposed an unexpected failure of the circuit card due to a broken aluminum bracket mounted on the circuit card. Damage accumulation analysis determined that the aluminum brackets had lost significant life due to shock loading.

Shetty, et al. [56] applied the LCM methodology for conducting a prognostic remaining-life assessment of the end effector electronics unit (EEEU) inside the robotic arm of the space shuttle remote manipulator system (SMRS). A life-cycle loading profile for thermal and vibrational loads was developed for the EEEU boards. Damage assessment was conducted using physics-based mechanical and thermomechanical damage models. A prognostic estimate using a combination of

damage models, inspection, and accelerated testing showed that there was little degradation in the electronics and they could be expected to last another twenty years.

Vichare, et al. [2] [57] outlined generic strategies for in-situ load monitoring, including selecting appropriate parameters to monitor and designing an effective monitoring plan. Methods for processing the raw sensor data during in-situ monitoring to reduce the memory requirements and power consumption of the monitoring device were presented. Approaches were also presented for embedding intelligent front-end data processing capabilities in monitoring systems to enable data reduction and simplification (without sacrificing relevant load information) prior to input in damage models for health assessment and prognostics.

Embedding the data reduction and load parameter extraction algorithms in to the sensor modules as suggested by Vichare et al., [57] can lead to reduction in on-board storage space, low power consumption, and uninterrupted data collection over longer durations. A time-load signal can be monitored in-situ using sensors, and further processed to extract (in this case) cyclic range (Δs), cyclic mean load (Smean), and rate of change of load (ds/dt) using embedded load extraction algorithms. The extracted load parameters can be stored in appropriately binned histograms to achieve further data reduction. After the binned data is downloaded, it can be used to estimate the distributions of the load parameters. The usage history is used for damage accumulation and remaining life prediction.

Efforts to monitor life-cycle load data on avionics modules can be found in time-stress measurement device (TSMD) studies. Over the years the TSMD designs have been upgraded using advanced sensors [58], and miniaturized TSMDs are being developed due to advances in microprocessor and non-volatile memory technologies [59].

Searls, et al., [60] undertook in-situ temperature measurements in both notebook and desktop computers used in different parts of the world. In terms of the commercial applications of this approach, IBM has installed temperature sensors on hard drives (Drive-TIP) [61] to mitigate risks due to severe temperature conditions, such as thermal tilt of the disk stack and actuator arm, off-track writing, data corruptions on adjacent cylinders, and outgassing of lubricants on the spindle motor. The sensor is controlled using a dedicated algorithm to generate errors and control fan speeds.

Strategies for efficient in-situ health monitoring of notebook computers were provided by Vichare, et al., [62]. In this study the authors monitored and statistically analyzed the temperatures inside a notebook computer, including those experienced during usage, storage, and transportation, and discussed the need to collect such data both to improve the thermal design of the product and to monitor prognostic health. The temperature data was processed using two algorithms: (1) ordered overall range (OOR) to convert an irregular time-temperature history into peaks and valleys and also to remove noise due to small cycles and sensor variations, and (2) a three-

parameter Rainflow algorithm to process the OOR results to extract full and half cycles with cyclic range, mean and ramp rates. The effects of power cycles, usage history, CPU computing resources usage, and external thermal environment on peak transient thermal loads were characterized.

The European Union funded a project from September 2001 through February 2005 named environmental life-cycle information management and acquisition for consumer products (ELIMA), which aimed to develop ways of better managing the life cycles of products using technology to collect vital information during a product's life to lead to better and more sustainable products [63] [64]. Though the focus of this work was not on prognostics, the project demonstrated the monitoring of the life-cycle conditions of electronic products by field trials. ELIMA partners built and tested two special prototype consumer products with data collection features, and investigated the implications for producers, users, and recyclers. The ELIMA technology included sensors and memory built into the product to record dynamic data such as operation time, temperature, and power consumption. This was added to static data about materials and manufacture. Both a direct communication (via GSM module) as well as a two-step communication with the database (RFID data retrieval followed by an Internet data transfer) was applied. As a case study, the member companies monitored the application conditions of a game console and a household fridge-freezer.

Skormin, et al., [65] developed a data mining model based for failure prognostics of avionics units. The model provides a means of efficiently clustering data on parameters measured during operation, such as vibration, temperature, power supply, functional overload, and air pressure. These parameters are monitored in-situ on the flight using time-stress measurement devices. The objectives of the model are (1) to investigate the role of measured environmental factors in the development of particular failure; (2) to investigate the role of combined effects of several factors; and (3) to reevaluate the probability of failure on the basis of known exposure to particular adverse conditions. Unlike the physics-based assessments made by Ramakrishnan and Pecht [53], the data mining model relies on the statistical data available from the records of a time-stress measurement device (TSMD) on cumulative exposure to environmental factors and operational conditions. The TSMD records, along with calculations of probability of failure of avionics units, are used for developing the prognostic model. The data mining enables an understanding of the usage history and allows tracing the cause of failure to individual operational and environmental conditions.

2.5 PHM Integration

Implementing an effective PHM strategy for an entire system will involve integrating different health monitoring approaches. An extensive analysis may be required to determine the weak link(s) in the system to enable a more focused monitoring process. Once the potential failure modes, mechanisms, and effects have been identified, a combination of BIT, canaries, precursor reasoning, and life-cycle

damage modeling may be necessary, depending on the failure attributes. In fact, different approaches can be implemented based on the same sensor data. For example, operational loads, such as temperature, voltage, supply current, and acceleration, can be collected by BIT. The current and temperature data can be used with damage models to calculate the susceptibility to electromigration between metallizations. Also, the supply-current data can be used with precursor reasoning algorithms for identifying signs of transistor degradation.

Case studies of the integration of different approaches of PHM can be found in work by CALCE [66] [56] and R. Orsagh, et al., [67], which used physics-based models for damage accumulation and precursor reasoning for system assessment. A detailed FMMEA [33] was conducted and time to failure was assessed for the failure mechanisms identified by the FMMEA using appropriate failure models. The time-to-failures were ranked and a risk assessment was made based on severity and occurrence before PHM implementation [66]. In another PHM study [68], an off-the-shelf 50-watt, DC-to-DC converter from a commercial power supply manufacturer was used. As in the CALCE studies [66] [56], a detailed a-priori analysis of power supply reliability issues was conducted in this case using the Pareto analysis of failures reported by the manufacturer. PHM techniques were then aimed at monitoring and predicting the most common failures.

Future electronic system designs will integrate sensing and processing modules that will enable in-situ PHM. Advances in sensors, microprocessors,

compact non-volatile memory, battery technologies, and wireless telemetry have already enabled the implementation of sensor modules and autonomous data loggers. For in-situ health monitoring, integrated, miniaturized, low-power, reliable sensor systems operated using portable power supplies (such as batteries) are being developed. These sensor systems have self-contained architecture requiring minimum or no intrusion into the host product in addition to specialized sensors for monitoring localized parameters. Sensors with embedded algorithms will enable fault detection, diagnostics, and remaining life prognostics that would ultimately drive the supply chain. The prognostic information will be linked via wireless communications to relay needs to maintenance officers and automatic identification techniques (RFID being the most common current example) will be used to locate parts in the supply chain--all integrated through a secure web portal to acquire and deliver replacement parts quickly on an as-needed basis.

Chapter 3: Prognostics Using Environmental and Usage Loads

3.0 Introduction

This chapter presents the prognostic approach that is based on accumulating damage due to environmental and usage exposures. This chapter discusses the approach and its implementation setup for electronic prognostics used in this research. The key challenges in implementing this approach are presented. These challenges and proposed solutions will be discussed in more details in individual chapters.

3.1 Approach

The basic philosophy underlying the type of PHM approach is that damage is a function of the loads experienced by the product in the life cycle environment. The life cycle environment of a product consists of manufacturing, storage, handling, operating and non-operating scenario. The life cycle loads consists of thermal (steady-state temperature, temperature ranges, temperature cycles, temperature gradients), mechanical (pressure levels, pressure gradients, vibrations, shock loads, acoustic levels), chemical (aggressive or inert environments, humidity levels, contamination), physical (radiation, electromagnetic interference, altitude), environmental (ozone, pollution, fuel spills) and usage loads (usage frequency, usage severity, usage time, power, heat dissipation, current, voltage etc.) [2] [57]. These loads either individually or in various combinations may lead to performance or physical degradation of the product and subsequently reduce its service life. The

extent and rate of product degradation depends upon the nature, magnitude, and duration of exposure to such loads

For implementation of this approach, strategies are required to design an effective PHM process for the product and application specific needs. Environmental and usage load profiles need to be efficiently and accurately captured in the application environment, and utilized in real time or near real time health assessment and prognostics. It is essential to simplify or pre-process the "raw" sensor data to make it compatible with the damage models and algorithms needed to conduct prognostics. In particular, it may be necessary to extract the relevant load parameters including cyclic mean, amplitudes, ramp rates, hold periods, power spectral densities, etc. Commonly used load parameter extraction methods include: cycle counting algorithms for extracting cycles from time-load signal, Fast Fourier transforms (FFT) for extracting the frequency content of signals, etc. Depending on the application and type of signal, custom load extraction methods may be required.

Figure 5 is a schematic of the in-situ monitoring, pre-processing, and storage of environmental and usage loads. A time-temperature signal is monitored in-situ using sensors, and further processed to extract (in this case) cyclic temperature range (ΔT), cyclic mean temperature (T_{mean}), ramp rate (dT/dt), and dwell time (t_D) using embedded load extraction algorithms. The extracted load parameters are stored in appropriate bins to achieve further data reduction. The binned data is downloaded to estimate the distributions of the load parameters for use in damage assessment, remaining life estimation, and the accumulation of the products use history.

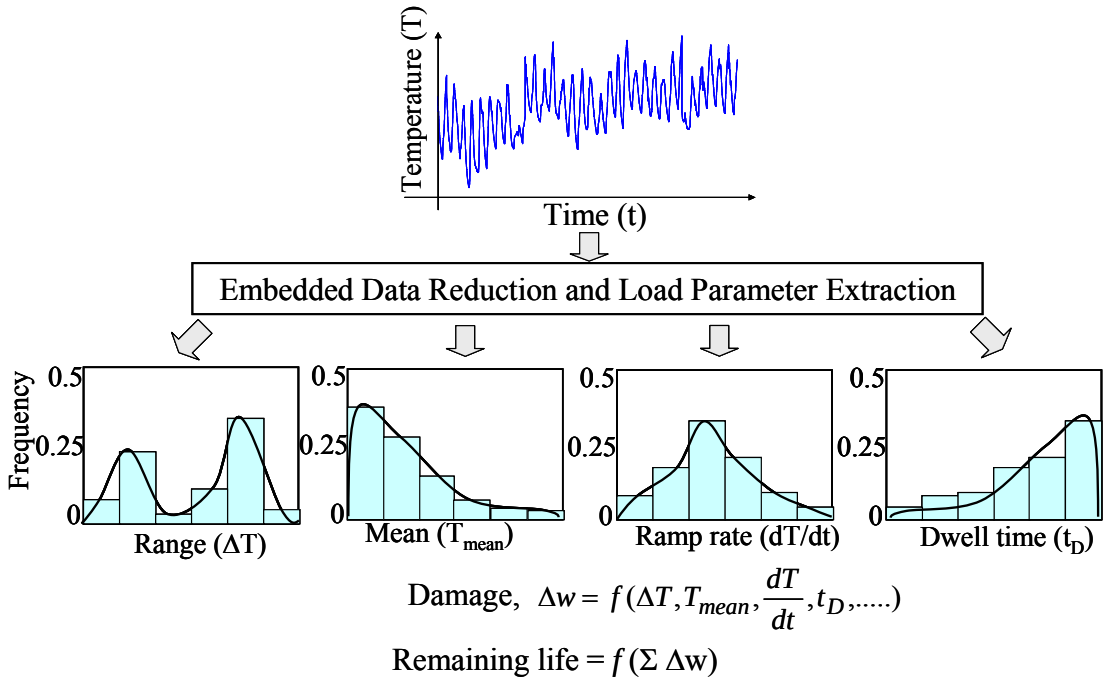

Figure 5. Prognostic approach using environmental and usage loads

Once these load parameters are obtained, they can then be used in conjunction with damage models in Table 4 to assess the damage at various failure sites due to different failure mechanisms for a given electronic assembly. A comprehensive listing of loads, models, and failure mechanisms can be found in the following documents JESD659-A: Failure-mechanism-driven reliability monitoring, JEP143A: Solid-state reliability assessment and qualification methodologies, JEP150: Stress-test-driven qualification of and failure mechanisms associated with assembled solid state surface-mount components, JESD94: Application specific qualification using knowledge based test methodology, JESD91A: Method for developing acceleration models for electronic component failure mechanisms, SEMATECH, #00053955A-XFR: Semiconductor device reliability failure models, SEMATECH, #00053958A-XFR: Knowledge-based reliability qualification testing of silicon devices, and

SEMATECH, #99083810A-XFR: Use condition based reliability evaluation of new semiconductor technologies [69] [70].

Table 4. Failure mechanisms, relevant loads, and models in electronics

Failure Mechanisms	Failure Sites	Relevant Loads	Sample Models
Fatigue	Die attach, Wirebond/TAB, Solder leads, Bond pads, Traces, Vias/PTHs, Interfaces	Δ T, Tmean, dT/dt, dwell time, ΔH, ΔV	Nonlinear Power Law (Coffin-Manson)
Corrosion	Metallizations	M, ΔV, T	Eyring (Howard)
Electromigration	Metallization	T, J	Eyring (Black)
Conductive Filament Formation	Between Metallization	M, ∇ V	Power Law (Rudra)
Stress Driven Diffuison Voiding	Metal Traces	s, T	Eyring (Okabayashi)
Time Dependant Dielectric Breakdown	Dielectric layers	V, T	Arrhenius (Fowler-Nordheim)
Δ: Cyclic range ∇ : gradient	V: Voltage M: Moisture	T: Temperature J:Current density	s: Stress H: Humidity

3.2 Implementation Setup

The experiment was setup to implement the PHM methodology based on damage accumulation due to environmental and usage exposures for predicting remaining life of solder joint interconnects under temperature cycling loads. An electronic test board was exposed to a completely irregular temperature profile. The test board used for this research is shown in **Figure 6**. The board contains 12 surface mount components soldered on a 62 mil thick high Tg FR-4 substrate using eutectic Sn-Pb solder. The components are dummy packages with small size silicon die. All components are daisy chained to facilitate continuity monitoring during testing. A daisy chain is a conductive path that connects several interconnections of a

component. In this experiment a failure (refer to failure definitions in the main document) of any daisy chain indicates the failure of the component. The overall dimensions of the board are 8" X 5.5" and the pad finish is immersion silver

The profile simulated field conditions by exposing the board to random temperature variations similar to those experienced due to random usage. This profile was generated in a programmable oven, such that each successive profile has completely different peak temperatures, ramp rates, and dwell times. The environmental chamber used for this work was the Thermatron 2800 S1.2, which is capable of storing 255 discrete time-temperature intervals and sequencing them in different loops. An example of the temperature profile for the first 20 days is shown in **Figure 7**. During testing, the temperatures at various locations of the board were measured in-situ using sensors placed on the board. The temperature was monitored every 10 seconds. Two instruments were used, one is a prototype miniature sensing and data recording systems (HUMS) provided by European Aeronautics and Defense Space (EADS) systems. However, for most part of the experiment, a multi-channel data logger (from Agilent) with multiplexing units was used.

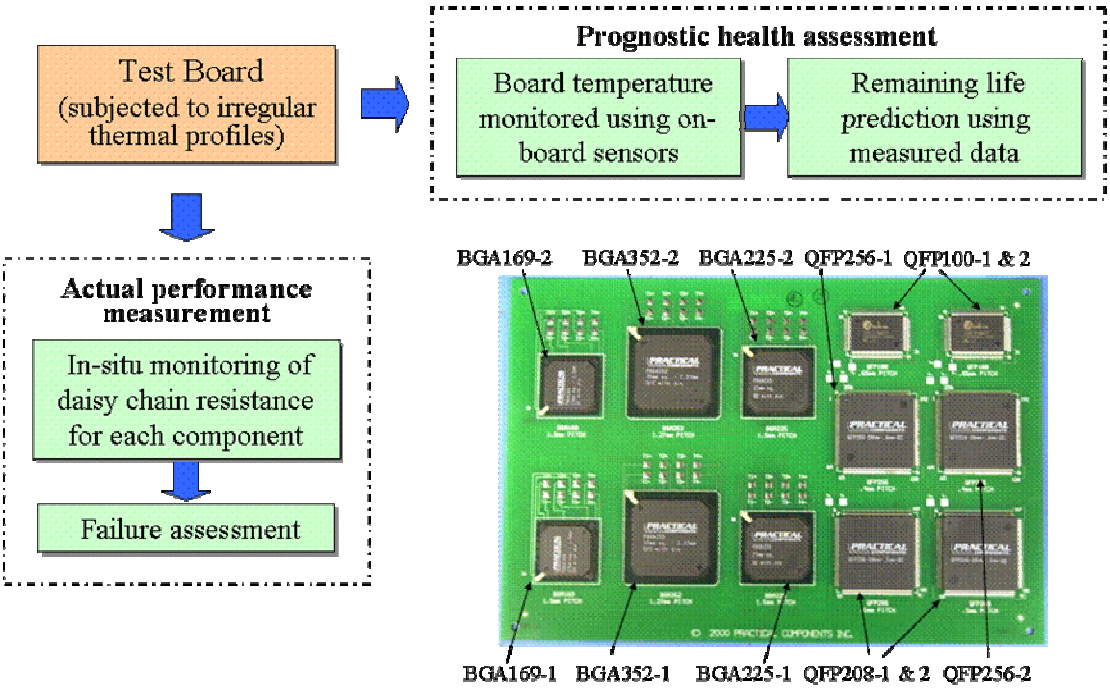

Figure 6. Experimental setup for PHM implementation on electronic board

The test board was thoroughly characterized in the oven with thermocouples on all components and at various locations of the board. However, we found that the temperature variation on the board was within 5°C. Hence, the temperature was monitored using 3 sensors, two on components and one on the board. The raw sensor data was fed in the novel load parameter extraction algorithm discussed in the chapter 5, to extract the cyclic range, mean, ramp-rate and the dwell times (with temperature of dwell).

The next step in the PHM process is the damage estimation and accumulation. The results of load parameter extraction algorithm were fed in the first order thermal fatigue model. This model is based on the work of CALCE researchers and has been implemented using custom software after calibrating against various experimental

studies. Using this thermal fatigue model and the board and component specific information on material properties and geometry, the model was used to assess the damage of solder joints on the test board. The model has been used extensively for calculating solder fatigue and provides rapid assessment which makes it more attractive for in-situ assessments for PHM application.

The package geometries namely, the size, shape, and areas of the solder balls and the gull wing interconnects were supplied by the manufacturer. Some of these values were verified by actual measurement. The material properties of solder, board, interconnect, and packages were obtained from the manufacturer. For routinely used materials such as Pb-Sn solder, and FR-4, these properties are stored in the database of the CalcePWA software that was used for building the model. These properties have been derived from several experimental results and from literature.

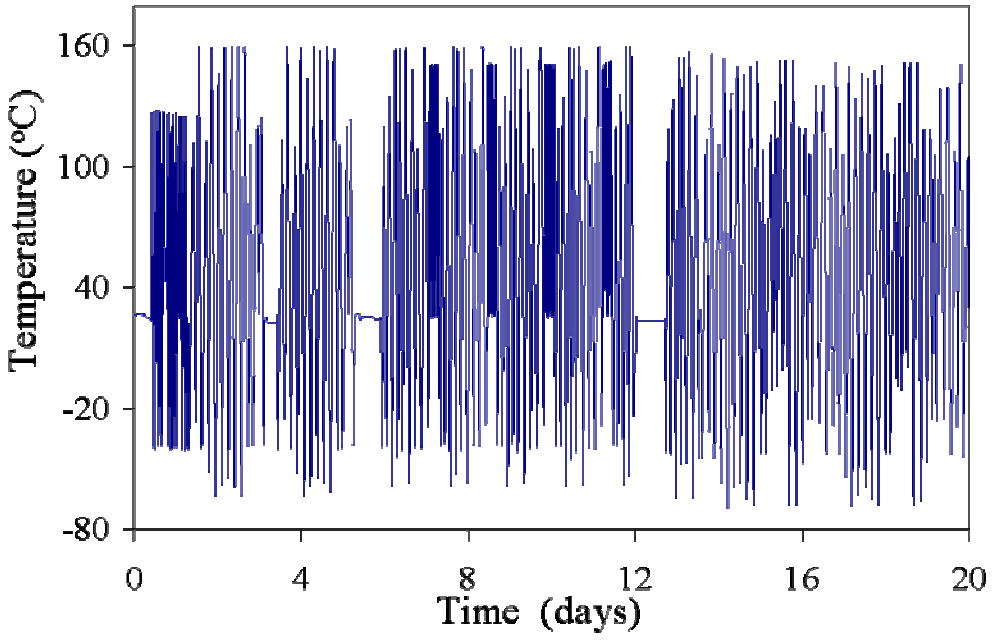

Figure 7. Illustration of temperature measured on the board for first 20 days

Prior to exposing the test board to irregular cycles, another board of the exact same design was exposed to constant thermal cycling profile ranging from -40^{o}C to 125^{o}C, with a 15 minute and 10 minute dwell at maximum and minimum temperatures. The temperature ramp-up and ramp-down rate was set at 5.5^{o}C/minute and 8.5^{o}C/minute. The accuracy of the damage model was assessed by comparing the model predictions with results from testing to actual failure due to temperature cycling. Additionally, a range of different thermal cycling conditions were simulated. The results from testing were compared with modeling. Four thermal cycling parameters namely the temperature amplitude (ΔT), cyclic mean temperature (Ts), ramp rate from low to high temperatures, and dwell time at high temperature (t_D), were studied and the impact of each parameter on the life of solder joints was assessed by sensitivity studies.

The thermal-fatigue model provides a damage fraction due to each thermal cycle exposure, which is accumulated linearly using Miner's hypothesis. The damage fraction greater than or equal to 1 indicates failure or end of life of the product being monitored. Along with the temperature, the daisy chain resistance (actual electrical performance) of the solder interconnects is measured in-situ. The failure criteria for the solder joints was set as per IPC standard IPC-SM 785 [71], that states that failure manifests itself in form of resistance spikes of short durations >300 Ω and failure is defined as the first interruption of electrical continuity that is confirmed by 9 additional interruptions with an additional 10% of cycle life. The failure of the solder joints obtained from the resistance measurement indicates the actual failure. The

actual (measured) failure of the solder joint is compared with the prediction made using PHM (temperature measurement and damage accumulation) to validate the PHM methodology. The details of damage assessment and life prediction will be presented in chapter six.

3.3 Summary

The prognostic approach based on monitoring and modeling of environmental and usage loads was presented. The experimental setup for demonstrating the PHM technique for an electronic board was discussed. The temperature data from this experiment was used for demonstrating the load parameter extraction algorithm and the method for optimal binning (chapter 5). Also, the temperature data was used with damage models for enabling prognostics of solder joints in thermal cycling (Chapter 6). Finally, the in-situ resistance measurements, along with the temperature were used for identification and trending of failure precursors (chapter 7).

Chapter 4: Methods for In-situ Monitoring

4.0 Introduction

A major challenge in PHM is its implementation in the application environment. Strategies are required to design an effective PHM process for the product and application specific needs. Environmental and usage load profiles need to be efficiently and accurately captured in the application environment, and utilized in real time or near real time health assessment and prognostics. This paper outlines generic strategies both for load monitoring and conversion of the sensor data into a format that can be used in physics-of-failure models, for both damage estimation and remaining life prediction due to specific failure mechanisms. The selection of appropriate parameters to monitor, design of an effective monitoring plan, and selection of appropriate monitoring equipment are discussed. Methods to process the raw sensor data during in-situ monitoring for reducing the memory requirements and power consumption of the monitoring device are suggested. Conceptual approaches are also presented for embedding such processing capabilities in monitoring systems to enable data reduction and simplification (without sacrificing relevant load information) prior to model input for health assessment and prognostics. The strategies presented are generically applicable to electronic health monitoring processes and are illustrated using a case-study of in-situ monitoring of a note-book computer.

4.1 In-situ Monitoring of Environmental and Usage Loads

The requirements for data collection may be well known or already specified for some applications. However, in many applications, it is not always à priori known what parameters need to be measured, nor with what frequency or precision. It may be useful to conduct preliminary field tests and collect additional data that may not be justified in a fully operating system, so as to understand what data is actually relevant. If the objective of data collection is for use in an ongoing product design phase, the aim would be to gather maximum data in a minimum time frame. For health assessment as well as design decisions, monitoring plans are required to capture the distribution of loading parameters and usage profiles. The life cycle loads further depend on the usage conditions such as usage frequency, severity, and period of use. The following sections outline the steps in implementing a process for effective monitoring of life cycle loads.

4.1.1 Selection of Load Parameters for Monitoring

The first step in the data collection process is to select the life cycle parameters to be monitored. Parameters can be identified based on factors that are crucial for safety, are likely to cause catastrophic failures, are essential for mission completeness, or can result in long downtimes. Selection can also be based on knowledge of the critical parameters established from past experience and field failure data on similar products, and qualification testing. More systematic methods such as failure mode and effects analysis (FMEA) or failure mode mechanisms and effects analysis (FMMEA) [33] can be used to determine parameters that need to be monitored.

Table 4 (previous chapter) provides a listing of common failure mechanisms in electronics with the relevant loads and associated models compiled from JEDEC standards JEP122B (Failure Mechanisms and Models for Semiconductor Device) and JEP 148 (Reliability Qualification of Semiconductor Devices Based on Physics of Failure Risk and Opportunity Assessment). The failure mechanisms and models can serve as a starting point for selecting the appropriate parameters.

4.1.2. Selection of Monitoring Equipment

The main attributes of a sensor system for environmental and usage monitoring include level of integration, power consumption and management, on-board memory and utilization, size and weight, wireless communication, embedded computational power, software support, and product maturity. Each attribute is discussed in detail below.

Level of Integration

A completely integrated sensor system consists of the sensing elements, on-board analog to digital converter, on-board memory, embedded computational capabilities, ability to communicate with other sensor nodes, and completely supported by indigenous power supply. For in-situ monitoring, the requirements for data collection may be well known or already specified for some applications. However, in many applications, it is not always a-priori known what parameters need to be measured, nor with what frequency or precision. Hence, sensor systems with modular architecture consisting of integrated core central nodes and easy add-on nodes are preferred.

Sensor systems for environmental monitoring need to be a self-contained, requiring minimum or no intrusion into the host product. This can facilitate monitoring of legacy systems without the need for any testing or qualification. Flexible sensor ports that support a wide variety of sensors (such as ports for all sensors with input requirements between 0-3V) are preferred over rigid customized ports (such as ports designed specifically for particular sensor types say thermocouples). An example of integrated sensor system is shown **Figure 8**.

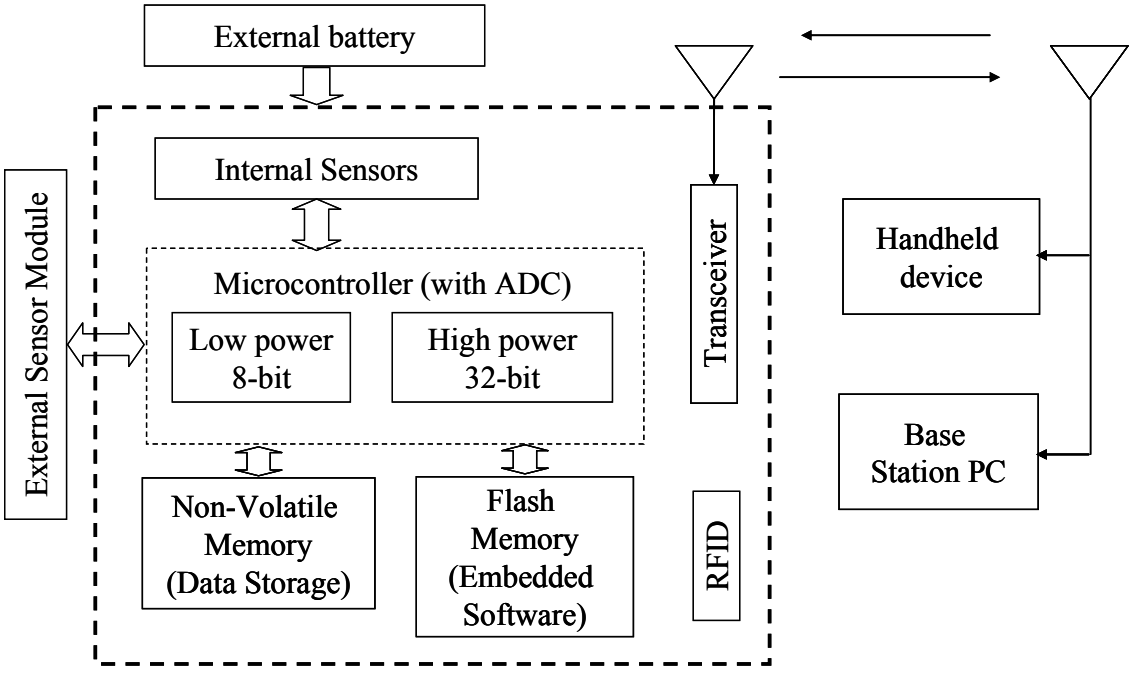

Figure 8. Conceptual schematic of integrated sensor system

Autonomous Power and Power Management Features

One of the major constraints that strongly influences the selection of components and hence the size, weight, and cost of the monitoring system is power consumption. The power consumption of sensor systems can be divided into three domains: sensing, communication, and processing. The power consumed for sensing

varies depending on the parameter being monitored. Periodic sensing can consume less power than continuous monitoring; however there is a risk of missing important data. Power consumption is also controllable by making measurements at events triggered by defined thresholds. The need for power management is even more challenging in wireless sensor systems running on batteries. In the case of wireless sensors, maximum energy is expended in communication, which involves both the data transmission and reception.

On- board Memory and Utilization

Effective utilization of memory is also an important attribute in setting up the sensor system. Memory requirements are affected by the monitoring interval and frequency. In selecting the monitoring frequency, the user has to ensure that the relevant loads are recorded and, at the same time, the memory is not flooded by irrelevant load data. The user should be able to define threshold values for measurement. Appropriate setting of thresholds can facilitate efficient data collection. For example, measurements can be recorded or a scan can be triggered only if the stimulus meets the set threshold. Events can be set to trigger above or below an absolute value, for example, recording acceleration levels above 2g or humidity levels above 80% R.H. Users can also set thresholds based on the value of the slope (positive or negative) of the curve formed by the measurements made by the sensor. This strategy allows usage-based data recording, which can result in a substantial saving in disk space and extend the battery life of the equipment. Other means of memory utilization involve effectively dividing the memory between

periodic measurements and threshold based measurements. A strategic combination of measurement intervals (for periodic measurements) and thresholds can enable recording a higher number of relevant measurements.

Miniature Size and Low Weight

In some applications, the size of the sensor may become the significant selection criteria due to limited space available for mounting the sensor or due to the inaccessibility of locations to be sensed. The weight of the sensor may be important in certain applications such as vibration and shock measurements using accelerometers, since the added mass can change the system response. In the case where a fixture is required to mount the sensor, the added mass of the sensor and fixture may change the system characteristics. Users should consider the entire weight of the sensor system, which includes the battery and other accessories such as communication antennas and cables.

Wireless Capabilities

Wireless monitoring has emerged in recent years as a promising technology that can impact in-situ environmental monitoring. Wireless sensor nodes can be used to remotely monitor inhospitable and toxic environments. In some applications, sensor(s) must operate remotely with data stored and downloaded by telemetry to a centrally located processing station. Also, wireless sensor systems are not dependent on extensive lengths of coaxial wires for the transfer of sensor measurements, thus saving installation and maintenance costs. The real benefit from wireless sensor

nodes can be achieved by embedding micro-controllers with the sensor nodes to improve the data analysis capabilities within the wireless sensing nodes themselves.

The use of portable devices (such as a PDA) in conjunction with wireless sensor systems can enable efficient fault diagnosis and prognostics by integrating more complex algorithms in the hand-held device. Customized processing and reporting tools can be programmed on portable devices for efficient maintenance activities. For example, the data collected by a Bluetooth-enabled accelerometer system can be downloaded on a hand-held device by maintenance technicians and can be processed further using Fast Fourier Transforms (FFT) embedded on the hand-held device.

Embedded Computation Capability

Integrating embedded computational capabilities with on-board processors can reduce the power consumption of wireless sensor systems. These processing capabilities would enable immediate and localized processing of the raw sensor data. This in turn enables transmitting fewer amounts of data (processed instead of raw data) to the base station, and hence results in lower power consumption. In the case of a large number of sensor systems working in a network, this would allow decentralization of computational power and facilitate efficient parallel processing of data.

Additionally, embedding computational power with on-board processors can also facilitate efficient data analysis for environmental monitoring applications. Embedded computations can be set to provide real time updates for taking immediate action such as powering off the equipment to avoid accidents or catastrophic failures, and also for providing prognostic horizons for conducting next repair and maintenance activities. Power consumption and flash memory of the microprocessor may limit computationally intensive algorithms to be embedded with on-board processors. However, even using simple algorithms and routines to process the raw sensor data significant gains can be achieved for in-situ analysis.

Software Support

Sensor systems need host software that can effectively control and communicate with the hardware. Host software can include capabilities to guide the user in selecting measurement scans and thresholds values, communicating with the sensor module to check operational status, enabling operation based power management, and trouble-shooting or diagnosing the hardware in case of problems. Software modules with low memory requirement that can be operated from portable device such as PDA are advantageous for health monitoring applications. For certain applications modules for immediate data analysis can be a part of the host software.

4.1.3. Design of Monitoring Plan

The important aspect of the in-situ load monitoring process is the setup of data collection equipment before dispatching in the application environment. Once the

parameters to be monitored are selected the next step is to design the complete monitoring process. The user needs to select the monitoring equipment (sensors and data recorders), and setup the monitoring process. The important items in the setup include deciding the monitoring interval and frequency. In making this decision the user has to ensure that the relevant loads are recorded and at the same time the memory is not flooded by irrelevant load data. Table 5 provides a list of challenges and possible solutions that can guide in setting up the monitoring equipment.

Effective utilization of memory is also an important parameter in setting up the sensor system. The user should be able to define threshold values for measurement. Appropriate setting of thresholds can facilitate efficient data collection. Measurement will be recorded or a scan will be triggered only if the stimulus meets the set threshold. Events can be set to trigger above or below an absolute value, for example, recording acceleration levels above 2g or humidity levels above 80%R.H. Users can also set thresholds based on the value of the slope (positive or negative) of the curve formed by the measurements made by the sensor. This strategy allows usage based data recording, which can result in substantial saving in disk space and extend the battery life of the equipment.

Higher levels of threshold lead to greater abbreviation of the load history. However, it can also introduce errors in the damage assessment. The monitored loads are simplified and used as inputs to physics-based models for assessing the damage and failure susceptibility due to a particular failure mechanism. Hence, the threshold

selection strongly depends on the failure mechanism being monitored and is often a trade-off between the data reduction and error in the damage assessment process.

This is explained by a recent analysis conducted by the authors. The temperatures on an electronic board mounted on the exhaust manifold of a car were monitored in-situ. This data was processed using ordered overall range (OOR) method to convert the irregular temperature variations into a sequence of peaks and valleys. The OOR output was used in Rainflow cycle counting algorithm to extract the temperature cycles. The temperature cycles and a thermal fatigue model were used to assess the damage on the terminals of the components mounted on the board.

In case of the OOR a reversal elimination index, S (< 1) can be selected to filter amplitudes that differ from the largest measured amplitude by the specified fraction. This data was screened using different values of reversal elimination index (threshold). The accumulated damage was estimated using each data set. For simplicity it was assumed that the error in damage accumulation is zero when all amplitudes are considered for the analysis (S = 0). The error in damage accumulation due to use of reduced data for all other data sets was obtained by the formula

$$\text{Error} = \frac{\text{Accumulated damage } (S = 0) - \text{Accumulated damage } (S > 0)}{\text{Accumulated damage } (S = 0)}$$

Figure 9 illustrates the percentage error in damage accumulation and the percentage data reduction with change in S-parameter. It is observed that even when the S is zero, the data reduction is 84%. This is due to filtering all data points that are in a monotonic increasing or decreasing sequence. Also small values of S, ranging

from 0 to 0.1 resulted in more than 90% data reduction with only 1% error in the damage calculation. Higher values of S result in increasing error in damage accumulation. This is due to elimination of reversals with large magnitude and the dependence of the fatigue model on the temperature amplitude.

The answer to the question on selecting the S parameter can be answered by assessing the distribution of cycles that are obtained after screening the data. **Figure 10**, compares the number of temperature cycles obtained after processing the data with S = 0.1 against S = 0. By choosing S value as 0.1, all cycles with amplitude < 15^{o}C are eliminated. It cannot be directly concluded from **Figure 10** that all the temperature cycles with amplitude < 15^{o}C contributed negligibly to the fatigue damage and can be always neglected. For example, in this case, the failure mechanism being monitored is creep and stress relaxation enhanced fatigue due to thermal cycling. Hence, temperature cycles with small amplitude (say < 10^{o}C) but higher mean temperatures (say > 100^{o}C) can cause more damage than cycles with same small amplitude but low mean temperatures (say < 30^{o}C).

Figure 11, investigates the cyclic mean temperatures of the 2489 cycles with amplitudes < 10^{o}C that were eliminated from the analysis in **Figure 10**. The histogram shows that more than 60% of the thermal amplitudes have a mean temperature within 21^{o}C-30^{o}C, and only 6% of the cycles have a mean temperature greater than 100^{o}C. **Figure 9**, 10 and 11 provide the analysis on the trade-off that can guide the selection of threshold. A-priori estimate of the threshold can be based on

conducting simulation using the selected damage model, to understand what can be eliminated. As monitoring continues the threshold can be updated based on the measured data.

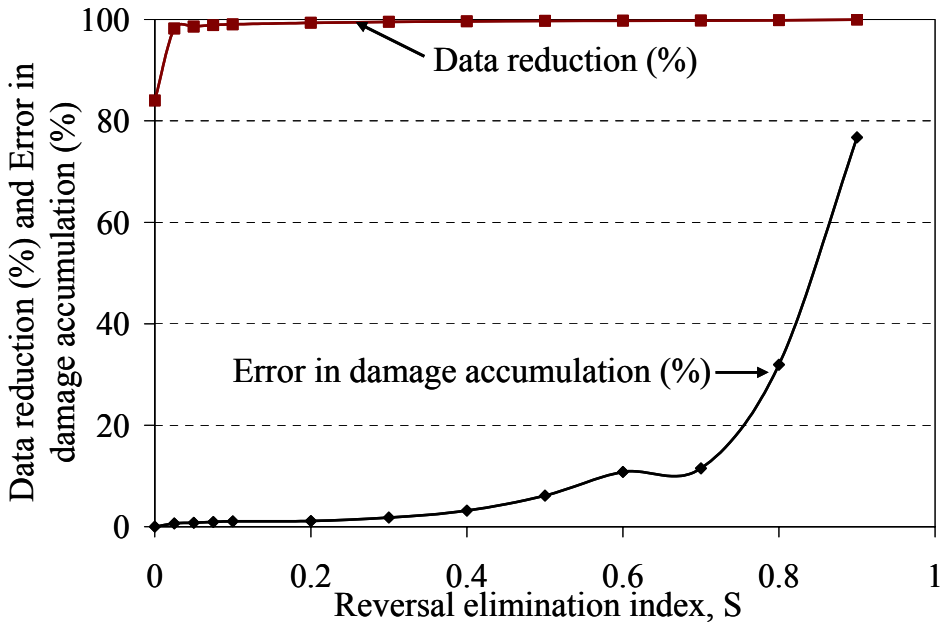

Figure 9. Example of percentage data reduction and error in damage accumulation

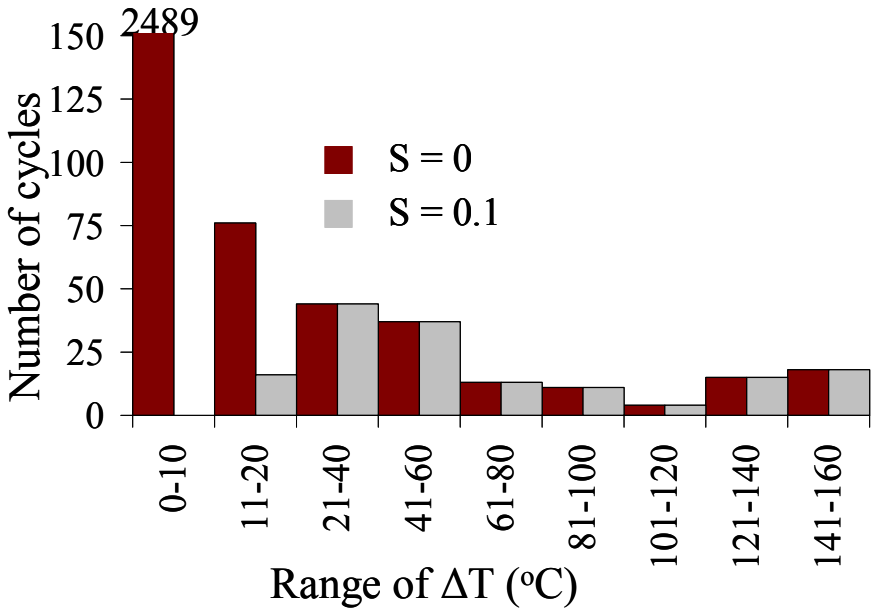

Figure 10. Comparison of histograms of filtered and non-filtered load cycles

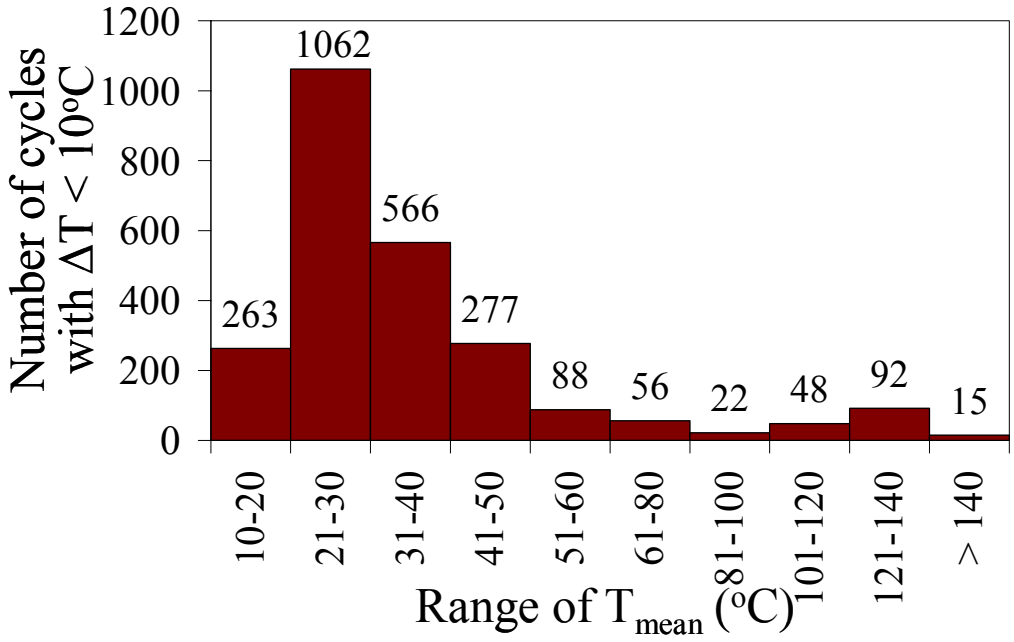

Figure 11. histogram of mean loads associated with the filtered cycles

The monitoring equipment should be setup by effectively dividing the memory between periodic measurements and threshold based measurements. A strategic combination of measurement intervals (for periodic measurements) and thresholds can enable recording more number of relevant measurements.

If the objective of data collection is to study the user behavior, the data collection process should be conducted across all board regions (continents or countries) where the product is used. If possible the monitoring process should not be known to user to avoid any kind of bias.

Table 5. Assessing product environmental and usage conditions

Environment and Usage	Possible Options
How is the product powered?	• Always ON • ON only for operation • OFF at end of day (or shift) • Auto OFF if not in use • Switches to low power mode if not in use • Doesn't matter
What is the usage rate?	• Continuously operated (e.g., production machine) • Irregular fixed number of times per day or week • Irregular and unknown
How may different users per day?	• Completely unknown (e.g., paper copier at Kinko's or clothes dryer in a commercial laundry) • Only qualified users • Doesn't matter
Average operating period per usage	• Fixed period every usage (e.g., starter motors) • Operating time varies within known intervals (e.g., electronics operating a bank ATM) • Predictable but depends on loading conditions (e.g., electronics for induction motor control) • Unpredictable operating time per usage (e.g., television, cell phone, etc.)
What are the special usage conditions if any?	• E.g., Regular battery operated products operating in low temperature environments

What does the life cycle environment comprise of?	• One time transportation, handling, installation followed by operation and maintenance in controlled environment. (e.g., electronics in machines tools) • One time transportation, handling, installation but operation and maintenance in uncontrolled environment. (e.g., telecommunication equipment in the field) • Portable and uncontrolled e.g., electronics in automobiles
What are the typical environmental extremes (temperature, humidity, radiation, altitude etc.) the product is expected to experience? (without considering usage loads)	• Controlled room or office environment • Atmospheric ambient in the region of use • More severe than atmospheric ambient (e.g., equipment used in oil well drilling)
What are the special environmental conditions unique for the product	• E.g., underwater installations, high shock loading, vacuum, etc.

4.1.4 Data Preprocessing for Model Input

The raw environmental and usage data from sensors is usually not in a form that is compatible with the required damage analysis and reliability prediction models. Hence for further analysis of the acquired data, it is essential to simplify the raw sensor data to a form compatible with the input requirements of the selected models.

Data reduction is often the first step in preprocessing and is important for reducing both data storage space and calculation time. By using information that is most relevant to the failure models, an efficient data reduction method should: 1) permit gains in computing speed and testing time, 2) condense load histories without sacrificing important damage characteristics, 3) preserve the interaction of load parameters if any, 4) provide an estimate of the error introduced by reducing and simplifying the data. Data reduction can be achieved using a variety of tools such as filters, Fourier transforms, wavelets, Hayes method, Ordered Overall Range (OOR), etc.

Subsequently the data may have to be processed to extract the relevant load parameters (such as cyclic mean, amplitudes, ramp rates, hold periods, power spectral densities, etc.) for PoF model input. In some cases the data reduction may be a part of the load parameter extraction algorithms. Commonly used load parameter extraction methods include: cycle counting algorithms for extracting cycles from time-load signal, Fast Fourier transforms (FFT) for extracting the frequency content of signals, etc. Depending on the application and type of signal, custom load extraction methods can be developed.

Embedding the data reduction and load parameter extraction algorithms with the sensor modules can lead to: reduction in on-board storage space, low power consumption, and uninterrupted data collection over longer durations.

4.2 In-situ Monitoring Case Study of Notebook Computer

The notebook computer characterized was a primarily-passively-cooled design, which incorporated a heat sink-fan assembly for managing peak transient loads. The processor, a Pentium II (233 MHz), had a worst-case power dissipation of 35 Watts, and a maximum base plate temperature rated at 75^{o}C. In such designs, the CPU heat sink fan is automatically activated when the processor base plate temperature exceeds its maximum rated temperature.

The microprocessor heat sink and Hard Disk Drive (HDD) housing were found to experience the largest absolute surface temperatures. Their surface temperatures were dynamically monitored using thin film RTD sensors calibrated to an accuracy of ±1^{o}C. **Figure 12** shows the microprocessor temperature recorded at the center of the heat sink base. Due to thermal contact resistance, the temperature drop between the heat sink base and base plate, was measured around 7^{o}C for the maximum CPU power dissipation. This was in line with the corresponding vendor specification. The HDD housing temperature was recorded at the center of its external top surface.

Measurements were recorded using an external battery powered portable data logger, having an integrated temperature sensor for external ambient air temperature measurement. The data logger had no physical interaction with the notebook computer. All data were recorded at a rate of one sample per minute. The experiments were conducted in College Park, MD, from October to December 2003.

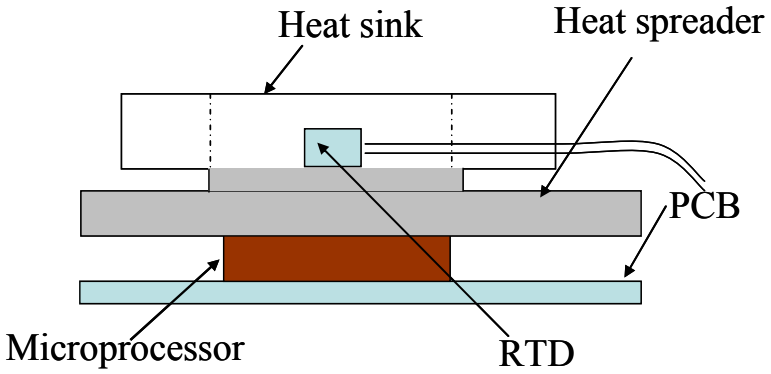

Figure 12. Location of RTD temperature sensor on CPU heat sink base

The recorded data were converted into a sequence of peaks and valleys using the Ordered Overall Range (OOR) method. The screening level was specified at 0% to include all peaks or valleys for cycle counting. The computed sequence of peaks and valleys (time-temperature history) was converted to temperature cycles that utilize the 3-parameter Rainflow cycle counting algorithm. The software calculates temperature cycle magnitude, cycle mean temperature, and cycle temperature ramp rate. The time-temperature history recorded for the CPU heat sink, HDD, and external ambient air temperature are shown in **Figure 13**. Three forms of temperature cycling are observed; that represent the notebook on-off cycles, variations in power dissipation associated with different usage intensity of the computing resources, and the external ambient air temperature variations.

The effect of computing resource usage on the CPU heat sink temperature is illustrated in **Figure 14**. As a computationally intensive numerical simulation is executed, CPU usage increases up to 80%, resulting in a 10^{o}C rise in CPU heat sink temperature. Such data can be valuable for the design of hybrid thermal management

solutions, that address peak transient thermal loads. The cooling effect of the fan on the CPU heat sink temperature is shown in **Figure 15**, where regions A-B and C-D denote the operating periods of the fan.

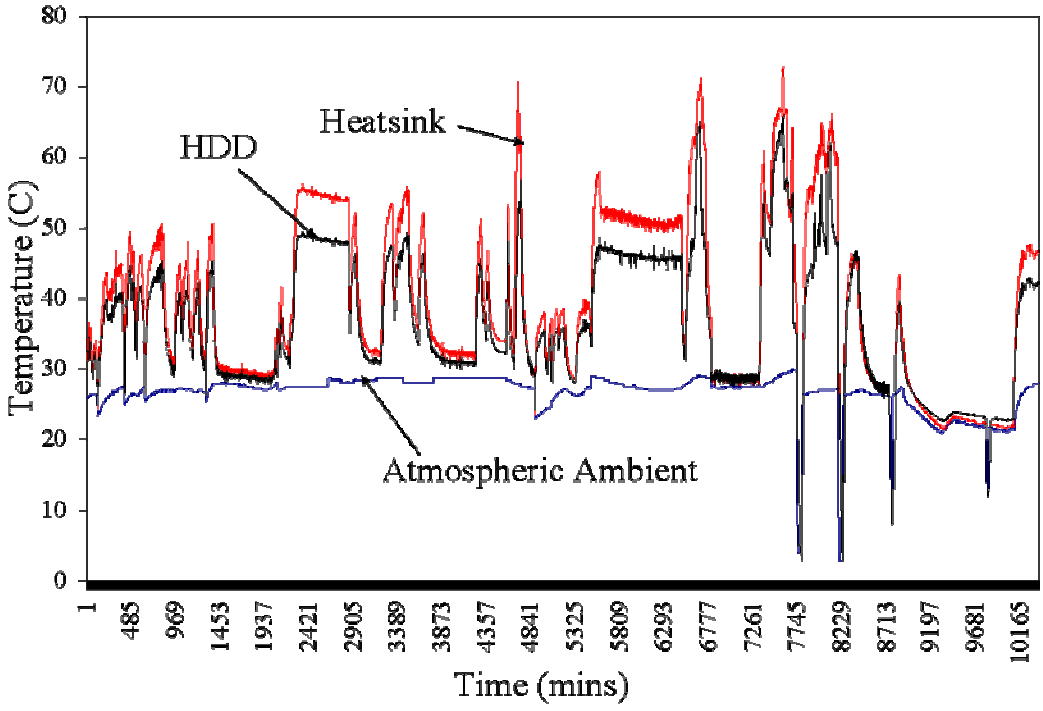

Figure 13. Measured temperature profiles of CPU heat sink, hard disk drive, and external ambient air.

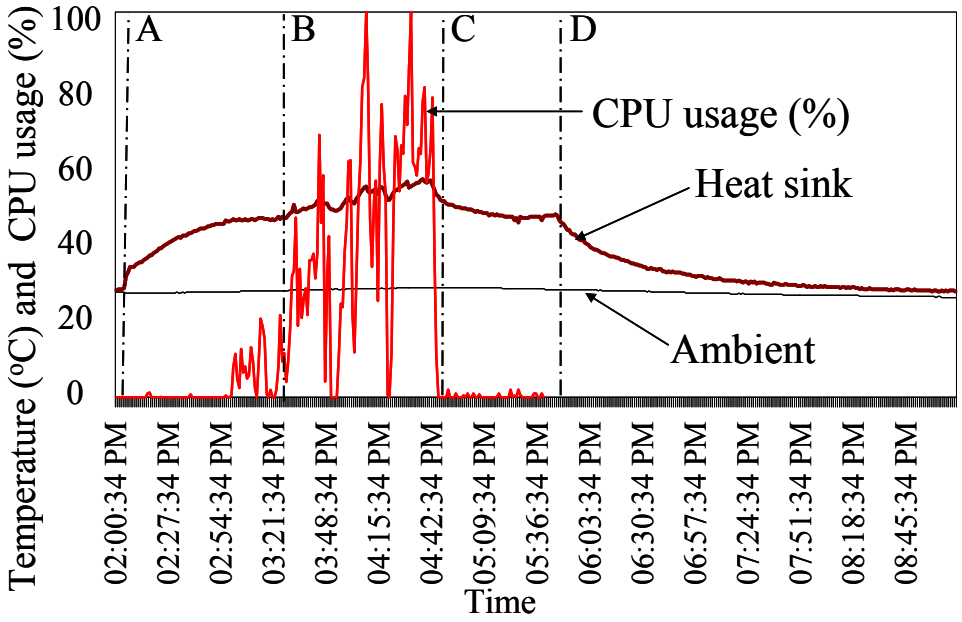

Figure 14. Measured CPU usage and CPU heat sink absolute temperature. Event A: notebook is powered on. Events B to C: numerical simulation is executed. Event D: Notebook is powered off

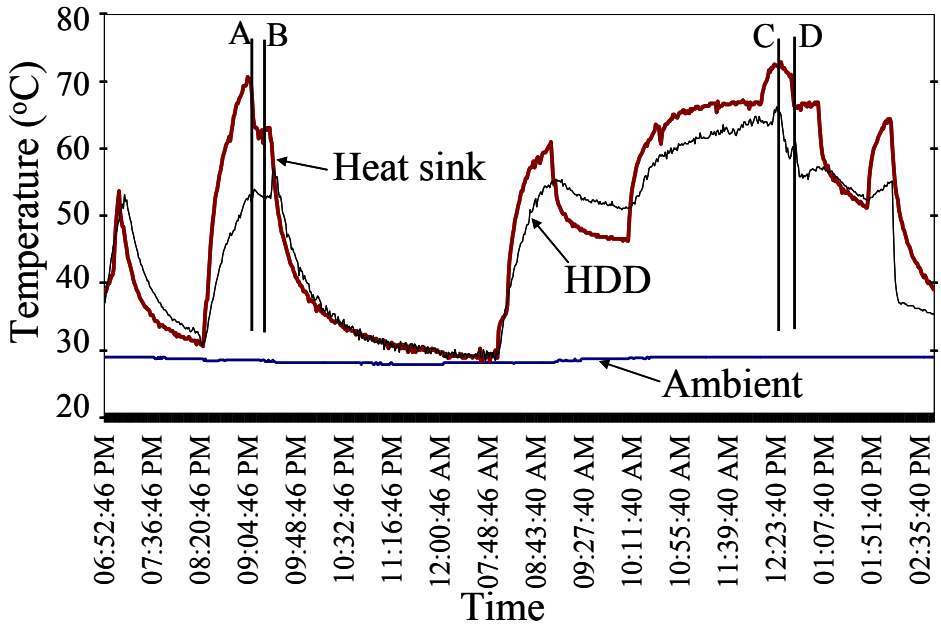

Figure 15. . Cooling fan operation in time periods A-B and C-D

The recorded temperatures presented in **Figure 13** range from 2°C, to 63°C for the HDD and 71°C for the CPU heat sink. The 2°C corresponded to the minimum external ambient air temperature recorded when the notebook was exposed to outdoor environments. The product usage profile observed in **Figure 13** is characterized by a large number of on-off cycles, relative to typical desktop computer usage, as well as temperature cycles of larger magnitude. The latter observation is attributed to exposure to large variations in external ambient temperature, covering both indoor and outdoor environments.

Using the data simplification methodology summarized in previous section, the distributions of absolute temperatures, temperature cycle magnitudes, and temperature ramp rates for both the CPU heat sink and HDD were extracted from the measurements in **Figure 13**. These analyses are presented in **Figure 16** to 18. **Figure 16** shows the fraction of total time during which the product experienced a given range of absolute temperature. **Figure 17** represents the number of occurrences of a range of temperature cycle magnitudes. **Figure 18** provides the fraction of total time during which the product experienced a given range of temperature ramp rate.

Figure 16 shows that the CPU heat sink base temperature exceeds its maximum rating, 68°C, over approximately 1% of the monitored time period. This may be due to the fact that the fan was not accurately synchronized with the CPU base plate temperature in the system design. However, the heat sink temperature does not exceed 55°C and 60°C over 90% and 95% of the time. This highlights the

potential conservativeness of thermal management solutions optimized based on worst-case operating conditions, 68°C.

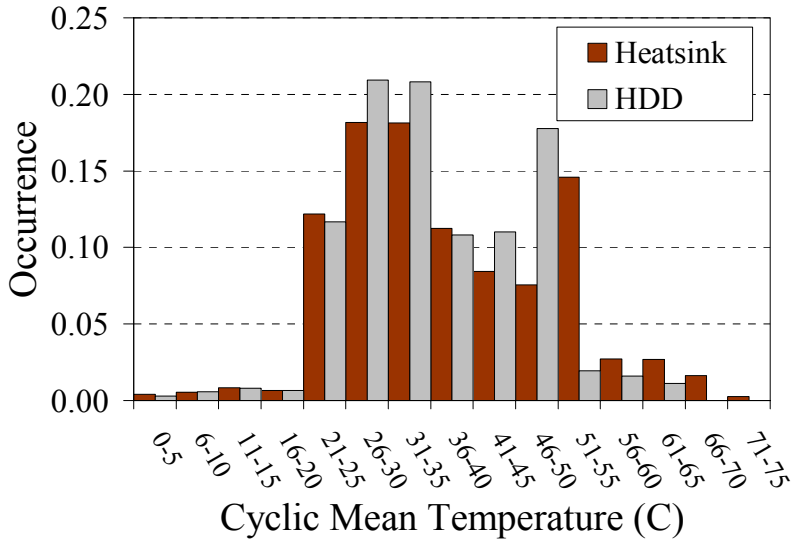

Figure 16. Distributions of measured absolute temperature for the CPU heat sink and hard disk drive

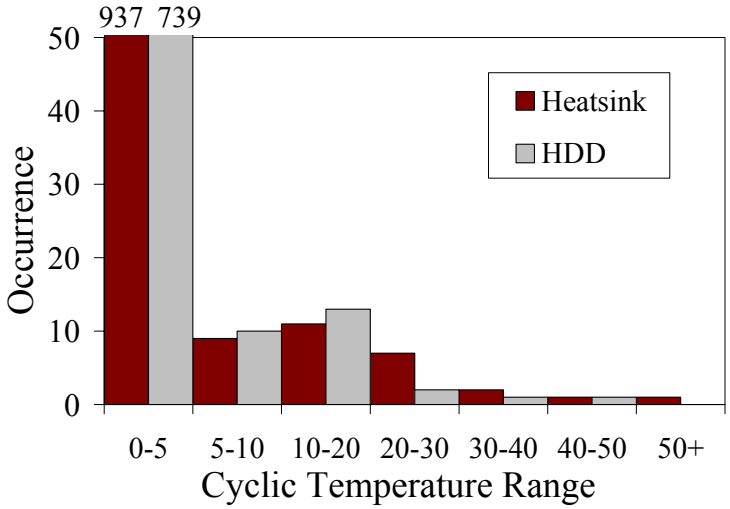

Figure 17. Occurrence of CPU heat sink and hard disk drive temperature cycles as a function of cycle magnitude.

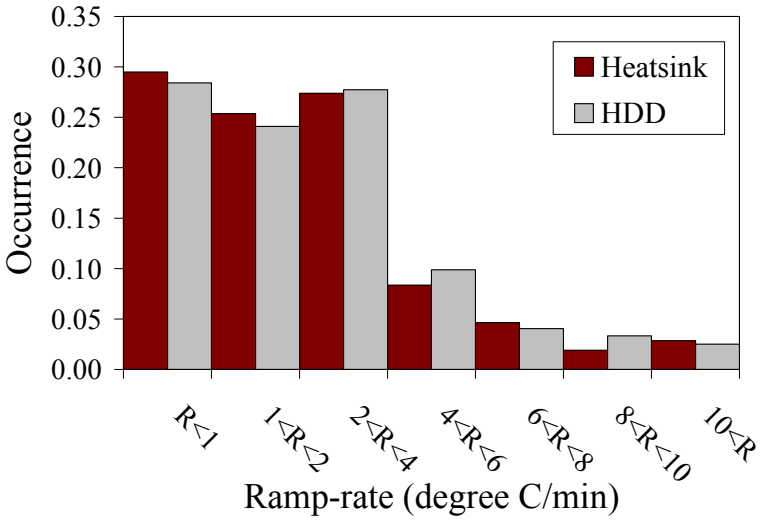

Figure 18. Distribution of measured temperature cycle ramp rates for the CPU heat sink and hard disk drive. R refers to temperature cycle ramp rate

Figure 17 indicates that about 97% of the temperature cycles experienced by either the CPU heat sink or HDD have amplitude of less than 5°C. In addition, the CPU heat sink experiences about 25% more such cycles than the HDD. While it is generally perceived that temperature cycles of small amplitude may not significantly impact on the reliability of electronic packaging interconnections, the potential damage induced also depends on variables such as the mean cyclic temperature, ramp rate, and dwell temperature, as highlighted by [118], [119] for solder joint fatigue. Pump-out of the thermally-conductive grease at CPU-heat sink interfaces, which lead to increased interface thermal resistance, has been attributed to temperature cycling having an amplitude comparable to those measured in this study, around 5°C [120]. The monitored temperature data therefore suggests that the effect of such multiple mini-cycles on interconnection reliability should be further investigated for the range of measured mean cyclic temperatures and ramp rates. This highlights the importance of recording such data. On the other extreme, temperature cycle

magnitudes of up to 50°C were also measured (see **Figure 17**). This exceeds the worst-case use condition specified by standard IPC SM-785 [71] for consumer and computer products, namely 30°C and 20°C respectively. Such a discrepancy between standardized and actual conditions provides a strong motivation for monitoring actual product application environments.

The measured temperature ramp rate distribution shown in **Figure 18** would also permit more accurate predictions of solder joint fatigue life to be obtained than using worst-case ramp rate specifications [71]. For example, **Figure 18** shows that over 80% of the total time period, the temperature cycles experienced by the CPU heat sink have a ramp rate of less that 4°C/min, while temperature ramp rates exceeding 10°C/min are observed over less than 3% of the total time.

Monitored life cycle temperature data, such as presented in **Figure 16** to 18, could be applied in a life consumption monitoring methodology, to provide both damage estimation and remaining life prediction due to specific failure mechanisms influenced by temperature. For example, measured heat sink base temperature data could be used to assess the reliability of component-to-heat sink adhesive attachments. Examples include [72], [73], [74] and [75], which evaluated the impact of differential thermal expansion and creep-induced degradation on component-heat sink adhesive joints, respectively. The measured data could also be used to determine the stress levels to be imposed in accelerated testing, refining product specifications, and setting product warranties.

While a comprehensive health monitoring process would involve other environmental variables, such as humidity, vibration and shock, apart from temperature, a line of approach similar to that presented in this study could be applied to monitor such life cycle loads. Similarly, the proposed approach could be extended to other electronic products. A list of variables (not exhaustive) for monitoring the entire laptop is proposed in Table 6.

Table 6. Environmental, usage and performance parameters for PHM of notebook computers

Parameters	Examples
Environmental and Usage	- Temperatures of microprocessor, hard disk drive, video card, RAM etc. - Vibrations/shock in application and handling, disk spin - Processor usage, memory usage, processor queue length, Cache fast reads/second etc. - Power cycles, number of on/off - Hard disk and monitor on/off - Strain in mother board flexing and torsion during handling and due to ageing - Pressure on keyboard and buttons - Force on latch, hinge, and connectors - Humidity and radiation exposure
Performance and system setup	- Fan ON/OFF, Fan speed - CPU core voltage, CPU I/O voltage - Hard disk parameters: spin-up time, flying head height, ECC count, data transfer rate - Power management settings (power schemes, hibernate, and stand-by settings)

4.3 Conclusions

A method of environmental, operational and usage data collection for enabling health monitoring of electronic products was presented. To implement this methodology in a real system, guidelines were provided on the selection of monitoring parameters and the design of a monitoring plan. An integrated hardware-software module was suggested for in-situ monitoring and processing of load data in the life cycle environment. The main attributes for selecting the sensor system for these applications were identified to be the level of integration, power consumption and management, on-board memory and utilization, low size and weight, wireless communication, embedded computational power, and software support. Methods to improve the efficiency of the data collection process by reducing power consumption, by making effective use of memory, and by integrating embedded computational power with sensor systems were discussed. Using field data the trade-off between data reduction and error in damage accumulation was demonstrated. The analysis showed that more than ninety percent data reduction only accounted for less than one percent error in damage accumulation.

The thermal loads in a notebook computer were dynamically monitored in-situ for typical usage, transportation and storage environments, and statistically analyzed. The effects of power cycles, usage history, CPU computing resources usage and external thermal environment on internal peak transient thermal loads were characterized.

The CPU heat sink temperature was found to be 13°C and 8°C lower than its maximum rating over 90% and 95% of the monitored time period, respectively. This highlights the potential conservativeness of thermal management solutions optimized based on worst-case operating conditions that rarely occur. Such findings could contribute to the design of more sustainable, least-energy consumption thermal management solutions.

About 97% of the temperature cycles experienced by either the CPU heat sink or HDD had amplitude of less than 5°C. However, the maximum temperature cycle amplitudes measured were found to exceed those specified by environmental standards for computer and consumer equipment. This provides a strong motivation for monitoring actual product application environments.

Chapter 5: Methodology for Extracting Load Parameters from Time-Load Signals

5.0 Introduction

This paper presents a novel method for processing the in-situ monitored load data to enable prognostic assessment of electronic products and systems. The proposed method processes the time-domain sensor data to extract load parameters including cyclic ranges, mean load, ramp-rates, and dwell times. The load parameters and their correlations are then used in conjunction with damage models for assessing and predicting the health due to commonly observed failure mechanisms in electronics. An algorithm was developed that enables significant reduction of large irregular time-load data without compromising load parameters essential for damage estimation and enables compact storage of load histories. The approach was demonstrated using a case-study of an electronic board subjected to irregular temperature cycles. The methodology can be used for processing other load signals in time domain including strain, humidity, voltage etc.

5.1 Review of Existing Load Parameter Extraction Methods

Several methods have been developed and reported that can extract parameters from time-load data [76-86]. Currently available methods are briefly discussed in Table 7. A cycle is defined when the time-load signal crosses it previous

peak or valley before changing its direction. In **Figure 19** b-c-b' is a complete cycle, while a-b-d is a half cycle.

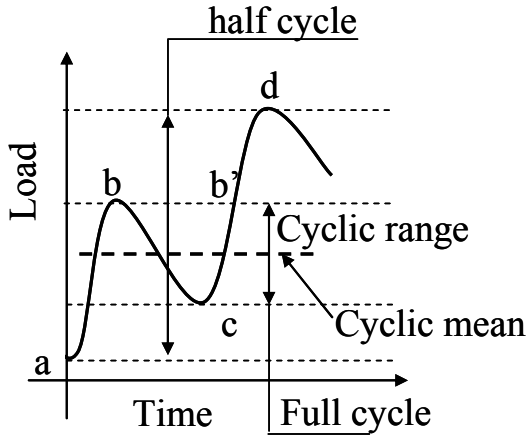

Figure 19. Geometric definition of a cycle

Table 7. Review of existing load parameter extraction methods

Load Extraction Method	Description
Hayes Method	Hayes' method identifies small ranges, which are interruptions of a larger range. An interruption is found for a peak-valley pair when the next peak is higher than the current peak. An interruption is found for a valley-peak pair when the next valley is lower than the current valley. Once damage is calculated for these cycles, they are screened out of the original block of data, producing the abbreviated blocks. The procedure is repeated to cover all blocks.
Ordered Overall Range	The OOR method (also called the Racetrack method) converts irregular data in sequence of peaks and valleys. The sequence of reversals in the original profile into a racetrack by offsetting the profile by a selected track width or screening level (S). Peaks and valleys that were originally separated by smaller interrupting ranges now become adjacent, creating larger overall ranges.
Level Crossing	In this method a count is recorded whenever an increasing

Counting	(positively sloped) portions of the load history crosses a certain level above the reference level. Likewise, a count is recorded when a decreasing (negatively sloped) portion of the load history crosses a certain level above the reference level. Cycles are constructed by counting in an order to form most damaging reversals.
Peak Counting	Peak counting records relative maxima and minima in the load history and their load levels. Generally only peaks and valleys above and below set reference levels are counted. Similar to level crossing the most damaging cycle is recorded between the largest peak and valley.
Simple-Range Counting	Simple range refers to the difference in the load levels of the successive reversals. Both positive and negative slopes can be counted. The method can be non-conservative and miss an overall large cycle.
Range-Pair Counting	In range pair counting, two subsequent ranges of opposite sign are considered together. If the second range is greater than or equal to the first range in size, the first range is counted, and the peak and valley are removed from consideration. If the second range is smaller then the next range is considered, and so on.
Rainflow Counting	In Rainflow counting two consecutive ranges are considered together. Based on a set of rules the algorithm scans the entire time-load history to identify full cycle and half cycles. The Rainflow method provides the mean stress in addition to the stress range during counting.

5.2 Limitations of Existing Methods

The limitations with existing load extraction methods for application in electronic prognostics and health assessment include (1) inability to extract ramp

rates and dwell time, (2) need for smart data reduction and filtering techniques, and (3) need for assessing correlation of load parameters, are discussed below.

5.2.1 Extracting ramp rates and dwell information

The existing load extraction methods provide the load range and mean load. These parameters can be adequate parameters for fatigue life estimation in elastic-plastic fatigue analysis of materials. However, for example, in case of thermal-fatigue loads (frequently observed in electronic systems), wherein the damage is characterized by plastic yielding and creep deformations, the estimation of dwell time and ramp rates is required in addition to the stress range and mean stress for accurate fatigue assessment. Ramp rates can be estimated with modifications in the Rainflow algorithm. However, extracting dwell times and corresponding load levels is more challenging since it depends on both the amplitude and ramp rate of the monitored load cycles.

Along with electronic applications, dwell times are also crucial in estimating fatigue life of other components. For examples of fan disk failures have been reported due to dwell sensitivity [87]. Hold periods of few minutes to several hours are applied in gas turbines [87], [88] and for weeks or more for power plant components that affect the remaining life of components. Other examples of applications were components are affected by creep-fatigue data are; electronic packaging, space shuttle nozzle liners, power plant components, gas turbine nozzles [89], furnace tubes [90].

Various materials that have been studied and have shown dwell sensitivity: solder alloys (96.5% Pb-3.5% Sn) and other solders commonly used in PCB assembly, copper alloy (NARloy and AMZIRC), low alloy steels (1-Cr-Mo-V, 1.25 Cr – Mo, and 2.25Cr-Mo), stainless steel (SS 316), titanium alloys (IMI 318 and IMI 829), and super-alloys (MAR M 002, waspaloy, Rene 95, Rene 90, inconel 617, In 100, PWA 1480 and MA 754) [91], [92].

5.2.2 Concerns with data reduction

Analysis of complex load histories typically involves a data reduction stage to enable efficient data processing and eliminating undesired load reversals. However, data reduction methods can eliminate important load information and avoid the extraction of certain loading parameters in subsequent stages. For example the Ordered Overall Range (OOR) can eliminate small cycles (as a fraction of large cycles) by choosing an appropriate value of S-parameter ($S < 1$). However, in the process it also deletes the dwell-time information. In **Figure 20**, the points and lines in light shade depict the original data before reduction. The dark line connecting the end points depicts the results obtained after OOR. The load information of 0.2 hours of dwell time at 60^{o}C is important for assessing damage due to creep mechanisms at various locations on the electronic assembly such as solder joints, plated through holes, and die-attaches.

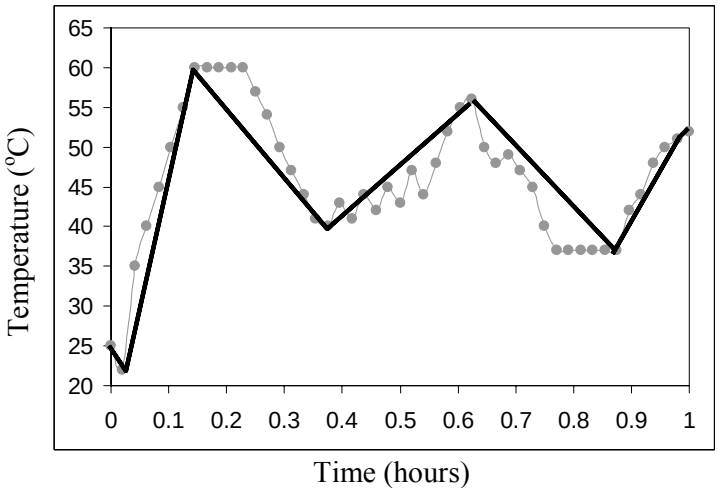

Figure 20. Data reduction methods can potentially eliminate dwell regions

5.2.3 Correlation of load parameters

Distributions of in-situ monitored temperature load parameters can be randomly sampled and used with the damage model in a Monte Carlo simulation. For accurate damage assessment the correlation between load parameters is important. Quantifying and using the correlations for damage assessment, enables generating realistic scenarios during random sampling. For example, the distributions of measured ΔT and T_{mean} can be used for assessing the solder joint damage due to cyclic thermal loading. However, it is essential to know the correlation between these two parameters, as cycles with small ΔT but higher T_{mean} values will cause more damage than the cycles with same ΔT values but lower T_{mean}.

5.3 Methodology for Load Extraction

An algorithm was developed to process a given a time (t) versus temperature (T) signal, to extract cyclic range ΔT, cyclic mean temperatures (Tmean), ramp rate (dT/dt) , dwell time t_D and temperature of dwell. Additionally, the correlation

between, dwell times versus temperature of dwell, cyclic range versus mean temperatures, and cyclic range versus ramp rates are quantified in terms of correlation coefficient. These load parameters can then be used in conjunction with damage models in Table 4 to assess the damage at various failure sites due to different failure mechanisms for a given electronic assembly. The entire process is implemented in a software program, which contains the details of the electronic board and component material properties and geometries, to enable rapid assessment.

The algorithm starts by processing the irregular time-load data using a moving average filter to remove the noise.

$$s'(t) = \frac{1}{a} \sum_{n}^{n+(a-1)} s(t)$$

In the above equation 'a' is the smoothening parameter. For the moving average to reduce the random noise while retaining the sharp response, the value of smoothening parameter 'a' is selected as the nearest integer of the square root of sampling frequency in Hz.

$$a = INT\left(\sqrt{fhz}\right)$$

Typically a filter with a smoothing factor derived from above equation has been reported to provide adequate noise reduction for various signal types without changing the original signal (**Figure 21**).

In the next step small ranges are merged into overall increasing, decreasing, or dwell data streams. A range threshold value is selected to merge small ranges. All

ranges in the given data set that are less than delta s are merged in the larger overall range. An optimal range threshold value enables efficient load data reduction method, permits gains in computing speed, condenses load histories without sacrificing important damage characteristics and preserves the most damaging reversals in the original loading

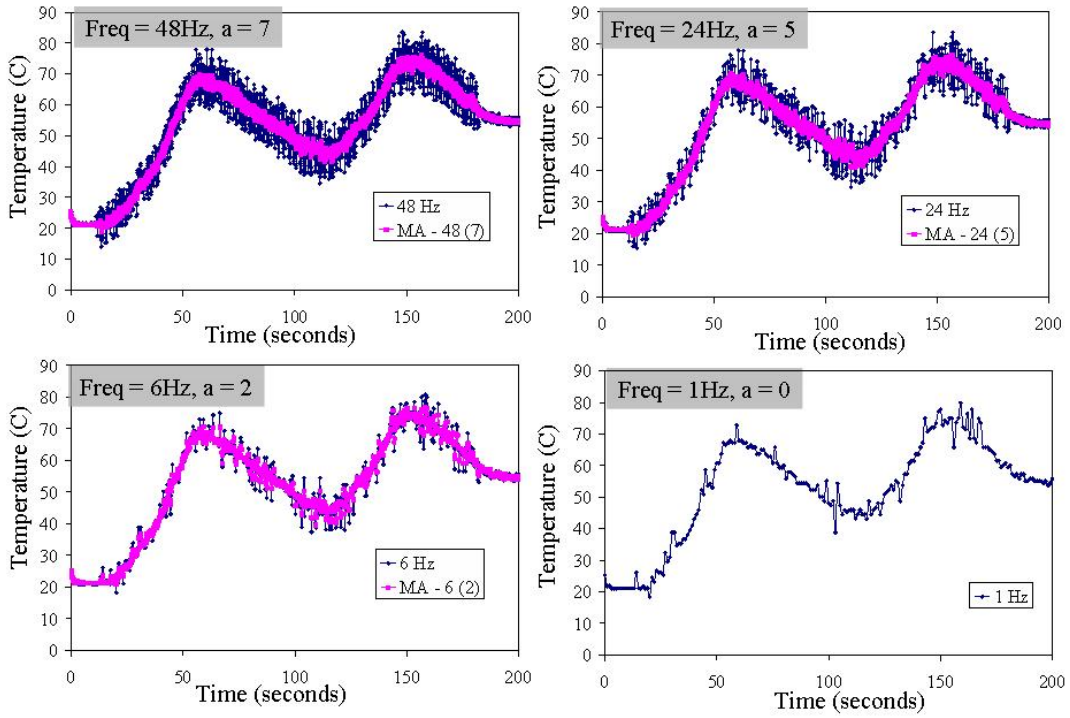

Figure 21. Results of MA filter with different smoothening parameter based sampling frequency

Range threshold value is based on the significance of the range in the damage model. For e.g., If, Damage α $(\Delta T)^n$, then for all n > 1, threshold range can be selected as the n^{th} root of the maximum ΔT measured i.e., = $(\Delta Tmax/2)^{(1/n)}$. For damage models with n between 0 and 1, the threshold range value = $(\Delta Tmax/2)^{(0.75)}$ can eliminate small cycles without introducing significant errors in the damage estimations (**Figure 22**).

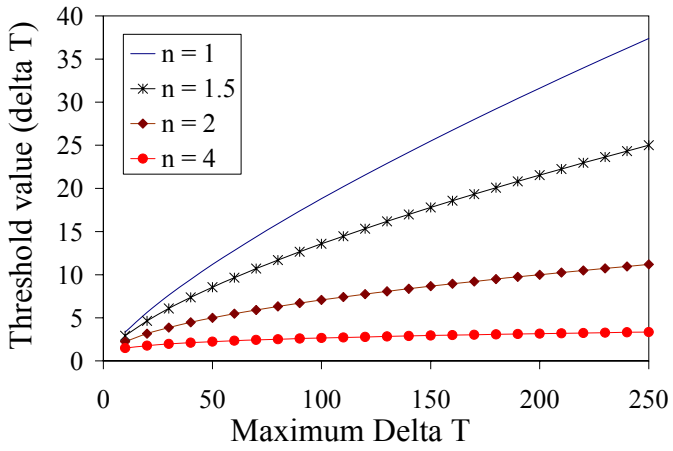

Figure 22. Threshold level increases as value of power in damage law (n) decreases

In case of measured field data it can be challenging to identify dwell temperature regions. This is because dwell regions may appear as a series of small cycles with a constant or near constant mean (**Figure 23**c), or it can also appear as a relatively large cycle with an extremely slow ramp rate (**Figure 23**c). For example, if the range threshold is ΔT less than $5^{o}C$, then several consecutive cycles with $\Delta T < 5^{o}C$ is considered dwell. However, a cycle with say, $\Delta T = 10^{o}C$ but a slower ramp-rate is also considered as dwell. Based on these criteria, the algorithm scans the time-temperature data and identifies the dwell temperatures and dwell times.

The correlation coefficient between dwell time and dwell temperatures is calculated and stored. The actual values of dwell time and dwell temperatures are then stored in a histogram with optimal bin-widths. The bin-data is used with kernel functions to estimate the probability density of the measured values. This method enables enormous on-board storage reduction and improves the ability of the sensor module to monitor for longer time durations. The significance of optimal binning and density estimation will be discussed in section 5.6.

The time-temperature data is then scanned for identifying full cycles. The geometric definitions of full and half cycle are well documented [80]. The time-temperature data is scanned to identify if ΔT_i is a full cycle based on the condition $\Delta T_{i-1} > \Delta T_i \leq \Delta T_{i+1}$ (**Figure 23**d). For each cycle the mean temperature and ramp-rate is recorded. The full cycle is then removed from the stream and the residual time-temperature containing half cycles is data is merged with original time stamp being retained. The process is iterated till all full cycles are identified and stored in the appending matrix. The remaining half cycles are then converted into full cycles. At the end of cycle counting the correlations between temperature range versus mean temperatures, and temperature range versus ramp rate are assessed and recorded. The load parameter values are then stored in histogram with optimal bins as described previously. The entire procedure for load parameter extraction is shown in Appendix I. The on-board memory is cleared by deleting the matrix containing the load parameters and only the histograms and correlation values are retained.

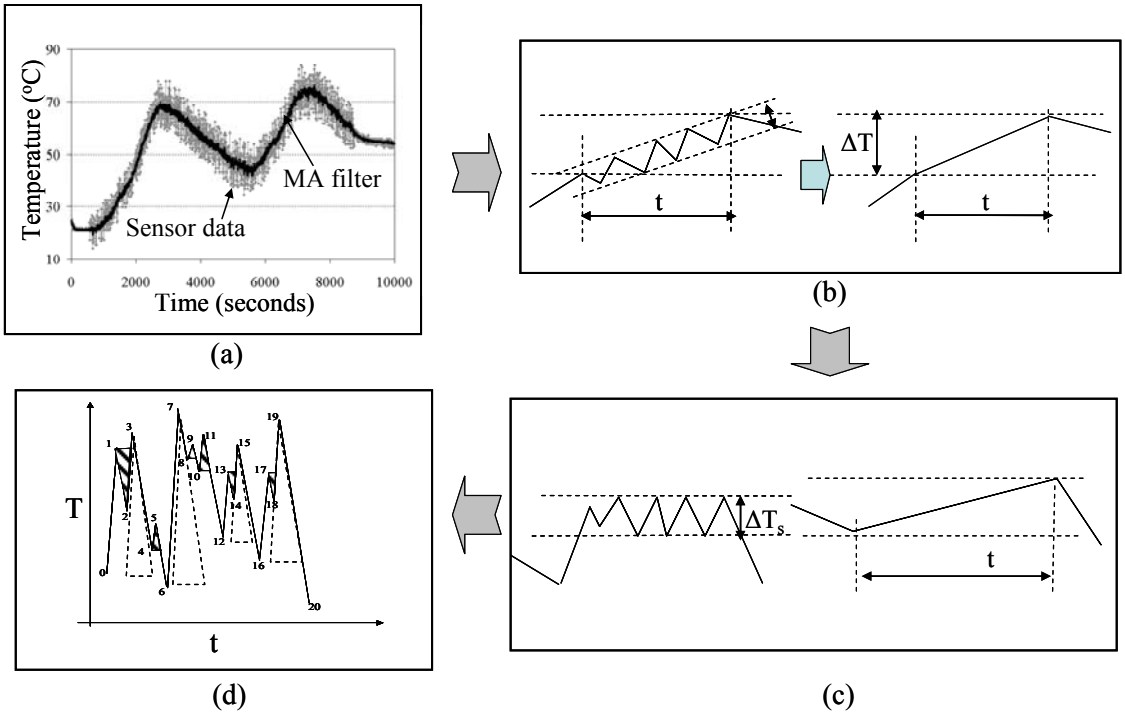

Figure 23. (a) Reduces noise using moving average filter (b) Eliminates monotonic data patterns and merges small ranges into overall data streams (c) Identifies dwells temperatures and time using ramp-rate and range (d) Scans the time-temperature data to extract cyclic load parameters

5.4 Demonstration

The proposed load parameter extraction method was first tested using simple data sets. Various time-temperature data series were generated to evaluate the ability of the algorithm to correctly identify dwell regions based on small cycles and ramp-rates. For the cycle counting part, the algorithm is primarily based on the proven and tested Rainflow cycle counting method, and hence additional rigorous testing was not required.

The application of the proposed method was then demonstrated for electronic prognostics by processing in-situ monitored temperature data. An electronic assembly was exposed to irregular temperature cycles using a programmable oven to simulate field conditions. The irregular profile was generated produce temperature cycles with a different ranges, means, ramp-rates, and dwell times. Temperature extremes ranged from -50^{o}C to 160^{o}C and dwell times were randomly selected as multiples of five between 0 to 30 minutes. Also long dwell times were recorded at room temperatures when the oven was shut-down to simulate non-operating conditions. A snapshot of 20 days of temperature exposure out of 110 days is shown in **Figure 7**.

The time-temperature data was processed using the steps shown in **Figure 23** and Appendix-I that were implemented in a visual basic for applications environment. The resulting distribution of cyclic temperature ranges, means, ramp rates, and dwell times is shown in Figure 22-25. The histogram of dwell times shows that the algorithm correctly identified the dwell regions that were programmed between 0 to 30 minutes (**Figure 26**). Also, the longer temperature dwell periods (> 160 minutes) programmed to represent the non-operating periods were correctly identified.

The correlation between the load parameters is shown in Figure 26-28. From **Figure 27** shows that the occurrence of the longer temperature dwell corresponds to temperatures in the range of 25-27^{o}C. The correlation coefficients (ρ) of -0.84 shows an inverse correlation, i.e., a low value from dwell time distribution corresponds to high value in dwell temperature distribution and vice versa. The use of these

correlations in Monte Carlo simulation for damage assessment will be discussed in the next chapter.

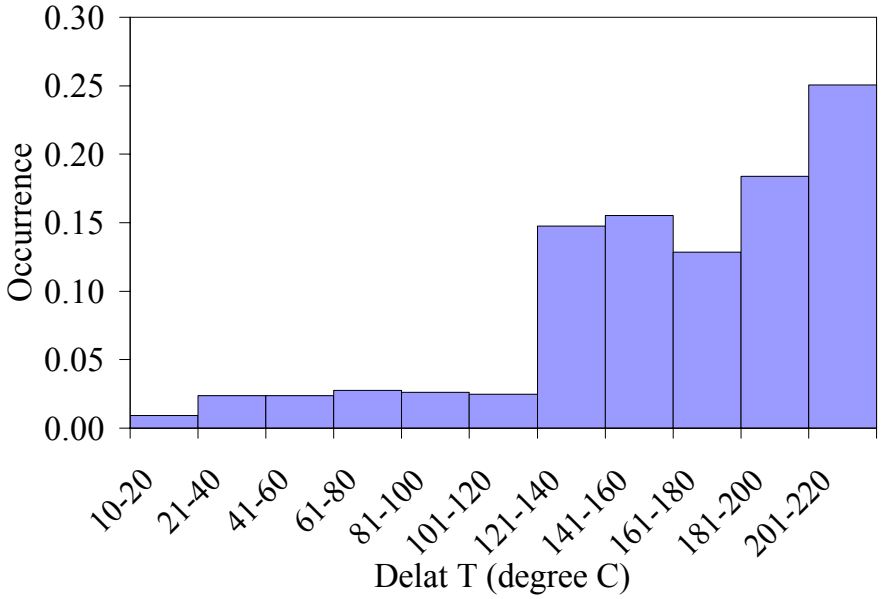

Figure 24. Histogram of cyclic range

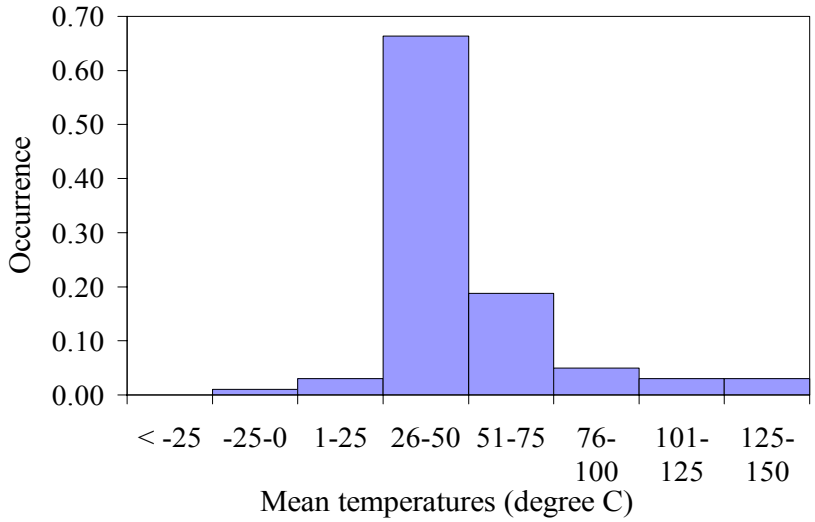

Figure 25. Histogram of cyclic mean temperatures

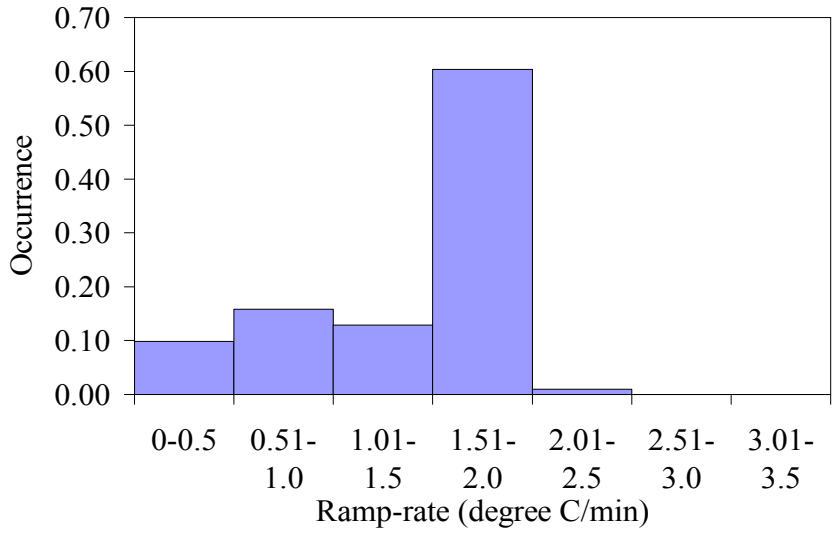

Figure 26. Histogram of ramp-rates

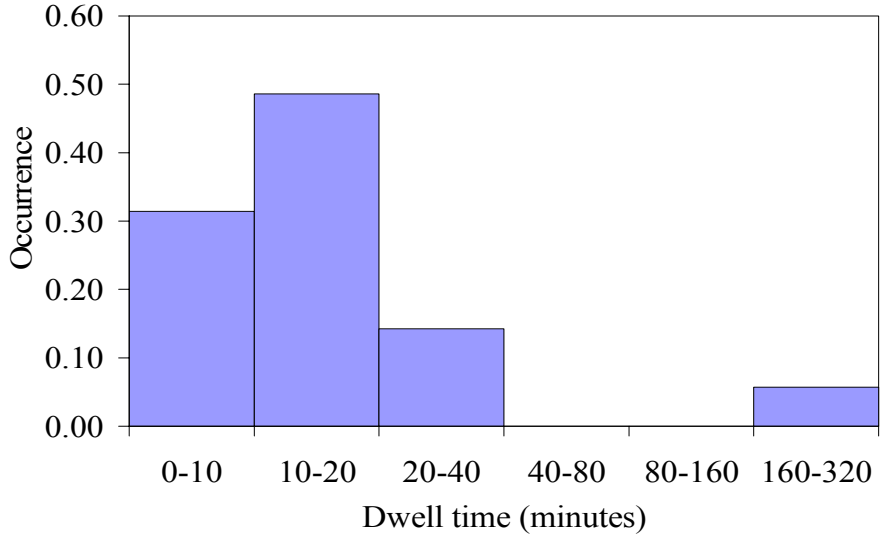

Figure 27. Histogram of temperature dwell times

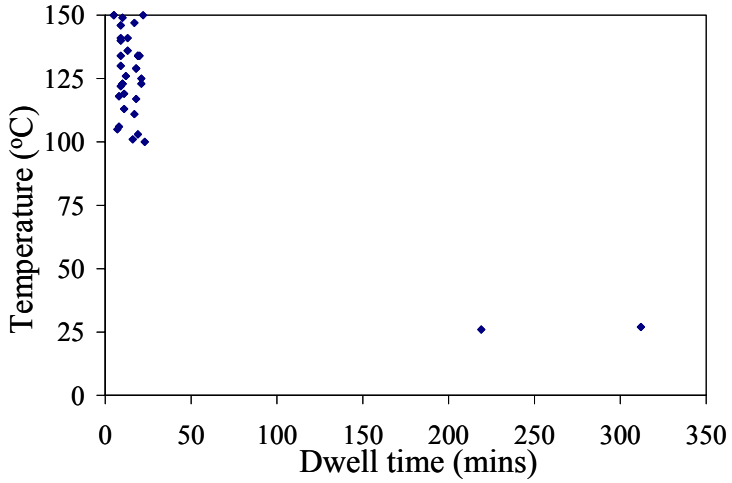

Figure 28. Correlation between dwell time and temperature

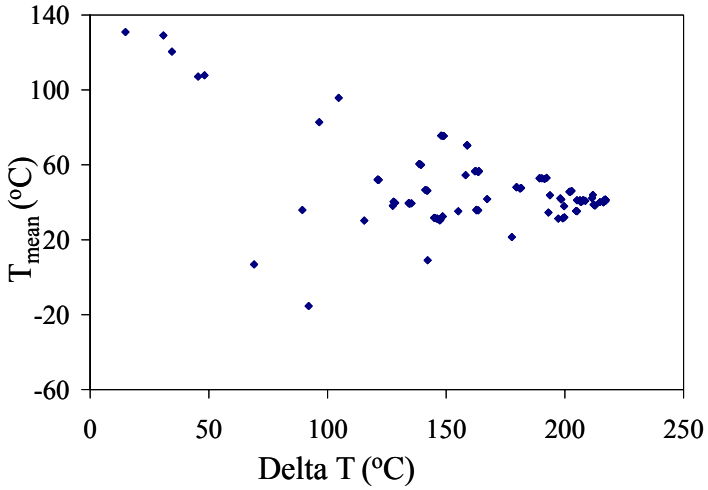

Figure 29. Correlation between delta T and mean temperatures

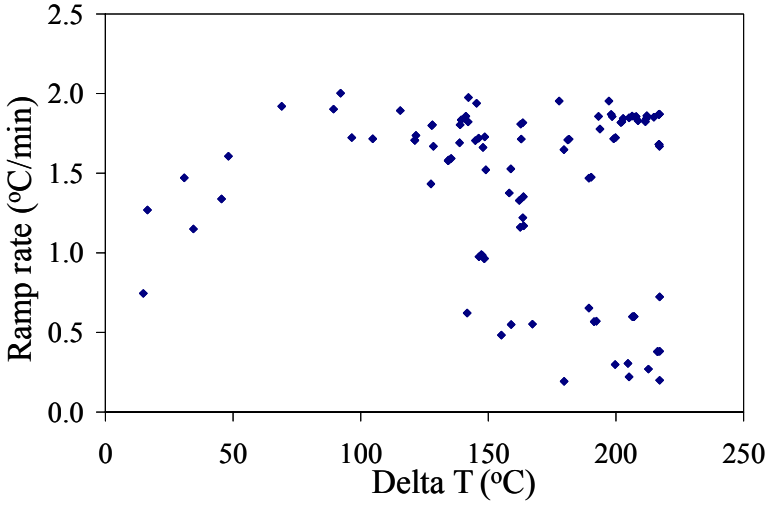

Figure 30. Correlation between delta T and ramp-rate

5.5 Method for Binning and Density Estimation

The extracted load parameters are stored in appropriate bins to achieve further data reduction. The binned data is downloaded to estimate the distributions of the load parameters for use in damage assessment, remaining life estimation, and the accumulation of the products use history. Since the accuracy of the damage assessment and remaining life prognostics depend on the accurate estimate of the probability density functions (pdf) of the loads derived from the binned data, it is essential to select the appropriate bin-width and number of bins a-priori.

This paper provides a method for applying optimal binning techniques for enabling condensed storage of in-situ monitored load histories. Optimal bin-widths relations are used in conjunction with non-parametric density estimation techniques, namely the histograms and kernels. The approach is then demonstrated.

5.5.1 Optimal Binning and Density Estimation

If the entire data set, without data binning, is retained, a parametric method can be used for density estimation. In that case the objective is to find a best fitting parametric function to the given data. Standard parametric functions include normal, lognormal, exponential, and Weibull, described by parameters such as mean and standard deviation. If the underlying distribution is non-standard (e.g., multi-modal), fitting a single standard parametric function to the data can result in errors, and fitting multiple parametric functions can make the problem solution non-unique. Non-parametric methods can be used to estimate the pdf without assuming any parametric

structure [93], [94]. Examples of non-parametric density estimation methods include histograms, Kernels, orthogonal series estimation, and nearest neighbor method. In our study, histograms and kernel estimators were used.

Histograms

A histogram is a graphical representation of a frequency distribution in which the height of the bins represents the observed frequencies. The choice of bin-width primarily controls the representation of the actual data. Smaller bin-widths may present too much details (undersmoothing) and larger bin-widths may present or too less details (oversmoothing), of the true distribution [93]. Histograms are based on an equally spaced bin-width hn where n denotes the sample size. If $\hat{f}(x)$ is the estimate of the true density f(x), then the global accuracy of the estimate can be evaluated by the integrated mean square error that is defined by.

$$IMSE = \int E\left[\hat{f}(x) - f(x)\right]^2 dx \tag{1}$$

The IMSE is the sum of the integrated square bias and integrated variance, the bias being the difference between the true density and the estimate. The bin-width that minimizes the IMSE is required for accurate estimation of the true pdf *f*(x). Scott, [95], derived the asymptotically optimal choice of bin width, h_n^* as;

$$h_n^* = \left(6^{1/3} \left(\int_{-\infty}^{\infty} f'(x)^2 \, dx \right)^{-1/3} \right) n^{-1/3} \tag{2}$$

Since h_n^* depends on the unknown pdf f(x), an estimate $\hat{f}(x)$ of f(x) can be plugged into equation 2. For the normal distribution, the approximate optimal bin-width is;

$$h_n^* = 3.49 s n^{-1/3} \tag{3}$$

where s is the sample standard deviation and n is the sample size. Freedman and Diaconis [96] suggested another bin width formula that can be applied to non-Gaussian data;

$$h_n^* = 2(IQR)n^{-1/3} \tag{4}$$

where IQR is the inter-quartile range of the data (Q3-Q1). Several other studies have focused on more quantitative and qualitative aspects of bin width selection [96]–[100]. Once the bin width is calculated, the histogram is defined as;

$$\hat{f}(x) = \frac{1}{nh} \quad \text{(number of } x_i \text{ in the same bin as x)} \tag{5}$$

Kernel Estimators

Kernel density estimators [101] are non-parametric methods used to estimate f(x) using the kernel estimator K (also called a window function) defined as;

$$\hat{f}_h(x) = \frac{1}{nh} \sum_{j=1}^{n} K\left(\frac{x - x_j}{h} \right) \tag{6}$$

where h is the bin width, also called as smoothing parameter or band width. Equation 6 can be considered as a pdf obtained by averaging the effect of a set of local functions K centered at each data point x. A variety of kernel functions with different mathematical properties have been reported [102]-[106]. Commonly used kernel functions include uniform, Gaussian, triangle, Epanechnikov, and biweight. Kernel functions are generally chosen based on the ease of computation and desired properties of the function. For example, the Gaussian kernel is used for its continuity and differentiability. The optimal bin width for the Gaussian kernel (equation 7) is obtained by minimizing the integrated mean square error (equation 8).

$$K(x) = (2\pi)^{-1/2} e^{-x^2/2} \tag{7}$$

$$h^{opt} = 1.06\hat{s}n^{-1/5} \tag{8}$$

where $\hat{s}$ is the estimate of standard deviation. The Gaussian kernel can be used for non-Gaussian data, since the kernel is used only as a local weighting function [94].

5.5.2 Implementation Approach for PHM

For in-situ monitoring over long durations, one can use the load measurements obtained in the past or the data monitored over initial few periods to obtain the estimate of sample size and standard deviation. The relations provided in equation (3) and (7) are then used for bin width calculations. Once the bin-widths are calculated, the data for the subsequent time periods is stored directly in the bins. At the end of the monitoring period, the bin-widths and frequency is used in conjunction with equations (5) and (6) to obtain the probability distributions. These distributions are then used for damage assessment and prognostics (see **Figure 31**).

The load parameters obtained during monitoring depend on the usage and environmental conditions during the monitoring period. Thus, depending on usage conditions, there could be differences between the estimated and actual values of sample size and standard deviation. These differences can lead to inaccuracies in the subsequent density estimation process. One approach to overcome this problem is by recording the actual values of standard deviation and sample size during monitoring

and using these values for density estimation. One can update the value of standard deviation every time a data point is added to the bins and also keep a track on the sample size. The advantage of continuously updating the standard deviation is that it does not require storing the complete data set. Optimal bin-widths can then be recalculated based on actual values of sample size and standard deviation to estimate the probability distribution (see **Figure 31**).

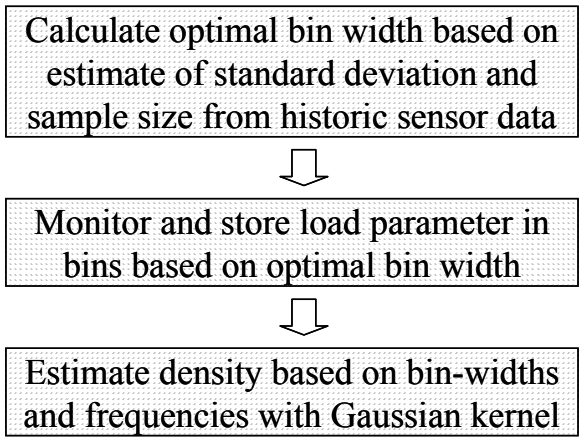

Figure 31. Approach for binning and density estimation of monitored load parameters

5.5.3 Results

The rest of the discussion will focus only on binning and density estimation of cyclic T_{mean}, values extracted using methods discussed in section 5.3. The same procedure used for binning and density estimation of all other load parameters. For the first five days of the experiment, the cyclic T_{mean} data was extracted and stored without any binning. The average samples size (n), standard deviation (s), and inter-quartile range (IQR) for each load parameter was then calculated (see Table 8). These values were used as estimates of s, n, and IQR in equations (3), (4), and (7) to calculate the optimal bin widths for both histograms and kernels. For the histograms,

the optimal bin widths obtained from equations (3) and (4) were within +/- 5%. This is in agreement with results reported in the literature [96].

After the fifth day, the load parameters were extracted and stored in the bins calculated from the five day estimate. The bin frequencies were downloaded and distributions of load parameters were derived using histograms (see equation 5) and kernel functions (see equation 6). The percentage of data reduction due to use of the bins was measured. The ability of histograms and kernel functions (using binned data) to represent the complete data set was assessed by comparing the histograms and kernel plots with the parametric distributions that were best fitted to the complete data set.

Table 8. Estimate of parameters used for the bin width calculation

Day	Sample size (n)	Inter-quartile range (IQR)	Standard deviation (s)
1	97	110.77	59.10
2	80	131.20	66.70
3	72	101.81	60.94
4	80	36.63	48.89
5	90	135.96	68.68
Average	84	103.27	60.68

The best fitting distribution for the complete data set of T_{mean} values obtained on day 6 was found to be a normal distribution (see **Figure 32**). The distribution obtained using histogram (equation 5), based on data binned as per equation 3, is shown in **Figure 32**. The solid dark line in the **Figure 32** shows the distribution of

T_{mean} values obtained from binned data and using the Gaussian kernel. It is observed that the true shape of the distribution obtained from the data is bi-modal, which is accurately represented by the kernel and histogram. This bi-modal nature of T_{mean} values was hidden by the smooth normal distribution.

When the distributions were used in the Monte Carlo simulation model for damage assessment, the samples of T_{mean} values drawn from the kernel resulted in more accurate estimates of damage, since the samples were drawn from a distribution that accurately represented the measured data. In comparison to the histogram, the kernel density estimate is smoother. Hence during random sampling, more number of distinct samples were drawn from the kernel distribution as compared to the histogram. This further improved the accuracy of the damage distribution resulting from the Monte Carlo.

In terms of data reduction, the use of kernels and histograms resulted in 78% and 85% less data per day compared to using the complete monitored data set. Assuming the same amount of data reduction, the sensor system with binning can now be used uninterrupted for 6.6 more days with histogram and 4.7 more day with kernels to consume the same storage space without binning. Similar results were obtained when the analysis was conducted from day seven onwards. This clearly demonstrates the importance of these methods to enable uninterrupted monitoring at low power and memory consumption.

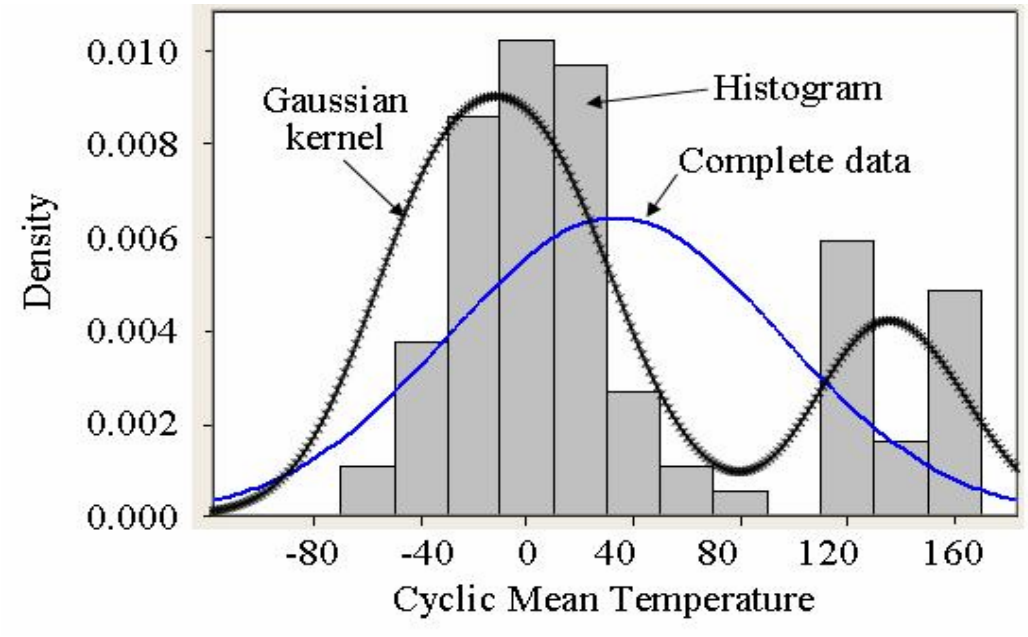

Figure 32. Comparison of density estimates for T_{mean} values of day 6

The sensitivity of the kernel densities to the difference between estimated and actual standard deviation and sample size were investigated by analyzing the experimental data for different time periods. For example, **Figure 33** compares three density estimates estimated using Gaussian kernel; distribution (1) is obtained using the complete data set and actual values of standard deviation and sample size for calculating is h_{opt}. Distribution (2) is based on binned data and estimated values standard deviation and sample size for calculating is h_{opt}. Distribution (3) is obtained from binned data and updated values standard deviation and sample size using the approach in **Figure 31**. In this example, the difference between the actual and estimated s was 38%. It is observed that the distribution (3) using updated value is a better estimate of the actual distribution (1). Similar results were obtained for

different sets of data collected in the study. More information is available in a paper on this work by the author [107].

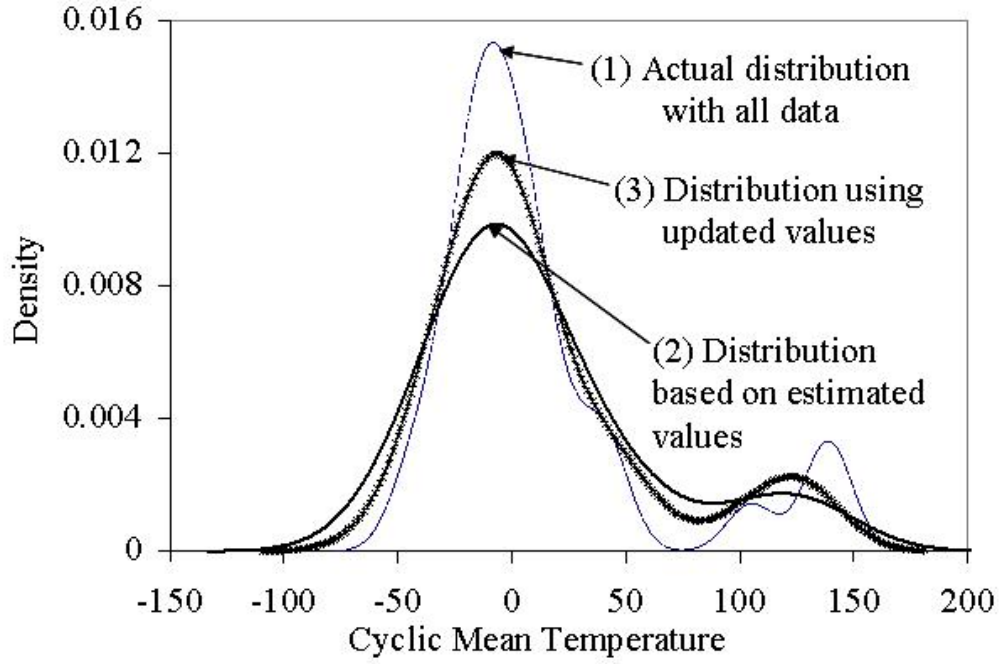

Figure 33. Comparison of distributions obtained from estimated versus actual parameters

5.6 Conclusions

A novel method was developed for extracting cyclic range, mean, ramp rates, dwell times and their correlations, from irregular time-temperature history. The application of this method for electronic prognostics and health management was demonstrated. The method for parameter extraction combined with storage of load parameters in bins resulted in 99.03% storage reduction per day, without compromising dwells regions. Thus embedding this algorithm with the sensor module can significantly enhance the ability of the module to monitor for longer durations

without running out of memory. The method can also be used for processing different time-load signals such as strain, acceleration, and humidity.

For prognostics and health management, the application of optimal binning and density estimation using histogram and kernel estimators for condensed storage of load histories, can significantly improve the ability of the sensor nodes to monitor for extended durations without interruptions and conserve memory and power. It was found that optimal bin widths can be calculated a-priori based on estimates of sample size and standard deviation of representative data sets. In using the binned data for representing the entire data set, kernel methods provided a better estimate of the probability density compared to histograms. It was shown that the difference between the estimated and actual bin-width and the resulting error in density estimation can be minimized by recording the sample size and standard deviation during in-situ monitoring, and using the recorded (true) values for density estimation.

Chapter 6: Prognostics Approach Considering Uncertainties

6.0 Introduction

The ability to predict a product's remaining life with the associated confidence limits, based on current and historic "health" conditions can enable effective maintenance and reduce the life cycle cost by decreasing inspection, downtime, and inventory costs. Remaining life predictions are made by assessing the accumulated damage due to measured environmental and usage exposure. However, often the effect of uncertainty and variability in the measurement and procedures used for making predictions is neglected. In this chapter, a generic method is developed for remaining life prognostics that accounts for the measurement, model-input, and model uncertainties. The method is demonstrated to predict the remaining life distributions of solder interconnects subjected to field temperature conditions. The details of the proposed method and the implementation case-study are presented.

6.1 Background

For electronics prognostics, a method to predict remaining life using life cycle loads was proposed by Ramkrishnan and Pecht 2003 [53], referred as life consumption monitoring (LCM). LCM methodology is a six-step process, (see **Figure 34**), that combines systematic study of the different failure modes and mechanisms of the product under consideration, monitoring of relevant environmental and/or operational parameters, and use of physics of failure models to asses the damage and ultimately predict remaining life. For demonstration of this approach to

electronic assembly, Mishra et al. 2002 [54] and Ramakrishnan and Pecht, 2003 [53] monitored the temperature, humidity, vibration and shock loads experienced by an electronic assembly operated in automotive under-hood environments. This monitored data was applied in conjunction with physics-of-failure models to estimate damage and predict remaining life. The PHM methodology was shown to accurately predict remaining life in the application environment.

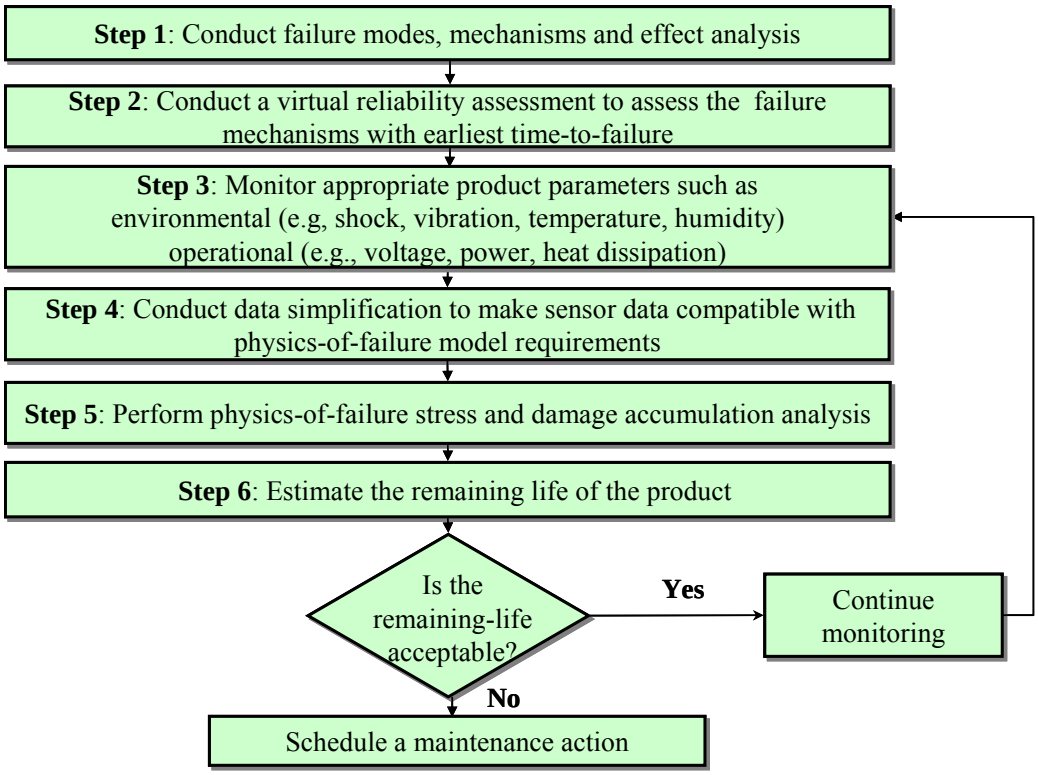

Figure 34. CALCE Life consumption monitoring methodology

One of the major drawbacks of this approach was the use of discrete values of loads for making damage assessments, which results in discrete values of damage fractions and remaining life. This approach did not consider the various uncertainties and variability that can significantly influence the prognostics. These uncertainties include i) measurement uncertainty, due to inaccuracies in the sensing, recording, use

of sampled information, and assumptions in data conditioning techniques. ii) Parameter uncertainty, which arises due to variability in the material and geometric parameters that are used in the damage model for health evaluations. iii) Model uncertainty, which may arise due to limitations in analyst's knowledge of phenomenon and deliberate simplifications introduced for modeling.

The essence of prognostics is the estimation of remaining life in terms that have consequence in the maintenance decisions process [108]. Using the life consumption monitoring approach with single point estimates of remaining life, without confidence intervals and confidence level, it may not be possible to take logistics decisions with certainty. Hence it is necessary to identify the uncertainties in the prognostic approach and assess the impact of these uncertainties on the remaining life distribution, in order to make risk-informed decisions.

In this work we have developed an approach to account for the measurement, parameter, and model uncertainties in the prognostics process. The approach combines sensitivity analysis and Monte Carlo based random sampling to provide a distribution of accumulated damage. Using regression analysis of the accumulated damage distributions, the remaining life is then predicted with confidence intervals and levels. The approach is demonstrated using a PHM setup discussed in chapter 3.

6.2 Overview of Methodology

A generic approach was developed for making predictions by considering the measurement, parameter, and model uncertainty. **Figure 35** presents the schematic of

the approach adopted in this work for estimating the confidence bounds on the remaining life predictions. The next few sections will discuss in detail on the building blocks of the approach.

6.2.1 Measurement Uncertainty

Environmental and usage load profiles are captured in the application environment, for utilizing in real time or near real time health assessment and prognostics using sensors and data loggers. This raw sensor data is simplified or pre-processed to make it compatible with the damage models and algorithms that are used to conduct prognostics. In particular, it may be necessary to extract the relevant load parameters including cyclic mean, amplitudes, ramp rates, hold periods, power spectral densities, etc. Commonly used load parameter extraction methods include: cycle counting algorithms for extracting cycles from time-load signal, Fast Fourier transforms (FFT) for extracting the frequency content of signals, etc. Depending on the application and type of signal, custom load extraction methods may be required.

Figure 5 (chapter 3), provides a schematic of the in-situ monitoring, pre-processing, and storage of environmental and usage loads. A time-temperature signal is monitored in-situ using sensors, and further processed to extract (in this case) cyclic temperature range (ΔT), cyclic mean temperature (T_{mean}), ramp rate (dT/dt), and dwell time (t_D) using embedded load extraction algorithms. The extracted load parameters are stored in bins with optimal bin-widths [107]. The binned data is downloaded to estimate the distributions of the load parameters using kernel

estimator for use in damage assessment, remaining life estimation, and the accumulation of the products use history. The kernel estimators are non-parametric methods of density estimation and hence the environmental and usage exposures are now expressed in terms of the load distributions that account for the uncertainties in each load parameter. These non-parametric distributions of individual load parameters reflect the uncertainties in measurement, sampling, and data simplification (such as cycle counting, FFT) combined.

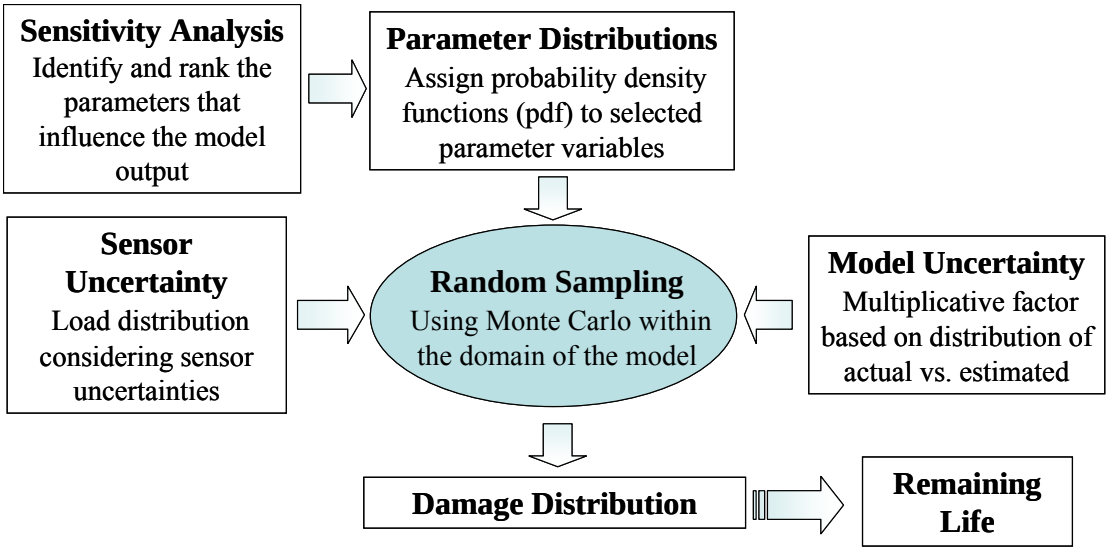

Figure 35. Prognostic health monitoring methodology considering uncertainty

6.2.2 Parameter Uncertainty

The parameter variables consist of decision variables and model-input parameters. Decision variables are the parameters over which the decision maker exercises control, such as sampling rate, measurement interval, download interval, variables in data conditioning etc. These variables can be explored and optimized based on accuracy and operational constraints. It is assumed that these decision variables are not a direct input to the mathematical or logical model used for damage

assessment. However, the selection of these variables can directly or indirectly influence the inaccuracies in the damage assessment process. The sensitivity analysis of decision variables has to be done just once, at the time of PHM implementation. This sensitivity analysis can probably lead to valuable recommendations such as need of different sensor, change of sensor location etc.

Model parameters are the terms in the mathematical model used for damage assessment. These can be geometric dimensions of the structure being analyzed, the material properties, constants used for fitting etc. Given a model there are various methods for sensitivity analysis. In this case a local sensitivity analysis method was selected as described below [109],

Let $y = f(x_1, x_2, ...x_n)$ be the model used in the PHM process

Wherein, $x_1, x_2, ...x_n$ denotes the model parameters

$\hat{x}_1, \hat{x}_2, ...\hat{x}_n$ denotes the nominal value of the parameters

For each parameter of interest, the first partial differentials were evaluated for values around a nominal value.

$$\left.\frac{\partial y}{\partial x_1}\right|_{\hat{x}_1-\Delta x_1}^{\hat{x}_1+\Delta x_1} \quad \left.\frac{\partial y}{\partial x_2}\right|_{\hat{x}_2-\Delta x_2}^{\hat{x}_2+\Delta x_2} \quad \ldots\ldots\ldots\ldots \quad \left.\frac{\partial y}{\partial x_n}\right|_{\hat{x}_n-\Delta x_n}^{\hat{x}_n+\Delta x_n}$$

A sensitivity index was obtained by considering the variability of the individual parameter by multiplying the sensitivity index by the standard deviation of the parameter. This accounts for considering the natural variability of the parameter, instead of the arbitrary selected criteria of say +/- 1%. Finally, we find the

dimensionless nominal sensitivity index by normalizing the results with the sensitivity index of all parameters considered. This enables the more accurate identification of the dominant parameters that influence the output of the damage model.

$$S_i = \left(\frac{\Delta y_i}{\Delta x_i} \right) \sigma_{x_i} \rightarrow \hat{S}_i = \frac{S_i}{\sqrt{\sum S_i^2}}$$

Based on the sensitivity analysis the parameters that results in the maximum variation in the time to failure can be selected. Probability distributions are then assigned for the selected parameters. The distributions were based on manufacturer data, tolerance limits, published literature, or prior knowledge.

This method is also known as the nominal range sensitivity method. It assumes that the user know the nominal values of the parameters and an expected range. There are several other sensitivity analysis methods such as global sensitivity, response surface, ANOVA, etc. However, our objective is to identify and rank the most sensitive variables for use in further analysis, which can be efficiently analyzed using this method [110] [111].

6.2.3 Model Uncertainty

Model uncertainty arises due to limitations in analyst's knowledge of phenomenon and the deliberate simplifications introduced for modeling. Thus model uncertainty would change significantly with the model being used. There have been several efforts to quantify the model uncertainty [112] [113] [114]. In this study,

model uncertainty has been accounted by using a multiplicative factor (or calibration factor) to the model output. This multiplicative factor is yi, and is defined as the ratio of measured value by the value estimated using the model under consideration. Here, yi is a random variable and has a distribution. yi can be obtained by fitting a best parametric distribution to data obtained from studies conducted to validate the model. Such data is often available from the model designer. However, data from multiple sources should be used to obtain un-biased results. Also, it needs to be ensured that the data used to generate yi belongs to studies with similar package, geometry and material configurations.

6.2.4 Random Sampling for Damage Assessment

The distributions of measured load parameters and the distributions of dominant model-inputs are then sampled randomly in a Monte Carlo technique using the damage model. In random variates are generated using the inverse cumulative function. The cut-off truncation method was used for generating random samples from truncated distributions for use in Monte Carlo.

Let f(x) is the pdf with $0 < x < \infty$ and F(x) is the cdf of random variable x. If the variates have to be between values 'a' and 'b'. We use the inverse cumulative function of that particular distribution for generating the random variates. However, the truncation is done as follows,

Generate x from F(x)

If $x \leq a$, let $x = a$,

If $x \geq b$, let $x = b$

In this case, the truncated distribution is given by,

$$F_t(x) = \begin{cases} 0, \text{ for } x < a \\ F(x) \text{ for } a \leq x \text{ , } b \\ 1, \text{ for } x \geq b \end{cases}$$

Also, since the load distributions were in form of Gaussian kernels or histograms, the random variates from these distributions were derived using the following procedure in [115]. Kernels are non-parametric distributions with output in the form specified in **Table 9**.

Table 9. Format of load distribution obtained in Gaussian kernel format

n	Interval	Probability p(x)	Cumulative F(x)
1	$x_{(i-1)} < x \leq x_{(i)}$	p_1	Σp_i
↓	↓	↓	↓
n	$x_{(n-1)} < x \leq x_{(n)}$	p_n	1

To generate the random variates, we first define R a random variable uniformly distributed over [0,1].

$$R = U[0,1]$$

Using values in **Table 9**, we calculate empirical slope as;

$$a_i = \frac{x_i - x_{i-1}}{F_i(x) - F_{i-1}(x)}$$

The inverse cdf is given by;

$$X = F^{-1}(R) = x_{(i-1)} + a_i[R - F_{i-1}(x)]$$

The stopping criteria for Monte Carlo simulation were based on minimizing the variance over the mean of the simulation results (Figure 36). For example,

If, d1, d2, …..dm are the results of Monte Carlo. Then, Stop Monte Carlo when, standard error of the mean (μ):

$$\frac{\sigma}{\sqrt{m}} \leq 0.01\mu$$

Here, mean, variance, and standard error over the mean are calculated as follows:

$$\mu = \frac{1}{m}\sum_{i=1}^{m} d_i \qquad \sigma^2 = \frac{1}{m-1}\sum_{i=1}^{m}(d_i - \mu)^2 \qquad \sqrt{Var|\mu|} = \frac{\sigma}{\sqrt{m}}$$

Before Monte Carlo simulations, the correlations between load parameter distributions were assessed using correlation coefficient. This is conducted to ensure that only meaningful scenarios are generated during Monte Carlo. If the distributions are correlated, then the procedure used for sampling these distributions is given below [116],

Let the two load parameter distribution that are correlated be f(x) and f(y). Let the correlation coefficient between these two distribution be ρ. If, N = number of iterations of Monte Carlo, sample f(x), N times to get X = $\{x_1, x_2, \ldots x_N\}$. For each value of x_i estimate the value of y_i based on ρ, and variance in x and y, given by:

$$\hat{y}_i = \frac{\rho S_y}{S_x}(x_i - \bar{x}) + \bar{y}$$

Here, correlation coefficient: $\rho = \dfrac{\mathrm{cov}(x, y)}{S_x S_y}$

Covariance between x and y is given by: $\mathrm{cov}(x, y) = \dfrac{\sum (x_i - \bar{x})(y_i - \bar{y})}{n-1}$

The standard deviations of x and y are given by:

$$S_x = \sqrt{\frac{\sum (x_i - \bar{x})^2}{n-1}} \qquad S_y = \sqrt{\frac{\sum (y_i - \bar{y})^2}{n-1}}$$

Use new pairs of (x_i, y_i) together in the Monte Carlo simulation

This assessment provides a distribution of damage fractions. Each damage fraction is due to the effect each measured load parameter. However, the combined damage distribution (accumulated over the assessment period) has to reflect the effect of all load parameters that were measured. Since the output of Monte Carlo simulation is over 10000 data points, a large number of random samples n, each of size N (where N = number of cycles counted over the monitoring period being assessed) are drawn from the Monte Carlo results (**Figure 36**). Accumulated damage fraction is then defined as accumulated damage AD_i;

$$AD_i = \sum_{i=1}^{N} D_i$$

As this procedure is continued for n number of samples, we get accumulated damage fractions AD1, AD2, …..ADn. Using these data points the accumulated damage distribution is obtained, which is the best fit to given data points (**Figure 36**).

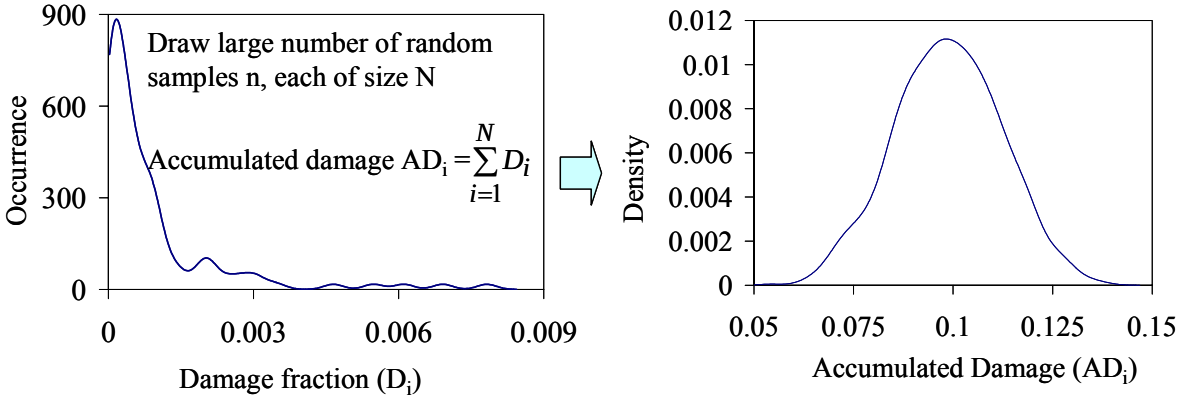

Figure 36. Accumulated damage distribution for the monitoring period being assessed

6.2.5 Damage Accumulation and Remaining Life Prediction

As the accumulated damage distributions over the monitoring period are obtained, these distributions can then be updated using the following procedure:

$$E(AD'_n) = E(AD'_{n-1}) + E(AD_n)$$

$$Var(AD'_n) = Var(AD'_{n-1}) + Var(AD_n) + 2Cov(AD'_{n-1}, AD_n)$$

Here, AD'_n is the accumulated damage distribution at the end of day n. AD_n is the accumulated damage distribution estimated over day n, and AD'n-1 is the accumulated damage distribution estimated at the end of day n-1. E denotes the expected value of the distribution and Var is the variance.

As the monitoring process continues the damage distributions are updated using the above procedure. The failure criteria is defined by Miner's rule, as the accumulated damage of greater than or equal to one. Thus if accumulated damage distributions are obtained at the end of time period X1, X2,….Xn. Then using regression analysis we can formulate the relation:

$$Y = \text{Normal}\ (mX + c, S_{yx})$$

Here, Y is the accumulated damage distribution, which has a mean of mX+c, and a standard deviation of Syx which is the standard error of y estimate.

$$S_{yx} = \sqrt{\sum_{i=1}^{n} \frac{(y_i - \hat{y}_i)^2}{(n-2)}}$$

Using the regression equation one can obtain the accumulated distribution of future time period by plugging the values of Xi, and calculating the corresponding Syx. Thus based on our failure criteria, the remaining life and its probability can be calculated for any value of Xi.

6.3 Case Study

The approach presented above was demonstrated for prognostics of an electronic printed circuit assembly. The experimental setup, in-situ monitoring and analysis, damage accumulation and life prediction considering uncertainty and variability are already discussed in chapter 3.

The demonstration process is explained by an example of BGA 225 a component on the test board. The potential sources of uncertainty in the damage assessment of this component were investigated (**Figure 37**). The sources are classified as geometric parameters, material parameters, model constants, and loads. This is the first step in the PHM uncertainty analysis. The next step is to determine which of these sources influence the damage assessment and hence the remaining life prediction.

6.3.1 Decision Variables

The decision variables are investigated first. One of the decision variables is the reversal elimination index (or threshold) in the ordered overall range algorithm, which is used for processing measured temperature data. The data reduction due to reversal elimination can be an important variable for remote monitoring systems working on portable power supplies. In such applications memory and power consumption can be most critical operational constraints. For OOR a reversal elimination index, S (< 1) can be selected to filter amplitudes that differ from the largest measured amplitude by the specified fraction. This data was screened using different values of reversal elimination index (threshold). The accumulated damage was estimated using each data set. For simplicity it was assumed that the error in damage accumulation is zero when all amplitudes are considered for the analysis (S = 0). The error in damage accumulation due to use of reduced data for all other data sets was obtained by the formula

$$\text{Error} = \frac{\text{Accumulated damage (S = 0)} - \text{Accumulated damage (S > 0)}}{\text{Accumulated damage (S = 0)}}$$

Figure 9 illustrates the percentage error in damage accumulation and the percentage data reduction with change in S-parameter. It is observed that even when the S is zero, the data reduction is 84%. This is due to filtering all data points that are in a monotone increasing or decreasing sequence. Also small values of S, ranging from 0 to 0.1 resulted in more than 90% data reduction with only 1% error in the damage calculation. Higher values of S result in increasing error in damage

accumulation. This is due to elimination of reversals with large magnitude and the dependence of the fatigue model on the temperature amplitude.

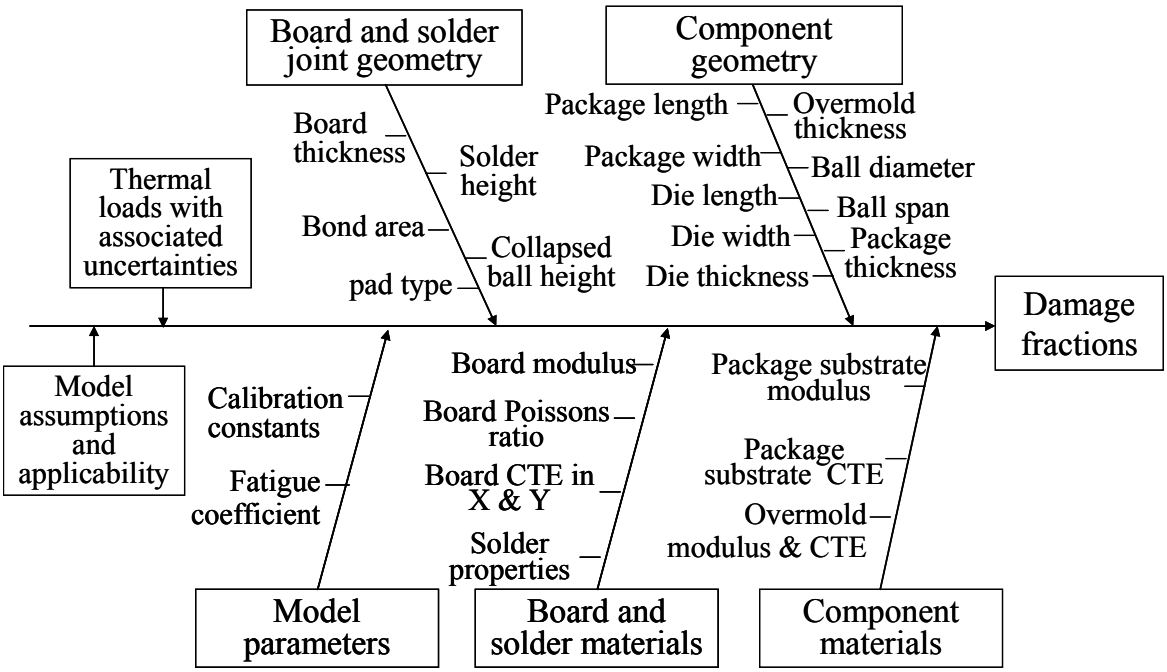

Figure 37. Sources of uncertainty in damage estimation and prognostics for BGA225

Another example of analysis of decision variable is the download frequency. The term download frequency denotes the number of times the monitoring system was interrogated for checking the status or making predictions. Interrogating the system more often results in breaking the data sets. Assuming the user is planning to download on a periodic basis, the decision on download frequency can be made based on analysis shown in **Figure 38**. Using the temperature data used for analysis in **Figure 9**, the damage analysis was conducted by using the complete data sets, breaking the data set into 3 parts, 5 parts and 10 parts. This is referred as signal interruption on the y-axis of **Figure 38**. The error was normalized with respect to the data set with no reversal elimination and signal interruptions. In this case all values are low, also it seems like the error has started to become constant. i.e., there is a

large change between 0 to 3 days. However, the difference between 5-10 days is not as much.

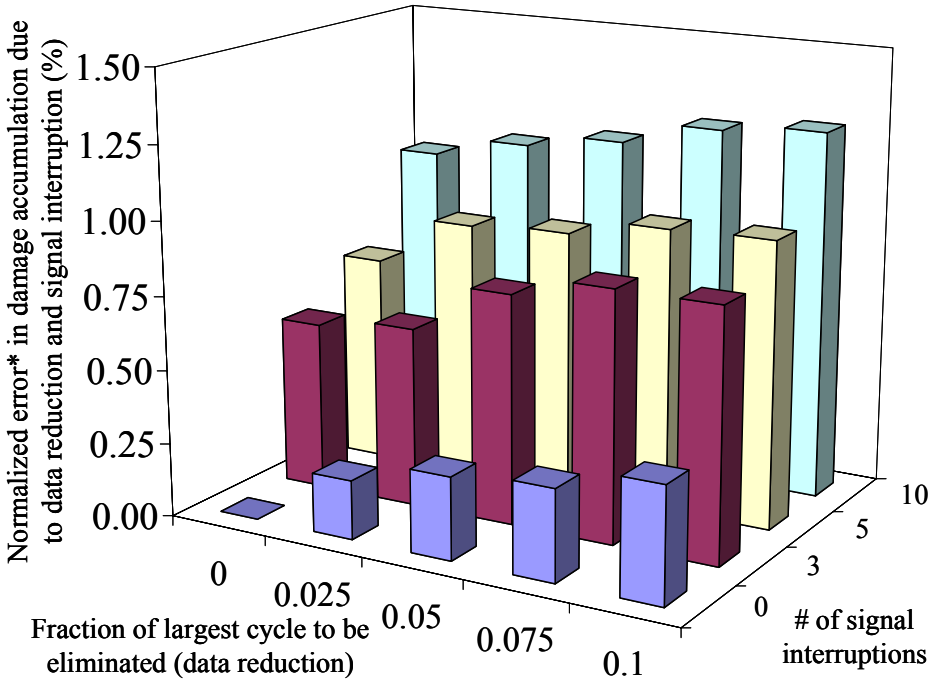

Figure 38. Error in damage accumulation due to reversal elimination and signal interruption

6.3.2 Model Parameters

Sensitivity analysis was conducted for the thermal fatigue model for BGA 225. The second column in Table 10 shows the change in the cycles to failure for a one percent change in the input variable around the nominal value. These values are then multiplied with the standard deviation of the model-input parameters, obtained from manufacturer data, literature, and measurements. The normalized range sensitivity index was calculated as shown in the approach (section 2). The final column shows that the ranks are rearranged by considering the natural variability of the model-input parameters. As per the new ranks, the top four model-input

parameters were assigned probability distributions and were used for in random sampling for damage assessment.

Table 10. Sensitivity analysis of model-input parameters

Model Parameters	% change in predicted cycles to failure*	Normalized sensitivity index	Rank
Collapsed ball height	2.45	0.00295	3
Board CTE	2.20	0.00412	1
Component CTE	1.26	0.00321	2
Diagonal length	1.26	0.00139	4
Overmold thickness	0.57	0.00091	6
Overmold modulus	0.50	0.00075	7
Package substrate CTE	0.44	0.00101	5
Package substrate modulus	0.19	0.00033	8
Pkg. substrate thickness	0.19	0.00028	9

6.3.3 Random Sampling

The four model-input parameters that were selected for Monte Carlo analysis for the damage assessment of the BGA 225 included, coefficient of thermal expansion (CTE) of the printed circuit board, CTE of component, collapsed solder ball height, and diagonal length of the component. The normal distributions assigned to each of these parameters are shown in **Figure 39**. The model-input parameter distributions and the measured load parameter distributions were randomly sampled using a Monte-Carlo technique within the damage model. The Monte-Carlo was stopped when the standard error over the mean was less than 1 percent of the mean

value. The resulting data on damage fractions was analyzed using the procedure in section 2 to obtain a distribution of accumulated damage. The stopping criteria of stabilizing the variance over the mean were utilized. Typically it required 10,000 runs of the Monte Carlo to satisfy this criterion (**Figure 40**).

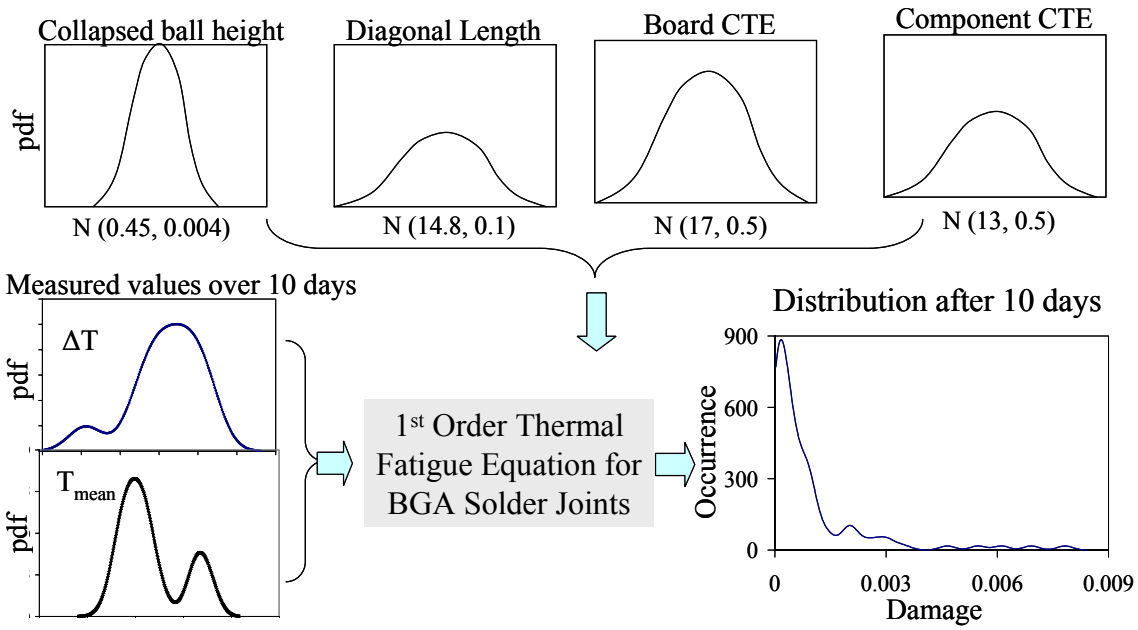

Figure 39. Monte-Carlo simulation for damage assessment

6.3.4 Model Uncertainty

The model used in this study is the first order thermal fatigue model for plastic ball grid arrays [117]. This model has been extensively used for various studies in industry and academia. The studies have compared the cycles to failure of BGA components obtained from accelerated testing with the results obtained from the model (estimated). Using the approach presented in section 2, the distribution of yi was derived using 48 data points obtained from CalcePWA manual for the model. The distribution of yi was randomly sampled and used as a multiplicative constant (**Figure 41**).

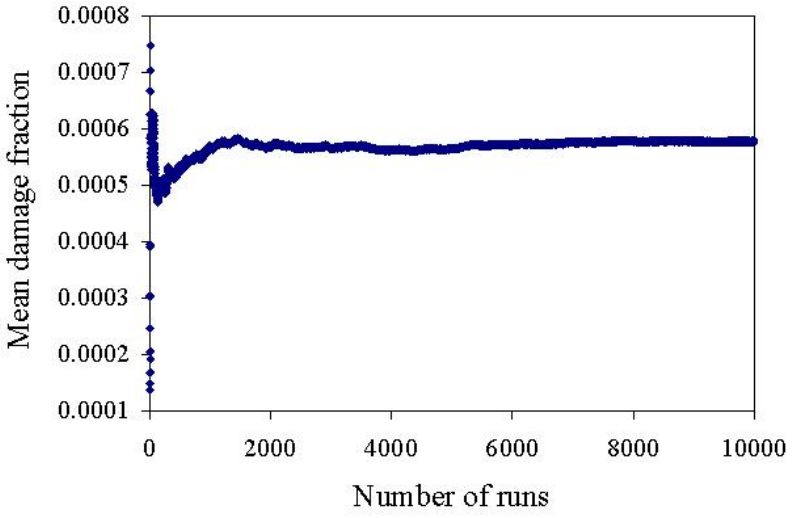

Figure 40. Monte Carlo results and stopping criteria

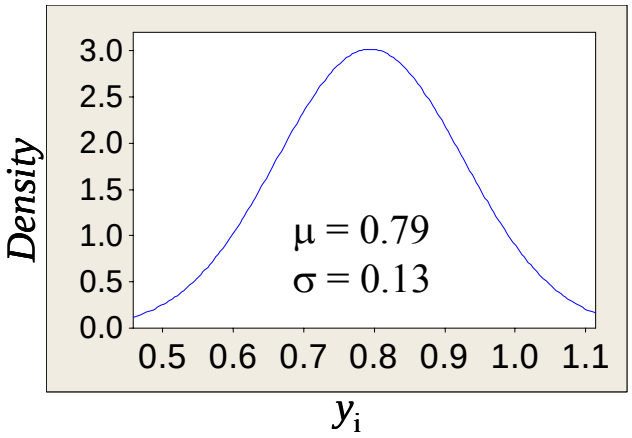

$$y_i = \frac{(N_f)_{measured}}{(N_f)_{predicted}}$$

$$D_i = \left(\frac{1}{y_i}\right) D_{estimated}$$

Figure 41. Distribution of calibration parameter for model uncertainty

6.3.5 Remaining Life Prognostics

Using the regression analysis presented in section 2, the distribution of accumulated damage after every ten days is shown in **Figure 43**. The actual failures in testing were observed on day 87 and 92. Based on the failure criteria, the remaining life prognostics are shown in Table 11. The first column shows the day on which the prediction was made, which represents the monitoring period data that was

used for prognostics. The spread of the remaining life distribution decreases as the time in use increases, i.e., the spread of the remaining life distribution made on day 60 is higher than the spread on day 84.

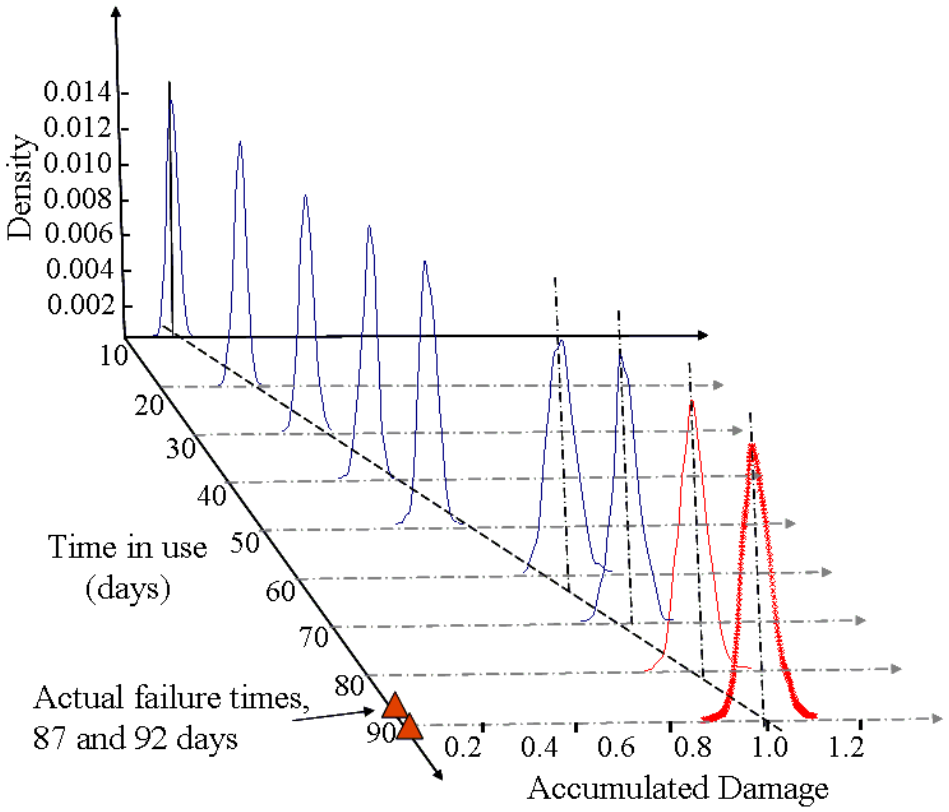

Figure 42. Accumulated damage distributions with time for BGA 225

Table 11. Remaining life distributions for BGA 225

Day of assessment	Remaining life with probability		
	0.5%	50%	95%
60	24	32	37
72	15	20	22
84	1	5	9

6.3.6 Damage Histories for Prognostics

For products and systems operated over long durations, the accumulated damage distribution can be stored in a condensed form. The user can track the change

in the damage distributions over time and use this information for assessing the future usage conditions, which can affect the remaining life prognostics. The normal distribution curves on the left corner of **Figure 43** shows the accumulated damage distributions of BGA 225. Each curve represents the distribution over a period of three days. The graph in the top right corner tracks the change in the mean of the damage distributions with time. This can enable to identify, periods of severe usage. The three histograms in the bottom contain the parameters of the accumulated damage distributions, specifically the mean, standard deviation, and kurtosis. Such damage histories can be stored for the entire product and can be used for generating scenarios for assessing mission survival under different usage conditions.

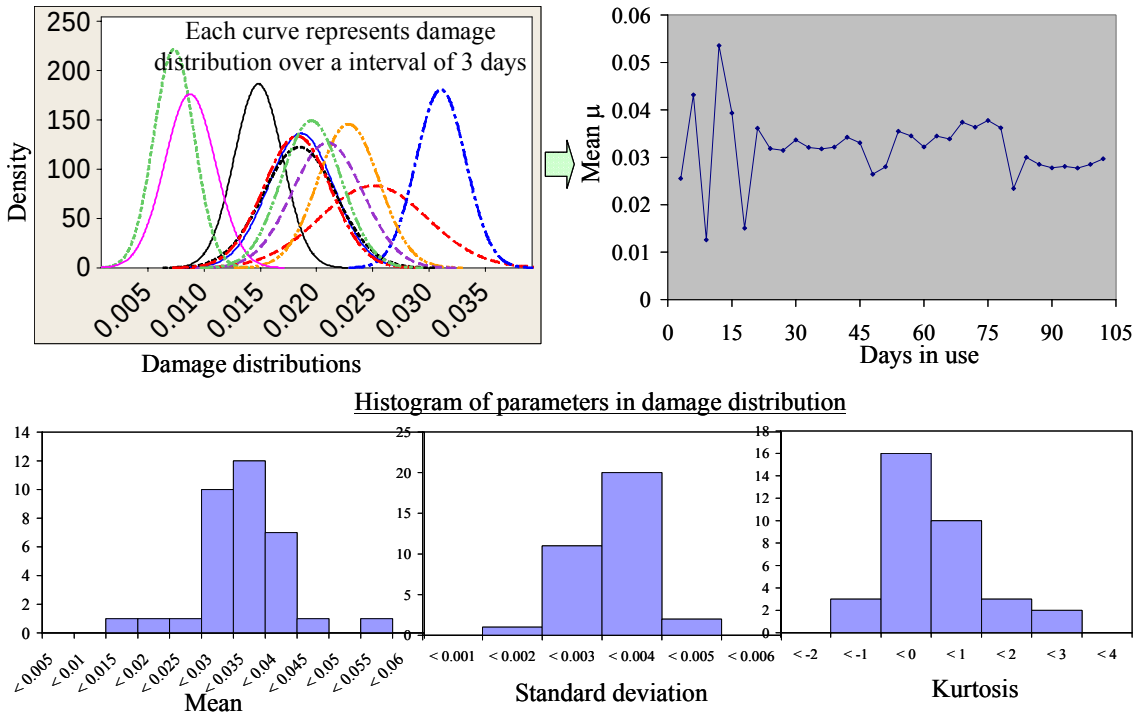

Figure 43. Distributions of accumulated damage over time

In the above experiment, each 3 day period can be considered as a mission. The prognostic assessments can be conducted at the end of each mission to ensure the number of failure free missions and the probability of surviving the next mission. Also, the load distributions can be stored in compact format (per mission) and retrieved for prognostic assessments when needed (**Figure 44**). The normal distributions represent the distributions of delta T over each 3 day (mission) period. The variations in the mean of the distributions over time are shown in the top right graph of **Figure 44**. The two graphs in the bottom show the histograms for the mean and standard deviation of the delta T distributions. The four graphs in Figure 43 can be used to reconstruct the temperature loading history of the entire missions.

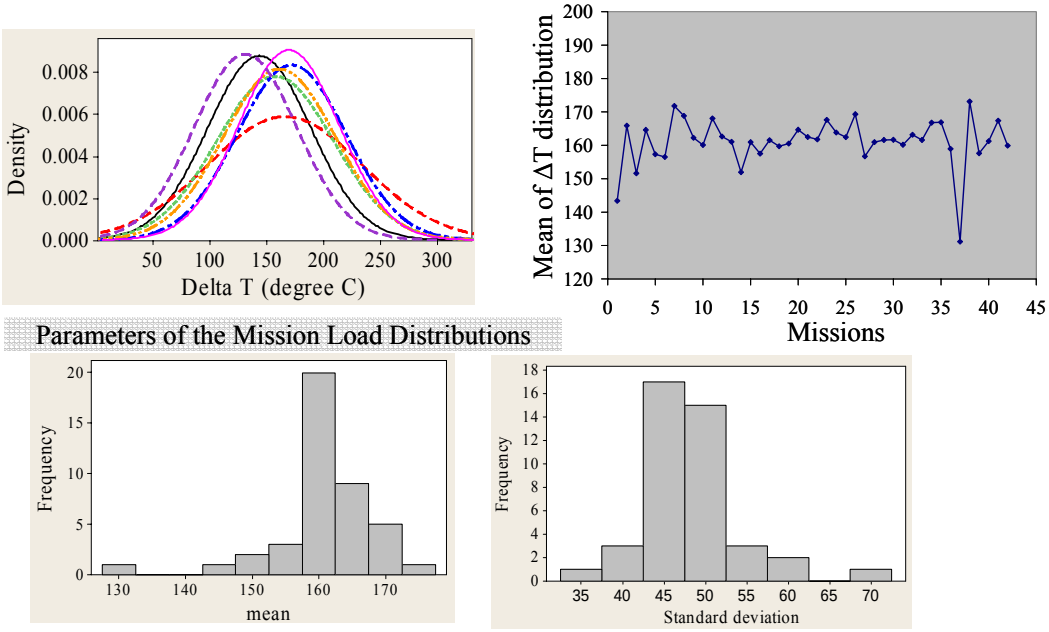

Figure 44. Condensed storage of load histories based on missions

Using the mission based approach, **Table 12** shows the predicated mean number of missions prior to failure. Two categories were considered. 1) The future

mission would be as severe as the mean value of all previous missions, and 2) the future mission will have a severity value equivalent to the worst case severity based on the previous missions. Actual failures were observed in mission 29 and 31.

Table 12. Remaining life prognostics in terms of missions

	Predicted mean number of missions prior to failure at 95% C.I.	
End of mission	Mission severity = mean	Mission severity = worst case
26	3.6	1.6
27	2.7	1.1
28	1.8	**0.6**
29	**0.9**	0

6.4 Conclusion

The sources of uncertainty in the prognostic approach based on environmental and usage exposure were identified. A generic approach to prognostics that can account for uncertainties in measurement, model-input, and damage models was developed and demonstrated to provide a distribution of remaining life.

It was found that given the measurement, parameter and model uncertainties, the actual failures in testing were observed within the predicted failure distribution. The sensitivity analysis procedure revealed that it is important to consider the standard deviation of parameter variables for calculating sensitivity indices, as it can strongly influence the ranking of the most sensitive variables. Prognostic approach consistently provided an advanced warning of failure for all components in the study.

It was observed that the prediction accuracy increased with the decrease in remaining life. This was attributed to the fact that with increased usage there was more data to support the prognostics.

Chapter 7: Failure Precursors Based on Resistance Analysis

7.0 Introduction

The previous four chapters discussed the methodology and case-studies for prognostics based on monitoring and modeling of life cycle environmental and usage loads. This chapter presents a different approach for prognostics using the same setup described in chapter 3. Instead of assessing the accumulated damage due to temperature cycles, the performance of the electronic board is directly monitored and analyzed to provide an advance warning of failure and estimate remaining life. The next few sections discuss the challenges in monitoring the performance, the methodology adopted for analysis or failure precursors and the results.

The failure mode being investigated here is solder joint cracking, which can introduce the complete fracture through the cross-section of the solder joint with the solder joint parts having none or partial adhesion to each other. The failure mechanism is creep and stress relaxation enhanced thermal fatigue due to temperature cycling. A failed solder joint is normally surrounded by solder joints that have not yet failed and therefore the solder joint fracture surfaces make compressively loaded contact. During thermal changes shear is the primary force of stress on the solder joints. As a result, the rough fractured surfaces of the failed solder joints slide relative to one another producing characteristic short duration electrical transients. There are several methods to detect solder joint failures, including destructive testing

to visually inspect cracks in the solder joints at periodic intervals, periodically measuring the electrical resistance of solder joints and define the failures based on the increase in original resistance, and continually monitoring electrical resistance of solder joints to detect electrical discontinuities as failures.

As mentioned in chapter 3, the test board used in this experiment has 6 different components and two components of each type making totally 12 components on the board. All components have a daisy chain for monitoring resistance continuity. A daisy chain is a conductive path that connects several interconnections of a component. In this experiment a failure of any daisy chain indicates the failure of the component. The daisy chain resistance of all components except the QFP 100 was measured in-situ for the entire period of the experiment. The QFP100 was not monitored in-situ, since the damage models and previous testing had predicted that the component was not susceptible to failure under the given conditions.

Thus in this experiment, the resistance of the daisy chains indicate the performance of the component. The daisy chains have a base resistance before start of the experiment. The daisy chain of the BGAs and QFPs extended onto the pads on the printed circuit board. Wires were soldered onto the pad and connected to an Agilent Model: 34970A data logger to take measurements of resistance every ten seconds. The base resistance of the daisy chain was measured and recorded prior to thermal cycling exposure. The data logger was operated in constant current mode at a source

current of 1mA, which passes through the daisy chains and reports the resistance of the path.

The plot of resistance versus days in testing is shown in **Figure 45**. As the component approaches failure, the short duration electrical spikes are observed in the resistance values. After the first spike the subsequent spikes occur within a short duration of time and ultimately the solder joint shows a complete open (infinite resistance). It is evident from the **Figure 45** that just by monitoring the resistance it is impossible to provide any indication of degradation prior to the occurrence of the first spike. The question asked here is that can we identify and estimate a degradation trend even before the occurrence of the first spike?

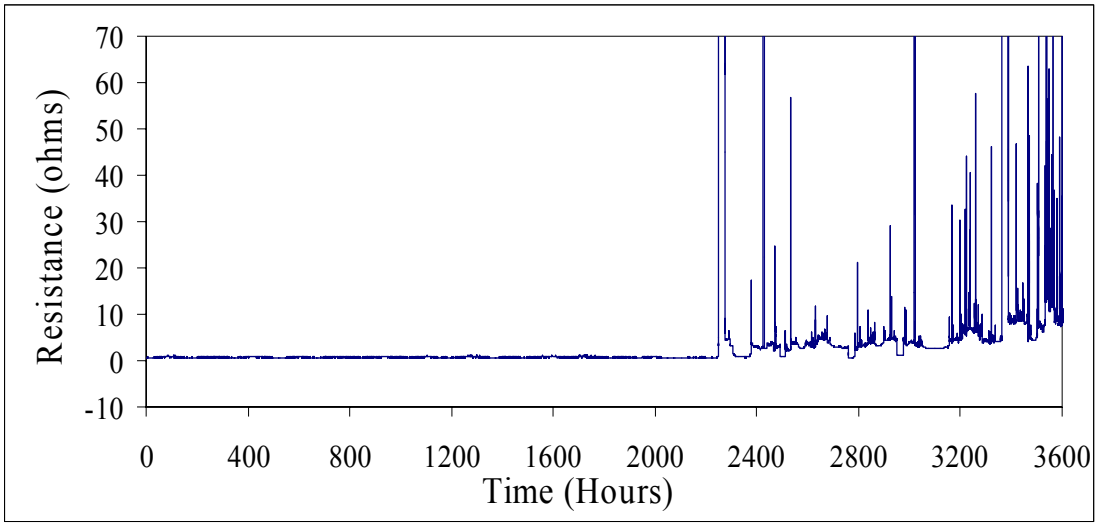

Figure 45. No indication of degradation before the occurrence of the first spike

Additionally, the challenge to identify a degradation trend is further complicated due to the constant change in resistance values during thermal cycling. The resistance increases with increase in temperature and returns back to normal as

shown in **Figure 46**. This is a typical representation for component PBGA 225. However, the change in the temperature-resistance is dependant on the component, base resistance, temperature cycle, and also the damage accumulation of the component. For example, the change in resistance for a temperature cycle with ΔT of 100°C is higher after 1000 cycles as compared to the start of the experiment. With continued thermal cycling the daisy chain resistance will gradually increase to indicate failure (crack growth leading to open connection), as shown in **Figure 45**. The resistance will increase with initial spikes and eventually lead to complete open with infinite resistance.

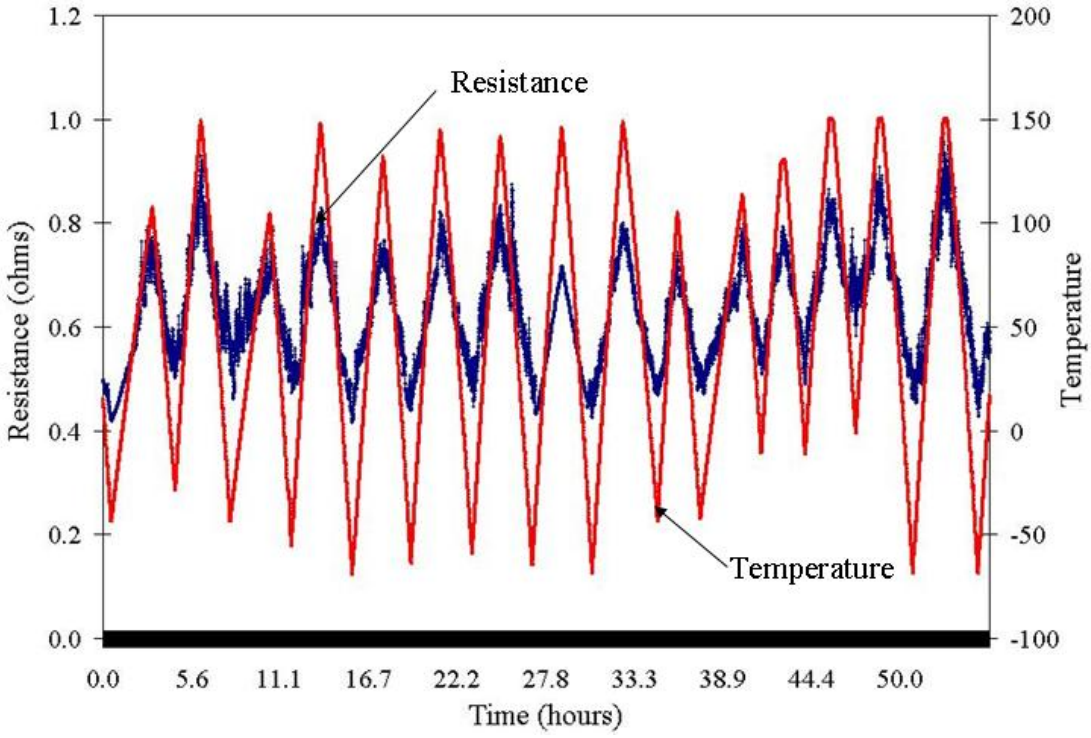

Figure 46. Change in resistance with temperature

7.1 Approach

Based on the above discussion there are two important issues: (1) the identification of resistance degradation trend before the occurrence of first spike and (2) the effect of temperature variations on resistance. The approach used to resolve both issues and enable the identification of the onset of degradation is shown in **Figure 47**.

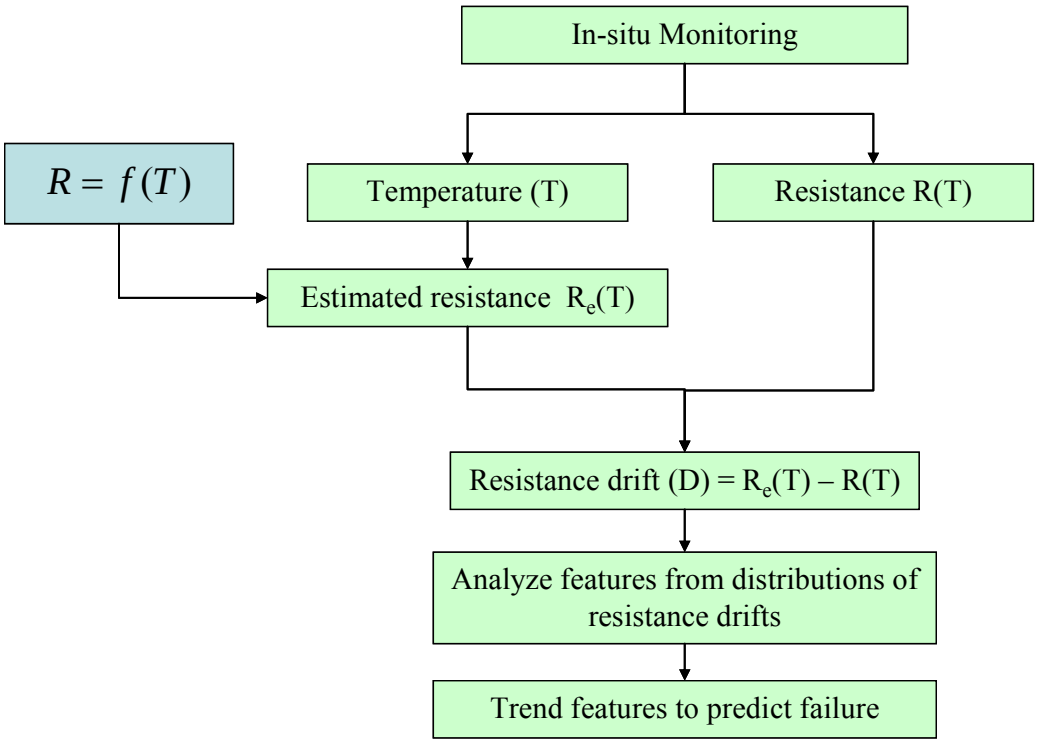

Figure 47. Approach for precursor identification and tracking using resistance drift values

The core of the approach is the relationship between temperature and resistance R = *F*(T), which is developed using in-situ monitored temperature and resistance data at the beginning of the experiment. This is equivalent to establishing a base-line performance. Since all components are in almost pristine condition, using this relationship, the resistance can be predicted as a function of temperature. Thus as the testing continues, the actual resistance R(T) is measured and recorded for the

component. Also, based on the temperature – resistance (TR) relationship, a value of resistance is estimated $R_e(T)$. The actual resistance value is then subtracted from the estimated value in time domain, to provide a resistance drift (D).

The resistance drift indicates a deviation from the expected normal condition. However, the values of drift in time domain also produce a noisy signal and cannot be directly used for identifying a degrading trend. Hence the values of drift are analyzed over windows of ten hours. Using these values on can track the shift in the distribution of drift values. Also the ten hour window covers the longest temperature cycle that can be observed in the experiment. Using the ten hour resistance drift data, various features were analyzed to identify the best (reliable) feature that can be used as a prognostic indicator. Failure criteria were set to 50% increase in the mean of the drift distribution. The 50% increase also corresponds to the first large spike that was measured during resistance monitoring.

7.1.1 Temperature – Resistance Model

A second order polynomial was fitted to predict the change in resistance with temperature. The coefficients α_1, α_2, and α_3 were calculated based on the first 3600 data points, with the corresponding 95% confidence intervals.

$$R = f(T) = \alpha_1 T^2 + \alpha_2 T + \alpha_3$$

The fit for component QFP 256 is shown in **Figure 48**, the details of the fit are shown in **Figure 49**. Table 13 gives the mean and 95% confidence values for α_1, α_2, and α_3. The R2 value for the fit is 98.9%. As observed from **Figure 49**, the residual values follow a normal distribution with a mean zero. The residual values are evenly

distributed around zero. Also, the scatter plot of fitted versus the residuals shows a uniform distribution with mean residual values around zero. The fitted values have a large spread from 0.2 to 0.45 ohms. Overall both **Figure 48** and 45 indicate that the model fits the data reasonably accurately.

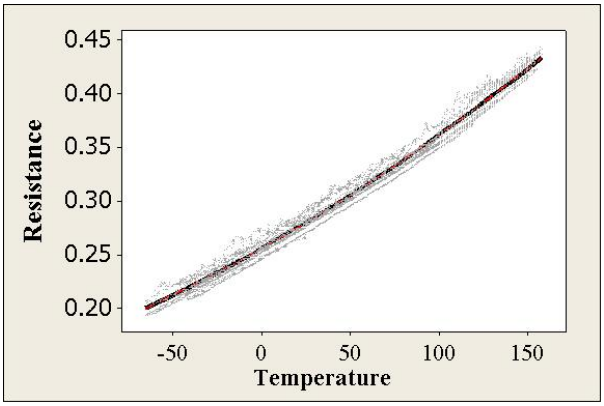

Figure 48. Second order polynomial fit between temperature and resistance

Table 13. Values of coefficients used in regression model

	Value	95% C.I.
α_1	1.31E-5	0.13e-5, 2.6e-5
α_2	9.36E-4	9.11E-4, 9.52E-4
α_3	0.2559	0.2548, 0.2561

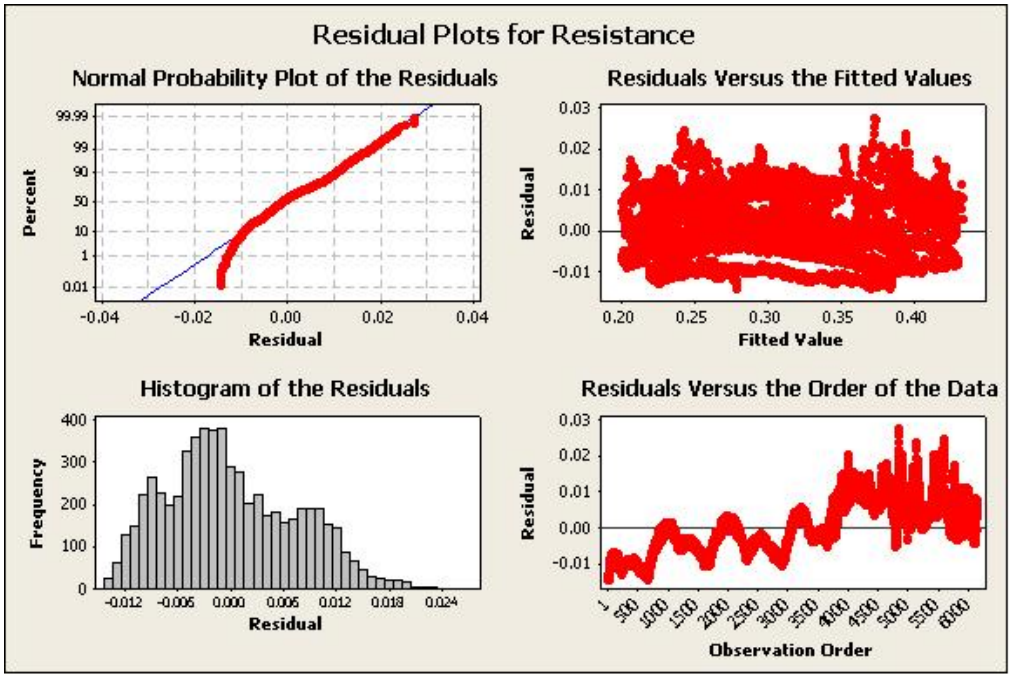

Figure 49. Details of prediction model

7.1.2 Features Investigated

The values of resistance drift and the features of the drift distributions over a ten hour period were monitored and analyzed to identify which features could be consistently used as a precursor to failure. The list of all feature investigated is shown in Table 14.

Table 14. Features investigated for determining consistent precursor

Feature	Formula
Resistance drift	$D = R_e(T) - R(T)$
Mean drift values	$\frac{1}{n}\sum D_i$
Mean peaks	$\left[t, \overline{D}^*\right], \overline{D}^* = Max(\overline{D}_i)$
Standard deviation	$\sqrt{\frac{1}{N}\left(D_i - \overline{D}\right)^2}$
95% cumulative distribution values	$F_{0.95}(D)$
95% cumulative peaks	$[F_{0.95}]_i^*$, $(F_{0.95})^*_i = \text{Max}\ (F_{0.95})_i$
Skewness	$\left[\sum_{i=1}^{n}(D-\overline{D})^3/n\right] \Big/ \left[\sum_{i=1}^{n}(D-\overline{D})^2/n\right]^{3/2}$
Skewness peaks	$\left[t, S^*_i\right], S^*_i = Max(S_i)$
Kurtosis	$\left[\sum_{i=1}^{n}(D-\overline{D})^4/n\right] \Big/ \left[\sum_{i=1}^{n}(D-\overline{D})^2/n\right]^{2}$
Kurtosis peak	$\left[t, K^*\right], K^* = Max(K_i)$
Third quartile	75^{th} Percentile

Over a period of ten hours the data was collected and the features listed in Table 14 were calculated. The feature values were plotted on a time scale to identify if there is any observable trend. This procedure was conducted using data for all the components on board (except for QFP 100). The objective was to find: (1) a

feature(s) that could be most reliable used for prognostics. Here the word reliable is used to indicate a degree of confidence, and (2) feature(s) that provided degradation trend across all components being investigated.

7.2 Results

Using the procedure in the previous section the results for QFP 256 are shown in **Figure 50** to 54. The following observations could be made about trending the different features. The values of resistance drift by itself were too noisy for trending and would lead to false alarms. The mean values of resistance drift distribution over a ten hour period were found to provide a good indication of degradation. As seen in Figure 46, for the component QFP 256, the mean drift values are close to zero or very low for the first 200 hours. This indicates that the data fits to the regression model and there is no deviation from the baseline performance.

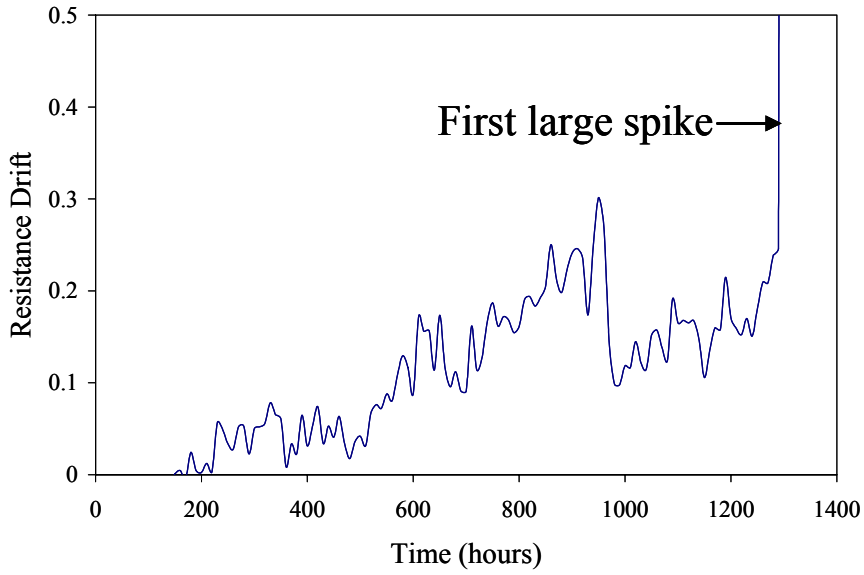

Figure 50. Trending mean values of resistance drift

After 200 hour to 500 hours, the value of mean drift fluctuates between zero to 0.7. However, after 500 hours a steep rise is observed, with a clear increasing trend. This would indicate a onset of fault and possible progression to failure. The mean drift value was found to be the most consistent feature across all components with similar trend. **Figure 51**, trends only the peak values of the mean drift (**Figure 50**). This is a better feature as there is no up or down trend (as observed with mean drifts and also few other features). The peaks are always increasing and hence the indication of degradation is clear.

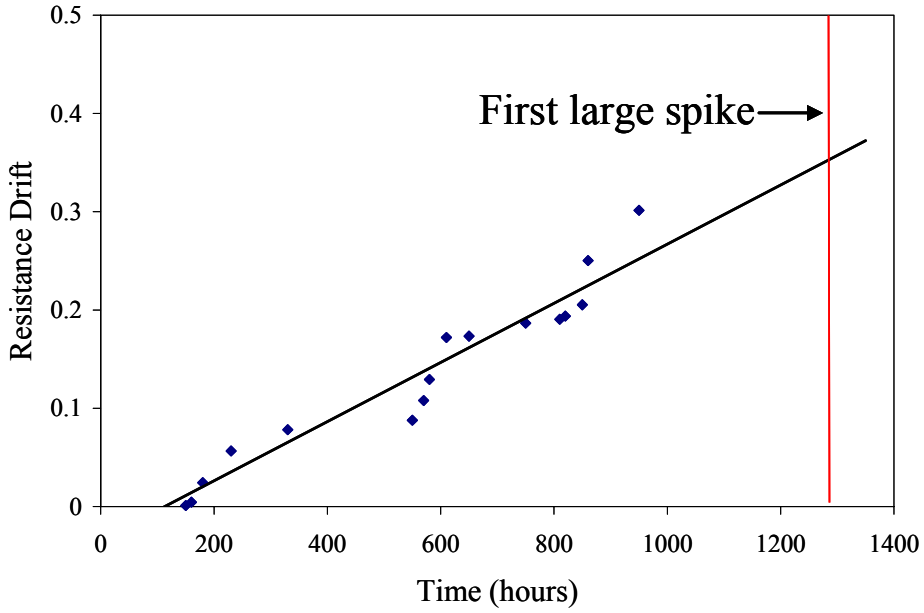

Figure 51. Trending mean-peak values of resistance drift

Figure 52, 51, and 52 show the standard deviation, skewness, and kurtosis values of the resistance drift. There is no change in the standard deviation values of the drift as the component approaches failure. One would expect that the standard deviation would increase with the mean (**Figure 50**), but it was not observed from the data. Skewness and kurtosis were considered to describe the drift distributions more accurately. High positive skewness values would indicate that the drift distribution is

getting skewed to the right, indicating more number of large positive drift values. However, for this component skewness values were not found to be a good indicator of degradation. Though, the peak skewness values (**Figure 57**) show a consistent increasing trend, it is difficult to use this trend directly, especially since the component failure is not defined in terms of skewness.

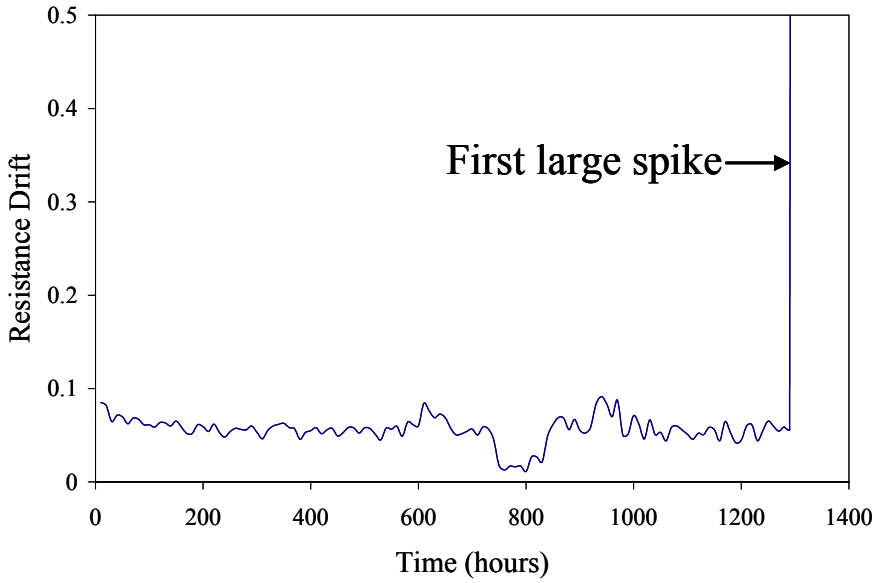

Figure 52. Trending values of standard deviation of resistance drift

The 95 percent cumulative distribution values of the resistance drift were found to be a good indicator of onset and progression of degradation. The progression of 95% cumulative values is similar to that observed for the mean values. The data (**Figure 53**) is characterized with low or no degradation till 200 hours followed by slow increase till 500 hours, and the final rise to eventual failure. Similar to mean peaks, the 95% cumulative peak values was found to be a good indicator for degradation indication. This is primarily because the peaks only capture the increasing values of the curve and hence it is easier to interpret. When similar exercise was performed with data for all components on the board, the mean drift,

mean peaks, 95% cumulative and cumulative peaks were found to be more robust features for prognostics.

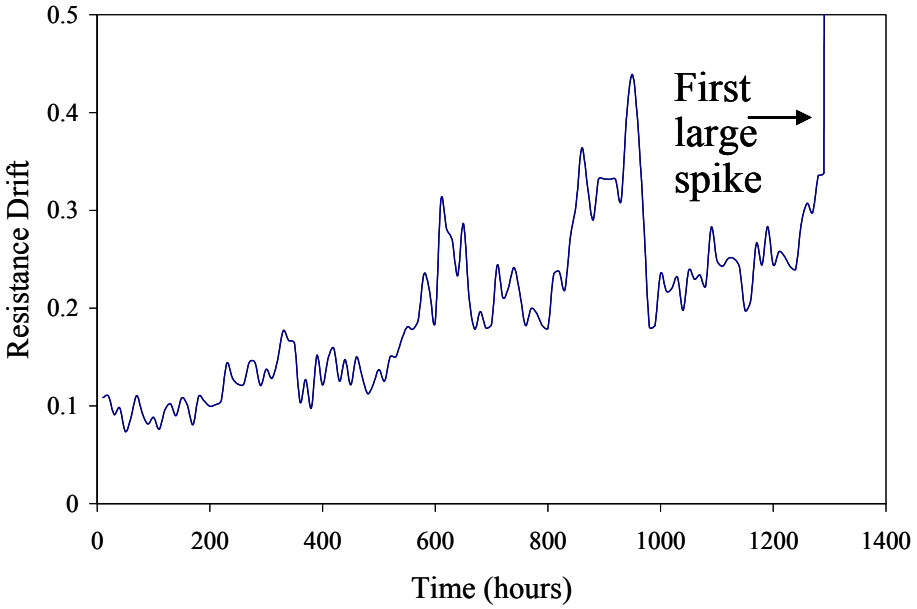

Figure 53. Trending values of 95% cumulative distribution values of resistance drift

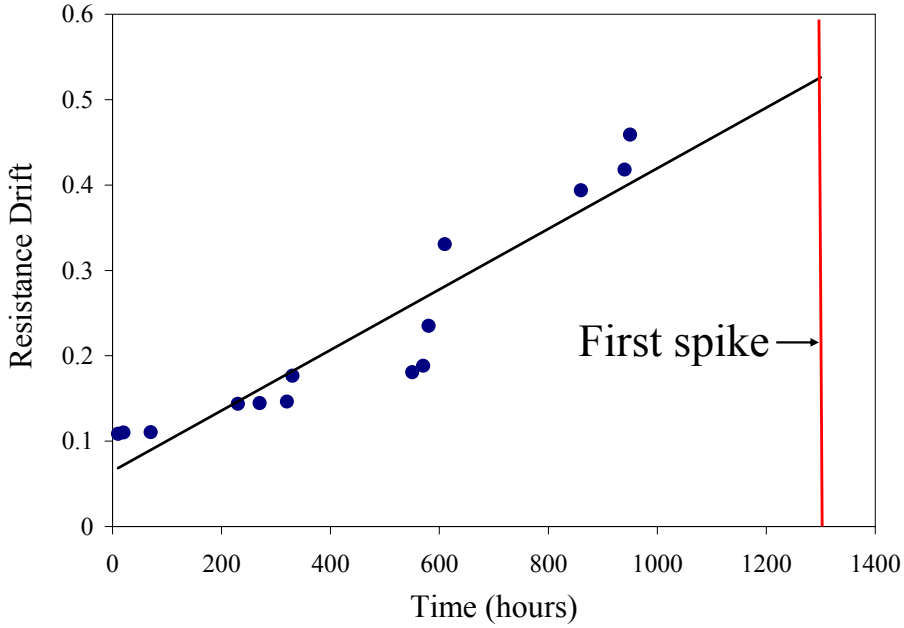

Figure 54. Trending values of 95% cumulative distribution peaks of resistance drift

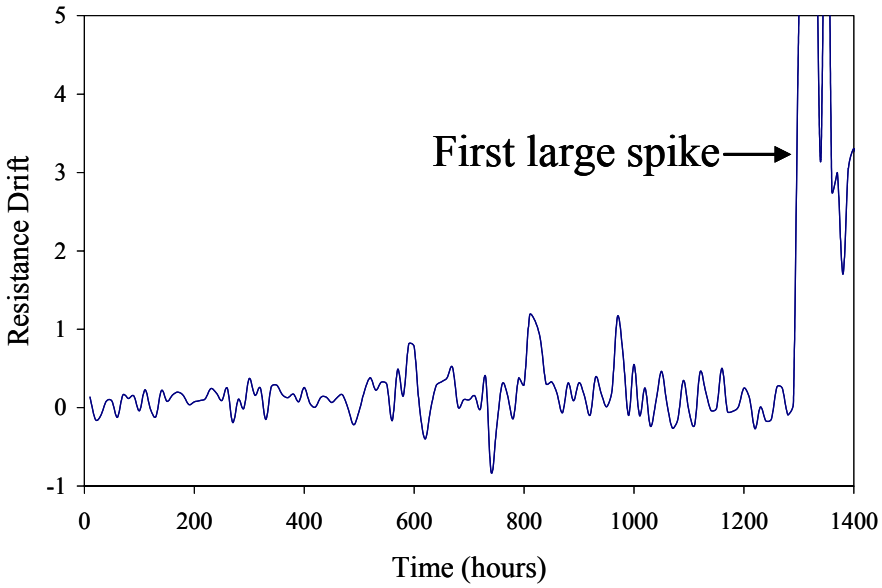

Figure 55. Trending skewness values of resistance drift

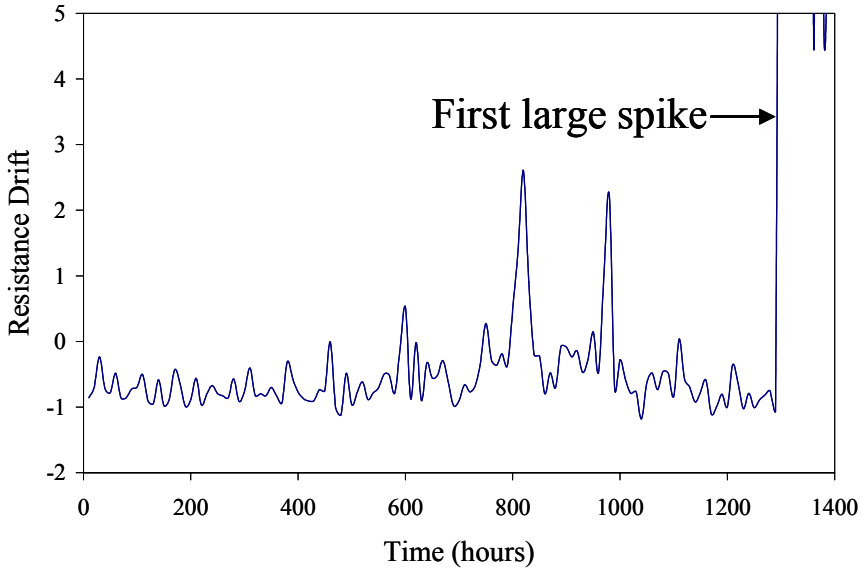

Figure 56. Trending kurtosis values of resistance drift

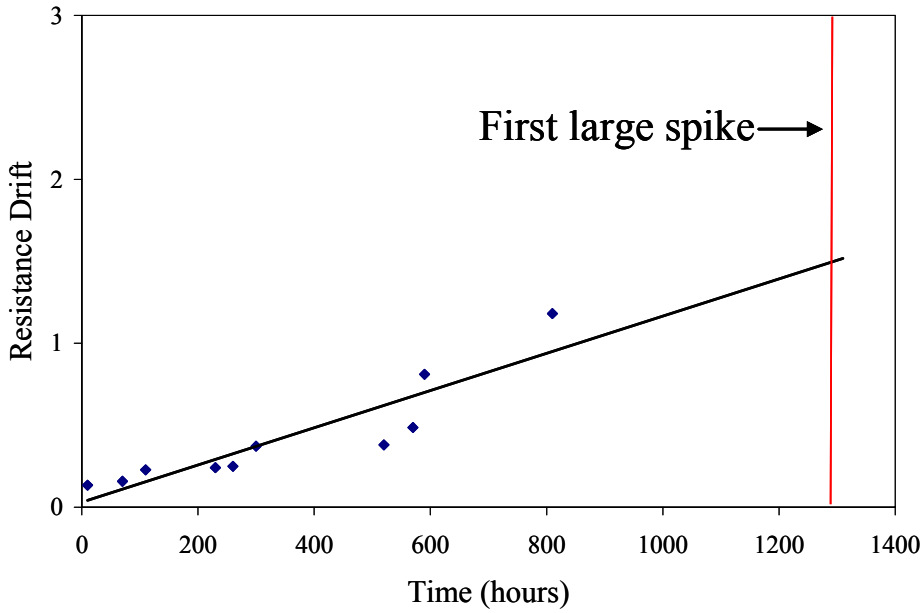

Figure 57. Trending skewness peak values of resistance drift

The mean peaks and 95% cumulative distribution peaks were fitted using linear regression to predict the failure (**Figure 58**). The prediction obtained after 950 hours using mean values of the drift distribution was 1780 hours. The prediction obtained using 95% cumulative distribution values was 1210 hours. The actual measured failure was at 1300 hours. The actual failure could be enveloped by trending these two features.

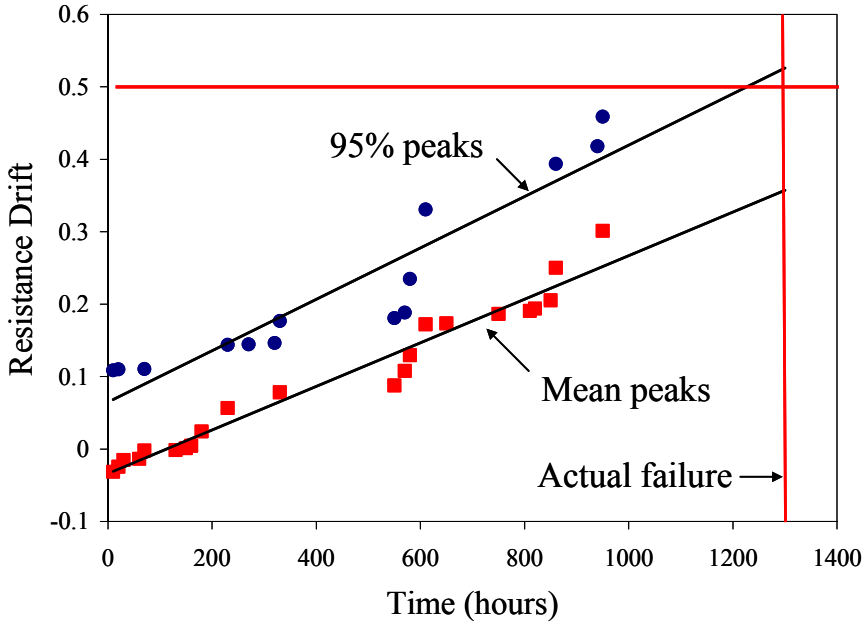

Figure 58. Failure prediction using two features

7.3 Conclusions

A novel approach was developed for predicting interconnect failure using in-situ resistance measurements. Resistance drift was identified as a primary indicator of health. The deviation of resistance drift from the established baseline was investigated using different features. The mean and the 95% cumulative values of the resistance distribution were identified as the most robust features for indicating degradation. The onset of degradation and the progression to failure could be explained using the mean values of resistance drift. For prognostics, the 95% cumulative peak trend always provided advanced warning of failure. The actual failures (measured) were observed between the failure prediction obtained from trending the mean peaks and 95% cumulative peak values.

Chapter 8: Contributions

The application of environmental and usage monitoring for health assessment of mechanical systems has been well studied. However, these concepts have rarely been applied for electronic products and systems. Electronics prognostics is evolving, but most solutions are still in design concepts, prototypes, and product-specific configurations. There are few actual realizations and even fewer commercialized solutions.

The specific contributions of this research include the development and demonstration of the algorithm to extract load parameters (cyclic range, mean loads, ramp rates, dwell times) required for assessing damage due to commonly observed failure mechanisms in electronics. The algorithm enables significant reduction of large irregular time-load data without compromising features such as load-dwell periods and small cycles with higher mean-load values that are essential for damage estimation.

The unique feature of this algorithm is the identification of dwell times and corresponding load levels by considering cycles with small amplitudes and cycles with lower ramp rates. The method also estimates the correlation between load parameters (cyclic range vs. mean, dwell time vs. load, cyclic range vs. ramp-rate)

using correlation coefficients to enable accurate damage assessment in subsequent steps.

This research is first to utilize the methods of optimal binning and non-parametric density estimation for prognostics and health management applications. Method to enable condensed storage of in-situ monitored loads was demonstrated using a-priori assessment of optimal bins for storage of load parameters. The binned data was used with Gaussian kernel functions to estimate the probability density of the load parameter. The method has shown to improve the ability of the sensor nodes to monitor for extended durations without interruptions and conserve on-board memory of sensor modules.

A generic approach for prognostics was proposed that accounted for measurement, parameter, and model uncertainties. This novel approach combines sensitivity analysis, Monte Carlo simulation, and regression modeling to predicting the distribution of remaining life. The approach was demonstrated for predicting the remaining life of solder interconnect failures on electronic boards under irregular thermal loading conditions. Methods were proposed for predicting the remaining life based on current and historic loads by utilizing the variations in the load distributions with time to assess future usage patterns and mission survivability.

An approach for remaining life prognostics of electronic components due to interconnect degradation by analyzing usage loads (temperature cycles) and

performance (resistance continuity) data was developed. The novel approach was based on a regression model for predicting the resistance using measured temperature values. The difference between actual and estimated resistance was then analyzed to predict the onset and progress of degradation. The method was shown to accurately predict remaining life by trending several features including means, mean peaks, kurtosis, and 95% cumulative values of the resistance drift distributions.

Appendix I

Flow chart of the load parameter extraction algorithm.

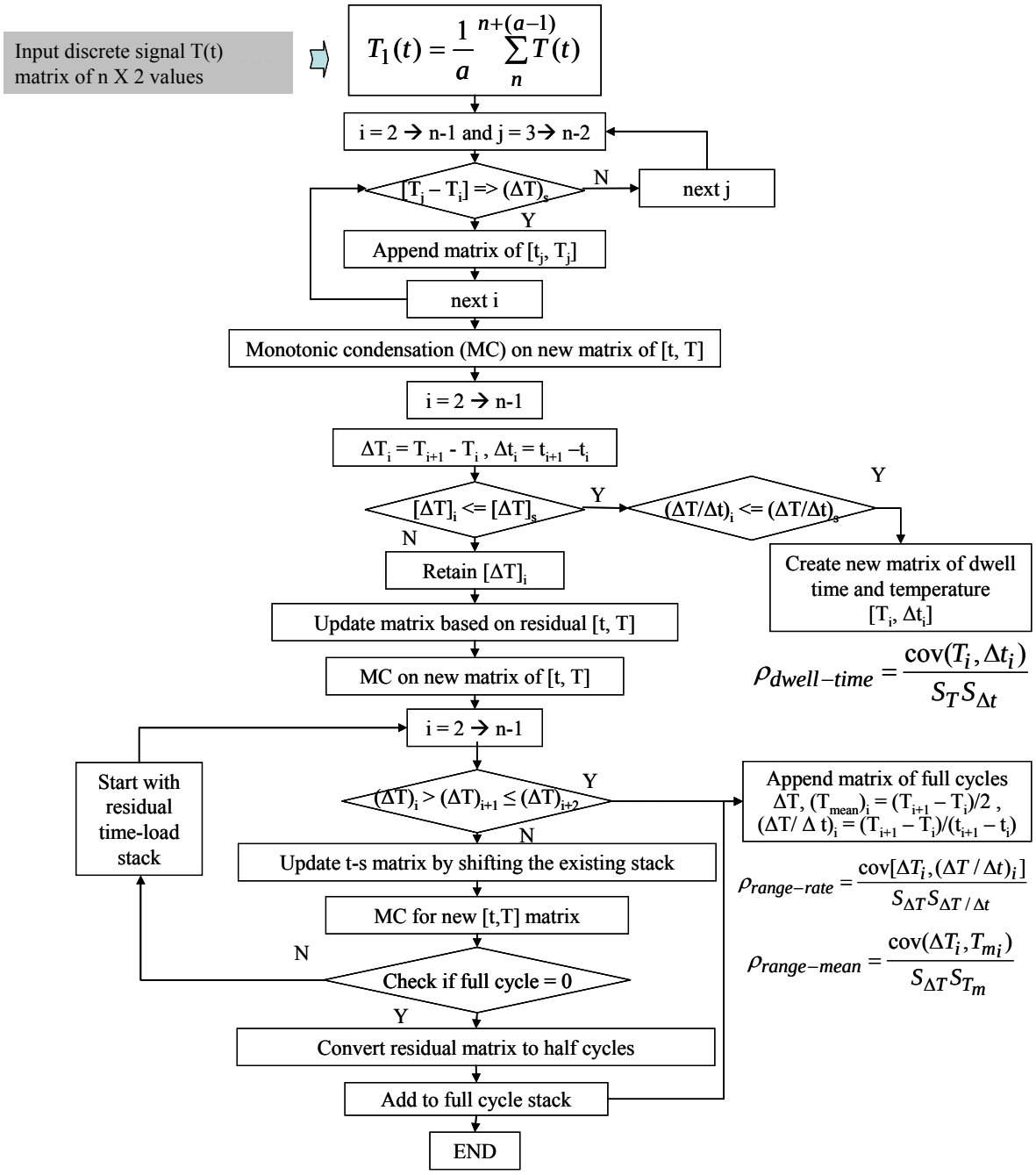

Appendix II

Models for Damage Estimation and Accumulation used for Assessing Solder Joints

First order thermal fatigue model for BGAs and gull wing QFPs was used for damage calculations. The model used contains all the first order parameters influencing the shear fatigue life of solder joints and comes from the fundamental understanding of the response of surface mount solder joints to cyclically accumulating fatigue damage resulting from shear displacement due to thermal expansion mismatches between the components and the substrate. These shear displacements, the global thermal expansion mismatch, cause time independent yielding strains, and time, temperature, and stress dependant creep/stress relaxation strains. These strains, on a cyclic basis form a visco-plastic stain energy hysteresis loop which characterizes the solder joints response to thermal cycling and those areas is indicative of the cyclically accumulating fatigue damage.

$$Nf = \frac{1}{2}\left(\frac{\Delta\gamma p}{2\varepsilon f}\right)^{\frac{1}{c}}$$

N_f = Mean number of cycles to failure

$\Delta\gamma_p$ = Inelastic strain range considering the local and global mismatch.

ε_f and c are material constants

For eutectic solder, ε_f = 0.325

$$c = -0.442 - 0.0006\,T_{sj} + 0.0174\ln\left(1 + \frac{360}{t_D}\right)$$

Where, Tsj = cyclic mean temperature of the solder in degrees C and t_D = dwell time in minutes at maximum temperature. . In the fatigue model, the ramp time

is considered in calculating the mean cyclic temperature, using the following expression

$$T_S = \frac{(T_{\max} \times \tau_{\max}) + (T_{\min} \times \tau_{\min}) + [(\frac{T_{\min} + T_{\max}}{2}) \times (\tau_{rampup} + \tau_{rampdown})]}{(\tau_{\max} + \tau_{\min} + \tau_{rampup} + \tau_{rampdown})}$$

Where,

τ_{max} = Dwell time at maximum temperature

τ_{min} = Dwell time at minimum temperature

τ_{rampup} = Ramp time from maximum to minimum temperature

$\tau_{rampdown}$ = Ramp time from minimum to maximum temperature

For BGAs the inelastic strain range due to global mismatch is given by

$$\Delta\gamma_g = \frac{0.5FI(\Delta\alpha L T_S - \Delta\alpha L T_C)}{h}$$

Where, I is the calibration factor internal to the software program. F = empirical factor "non-ideal" factor that accounts for deviation of real solder joints from ideal solder joints. h (mils) is the nominal height of the solder joints. Ts and Tc are temperatures of the substrate and component.

Similarly for gull wing QFPs the inelastic strain range due to global mismatch is given by

$$\Delta\gamma_g = \frac{0.5FI\,K_D(\Delta\alpha L T_S - \Delta\alpha L T_C)^2}{200Ah}$$

Where, K_D is the diagonal flexural lead stiffness for the gull wings based on the work of Kotlowitz and Taylor [1991].

The package geometries namely, the size, shape, and areas of the solder balls and the gull wing interconnects were supplied by the manufacturer. Some of these values were verified by actual measurement. The material properties of solder, board,

interconnect, and packages were obtained from the manufacturer. For routinely used materials such as Pb-Sn solder, and FR-4, these properties are stored in the database of the custom software (CalcePWA) that was used for building the model. These properties have been derived from several experimental results and from literature.

Damage Accumulation

Liner damage rule by Miner was used for damage accumulation. The basic assumptions of this rule are constant work absorption per cycle and characteristic amount of work absorbed at failure. The energy accumulation, therefore leads to linear summation of cycle ratio or damage.

Damage $D = \sum r_i = \sum \frac{n_i}{N_{fi}}$

Where, n_i = applied cycle at load of constant amplitude i

N_{fi} = total cycle to failure at load i

Failure is deemed to occur when, $\sum r_i = 1$

Appendix III

Publications Originated from Thesis Work

Journals

- Vichare, N., Pecht, M., "Prognostics and Health Management of Electronics", IEEE Transactions on Components and Packaging Technologies, Vol. 29, No. 1, March 2006, pp.222-229.
- Vichare, N., Rodgers, P., Pecht, M., "Methods for Binning and Density Estimation of Load Parameters for Prognostics and Health Management", International Journal of Performability Engineering, Vol. 2, No. 2, April 2006, pp.149-161.
- Vichare N., Rodgers P., Eveloy V., Pecht M. G., "In-Situ Temperature Measurement of a Notebook Computer - A Case Study in Health and Usage Monitoring of Electronics", IEEE Transactions on Device and Materials Reliability, vol. 4., No. 4, December 2004, pp. 658-663.
- Vichare N., Rodgers P., Eveloy V., Pecht M. G., "Environment and Usage Monitoring of Electronic Products for Health Assessment and Product Design", Accepted in the Journal of Quality Technology and Quantitative Management.

Conference Proceedings

- Vichare N., Rodgers P., Eveloy V., Pecht M. G., "Environment and Usage Monitoring of Electronic Products for Health (Reliability) Assessment and Product Design", IEEE Workshop on Accelerated Stress Testing and Reliability, Austin, Texas, Oct 3-5, 2005.
- Rouet, V., Foucher, B., Vichare, N., Rodgers, P., and Pecht M., "Improvement of a Miniaturized Health Monitoring Device for Advanced Alerts", International Conference on Condition Monitoring and Diagnosis, Changwon, Korea, April 2-5, 2006.
- Vichare N, and Pecht, M., "Enabling Electronic Prognostics Using Thermal Data", Thermal Investigation of IC's and Systems (THERMINIC), September 2006.
- Vichare, N., Rodgers, P., Azarian, M., and Pecht, M., "Application of Health Monitoring to Product Take-back Decisions", Proceedings of the Joint International Congress and Exhibition - Electronics Goes Green 2004, 6-8 September 2004, Berlin., Germany, pp. 945-951, 2004.

Working Papers

- Vichare, N. M., and Pecht, M., G., Load parameter Extraction Algorithm for Prognostic Health Monitoring
- Vichare N., Rodgers P., Pecht M. G., Prognostic Health Monitoring Approach for Electronics Considering Uncertainty
- Vichare N., Pecht M., Zhang, G., Kwan, C., Prognostics Using Resistance Drift as Failure Precursor

Bibliography

[1]. Vichare, N., Pecht, M., "Prognostics and Health Management of Electronics", IEEE Transactions on Components and Packaging Technologies, Vol. 29, No. 1, March 2006, pp. 222-229.

[2]. Vichare, N.; Rodgers, P., Eveloy, V., Pecht, M., "Monitoring Environment and Usage of Electronic Products for Health Assessment and Product Design", IEEE Workshop on Accelerated Stress Testing and Reliability (ASTR), Austin, TX, USA, October 2-5, 2005.

[3]. Lall, P., Pecht, M., and Hakim, E., "Influence of Temperature on Microelectronics and System Reliability", CRC Press, New York, 1997.

[4]. Pecht, M., Das, D., and Ramakrishnan, A., "The IEEE Standards on Reliability Program and Reliability Prediction Methods for Electronic Equipment," Microelectronics Reliability, Vol. 42, 2002, pp. 1259-1266.

[5]. Dasgupta, A., "The Physics-of-Failure Approach at the University of Maryland for the Development of Reliable Electronics," in Proceedings of Third International Conference on Thermal and Mechanical Simulation in (Micro) Electronics (EuroSimE), pp. 10-17, 2002.

[6]. Tumer, I., and Bajwa, A., "A Survey of Aircraft Engine Health Monitoring Systems", Proceedings of AIAA, 1999.

[7]. Carden, E. P., Fanning, P., "Vibration Based Condition Monitoring: A Review", Journal of Structural Health Monitoring, Vol. 3, No. 4, 2004, pp. 355-377.

[8]. Chang, P., Flatau, A., and Liu, S., "Review Paper: Health Monitoring of Civil Infrastructure", Journal of Structural Health Monitoring, Vol 3, No. 3, 2003, pp. 257-267.

[9]. Krok, M., and Goebel, K., "Prognostics for Advanced Compressor Health Monitoring", Proceedings of SPIE, Vol. 5107, 2003.

[10]. Kacprzynski, G. J., Roemer, M.J., Modgil, G., Palladino, A., "Enhancement of Physics of Failure Prognostic Models with System Level Features", IEEE Aerospace Conference Proceedings, Vol. 6, 2002, pp. 2925.

[11]. Xie, J., and Pecht, M., "Application of In-Situ Health Monitoring and Prognostic Sensors," 9th Pan Pacific Microelectronics Symposium Exhibits & Conference, Kahuku, Oahu, Hawaii, 10-12 February 2004.

[12]. Condition Based Maintenance Plus, http://www.acq.osd.mil/log/mppr/CBM%2B.htm, Viewed December 2005.

[13]. DoD 5000.2 Policy Document, Defense Acquisition Guidebook, Chapter 5.3 – Performance Based Logistics, December 2004.

[14]. Cutter, D. and Thompson, O., "Condition-Based Maintenance Plus Select Program Survey," Report LG301T6, January 2005, viewed from http://www.acq.osd. mil/log/mppr/CBM%2B.htm, October 2005

[15]. Kirkland, L.V.; Pombo, T.; Nelson, K.; and Berghout, F., "Avionics Health Management: Searching for the Prognostics Grail," Proceedings of IEEE Aerospace Conference, Vol. 5, 6-13 March 2004, pp. 3448 – 3454.

[16]. Leonard, C.T. and Pecht, M.G., "Improved Techniques for Cost Effective Electronics," Annual Proceedings of Reliability and Maintainability Symposium, 29-31 January 1991, pp. 174 – 182.

[17]. Karyagina, M., "Designing for Fault-Tolerance in the Commercial Environment," Proceedings of Reliability and Maintainability Symposium, 22-25 January 1996, pp. 258 – 262.

[18]. Shapiro, A.A.; Ling, S.X.; Ganesan, S.; Cozy, R.S.; Hunter, D.J.; Schatzel, D.V.; Mojarradi, M.M.; and Kolawa, E.A., "Electronic Packaging for Extended Mars Surface Missions," Proceedings of IEEE Aerospace Conference, Vol. 4, 6-13 March 2004, pp. 2515 - 2527.

[19]. Drees, R., and Young, N., "Role of BIT in Support System Maintenance and Availability," IEEE A&E Systems Magazine, August 2004, pp. 3-7.

[20]. Pecht, M.; Dube, M.; Natishan, M.; and Knowles, I., "An Evaluation of Built-In Test," IEEE Transactions on Aerospace and Electronic Systems, Vol. 37, No. 1, January 2001, pp. 266-272.

[21]. Motorola, "Motorola Built-In Test Diagnostic Software," http://www.dot21rts.com/products/mbit%20datasheet.pdf, June 2002, Viewed on December 2005.

[22]. Broadwater, S.P.; Oblak, T.A.; and Popyack, L.J., "Maintenance Processor/Time Stress Measurement Device (MP/TSMD) Use for Failure Trend Analysis," Annual Reliability and Maintainability Symposium, 1992, pp. 228-38.

[23]. Broadwater, S.P. and Cockey, E.A., "Time Stress Measurement Device Use for On-board Diagnostic Support," Proceedings of IEEE AUTOTESTCON '93, September 1993, pp. 251-8.

[24]. Johnson, D., “Review of Fault Management Techniques Used in Safety Critical Avionic Systems,” Progress in Aerospace Science, Vol. 32, No. 5, October 1996, pp. 415-431.

[25]. Allen, D., “Probabilities Associated with a Built-in-Test System, Focus on False Alarms,” Proceedings of AUTOTESTCON, IEEE Systems Readiness Technology Conference, 22-25 September 2003, pp. 643 – 645.

[26]. Gao, R.X. and Suryavanshi, A., “BIT for Intelligent System Design and Condition Monitoring”, IEEE Transactions on Instrumentation and Measurement, Vol. 51, No. 5, October 2002, pp. 1061 – 1067.

[27]. Rosenthal, D. and Wadell, B., “Predicting and Eliminating Built-in Test False Alarms,” IEEE Transactions on Reliability, Vol. 39, No. 4, October 1990, pp. 500-505.

[28]. Williams, R., Banner, J., Knowles, I., Natishan, M., and Pecht, M., “An Investigation of 'Cannot Duplicate' Failure”, Quality and Reliability Engineering International, Vol. 14, 1998, pp. 331-337.

[29]. Ramakrishnan, A.; Syrus, T.; and Pecht, M., “Electronic Hardware Reliability.” Avionics Handbook, CRC Press, Boca Raton, Florida, December 2000, pp. 22-1 - 22-21.

[30]. Mishra, S. and Pecht, M., “In-situ Sensors for Product Reliability Monitoring,” Proceedings of SPIE, Vol. 4755, 2002, pp. 10-19.

[31]. Ridgetop Semiconductor-Sentinel Silicon ™ Library, “Hot Carrier (HC) Prognostic Cell,” August 2004.

[32]. Anderson, N. and Wilcoxon, R., “Framework for Prognostics of Electronic Systems,” Proceedings of International Military and Aerospace/Avionics COTS Conference, Seattle, WA, August 3-5, 2004.

[33]. Ganesan, S.; Eveloy, V.; Das, D.; and Pecht, M.G, “Identification and Utilization of Failure Mechanisms to Enhance FMEA and FMECA,” Proceedings of the IEEE Workshop on Accelerated Stress Testing and Reliability (ASTR), Austin, Texas, October 3-5, 2005

[34]. Born, F. and Boenning, R. A., “Marginal Checking - A Technique to Detect Incipient Failures,” Proceedings of the IEEE Aerospace and Electronics Conference, 22-26 May 1989, pp. 1880 – 1886.

[35]. Pecht, M.G., Radojcic, R., and Rao, G., “Guidebook for Managing Silicon Chip Reliability”, CRC Press, Boca Raton, FL, 1999.

[36]. Smith, P.A. and Campbell, D.V., "Practical Implementation of BICS for Safety-Critical Applications," Proceedings of IEEE International Workshop on Current and Defect Based Testing-DBT, 30 April 2000 pp. 51 – 56.

[37]. Pecuh, I.; Margala, M.; and Stopjakova, V., "1.5 Volts Iddq/Iddt Current Monitor." Proceedings of the IEEE Canadian Conference on Electrical and Computer Engineering, Vol. 1, 9-12 May 1999, pp. 472 – 476.

[38]. Xue, B. and Walker, D.M.H., "Built-In Current Sensor for IDDQ Test," Proceedings of the IEEE International Workshop on Current and Defect Based Testing-DBT, 25 April 2004, pp. 3 – 9.

[39]. Wright, R.G. and Kirkland, L.V., "Nano-Scaled Electrical Sensor Devices for Integrated Circuit Diagnostics," IEEE Aerospace Conference Proceedings, Vol. 6, Mar 8-15, 2003, pp. 2549 - 2555.

[40]. Wright, R.G.; Zgol, M.; Adebimpe, D.; and Kirkland, L.V., "Functional Circuit Board Testing Using Nanoscale Sensors," IEEE Systems Readiness Technology Conference Proceedings AUTOTESTCON, 22-25 September 2003, pp. 266 – 272.

[41]. Wright, R.G.; Zgol, M.; Keeton, S.; and Kirkland, L.V., "Nanotechnology-Based Molecular Test Equipment (MTE)," IEEE Aerospace and Electronic Systems Magazine, Vol. 16, No.. 6, June 2001, pp. 15 – 19.

[42]. Kanniche, M.S. and Mamat-Ibrahim, M.R., "Wavelet based Fuzzy Algorithm for Condition Monitoring of Voltage Source Inverters," Electronic Letters, Vol. 40, No. 4, February 2004.

[43]. Lall, P., Islam, N., Rahim, K., Suhling, J., Gale, S., "Leading Indicators-of-Failure for Prognosis of Electronic and MEMS Packaging," Proceeding of Electronics Components and Technology Conference, Las Vegas, NV, pp. 1570-1578, June 1-4, 2004..

[44]. Lall, P., Islam, N., Suhling, J., "Prognostication and Health Monitoring of Leaded and Lead Free Electronic and MEMS Packages in Harsh Environments", Proceedings of the 55th IEEE Electronic Components and Technology Conference, Orlando, FL, pp. 1305-1313, June 1-3, 2005.

[45]. Self-Monitoring Analysis and Reporting Technology (SMART), PC Guide, http://www.pcguide.com/ref/hdd/perf/qual/featuresSMART-c.html, viewed on August 30, 2005

[46]. Hughes, G.F., Murray, J.F., Kreutz-Delgado, K., Elkan, C., "Improved Disk-drive Failure Warnings", IEEE Transactions on Reliability, Vol. 51, Issue 3, September 2002, pp. 350 – 357.

[47]. Gross, K., “Continuous System Telemetry Harness,” Sun Labs Open House, 2004, research.sun.com/sunlabsday/ docs.2004/talks/1.03_Gross.pdf, viewed in August 2005.

[48]. Whisnant, K.; Gross, K.; and Lingurovska, N., “Proactive Fault Monitoring in Enterprise Servers,” 2005 IEEE International Multi-conference in Computer Science and Computer Engineering, Las Vegas, NV, June 2005

[49]. Mishra, K. and Gross, K. C, “Dynamic Stimulation Tool for Improved Performance Modeling and Resource Provisioning of Enterprise Servers,” Proc. 14th IEEE International Symposium on Software Reliability Eng. (ISSRE’03), Denver, CO, November 2003.

[50]. Cassidy, K.; Gross, K. C.; and Malekpour, A., “Advanced Pattern Recognition for Detection of Complex Software Aging Phenomena in Online Transaction Processing Servers,” Proceedings of the International Performance and Dependability Symposium, Washington, DC, June 23 - 26, 2002.

[51]. Vaidyanathan, K. and Gross, K. C., “MSET Performance Optimization for Detection of Software Aging,” Proc. 14th IEEE International Symposium on Software Reliability Engineering (ISSRE’03), Denver, CO, November 2003.

[52]. Brown, D.; Kalgren, P.; Byington, C.; and Orsagh, R., “Electronic Prognostics – A Case Study Using Global Positioning System (GPS)," IEEE Autotestcon, 2005

[53]. Ramakrishnan, A. and Pecht, M., “A Life Consumption Monitoring Methodology for Electronic Systems,” IEEE Transactions on Components and Packaging Technologies, Vol. 26, No. 3, September 2003, pp. 625-634.

[54]. Mishra, S.; Pecht, M.; Smith, T.; McNee, I.; and Harris, R., “Remaining Life Prediction of Electronic Products Using Life Consumption Monitoring Approach,” Proceedings of the European Microelectronics Packaging and Interconnection Symposium, Cracow, June 16-18, 2002, pp. 136-142.

[55]. Mathew, S.; Das, D.; Osterman, M.; Pecht, M.G.; and Ferebee, R., ’’Prognostic Assessmsnt of Aluminum Support Structure on a Printed Circuit Board,” Accepted for publication in ASME Journal of Electronic Packaging, EP-05-1031

[56]. Shetty, V.; Das, D.; Pecht, M.; Hiemstra, D.; and Martin, S., “Remaining Life Assessment of Shuttle Remote Manipulator System End Effector,” Proceedings of the 22nd Space Simulation Conference, Ellicott City, MD, October 21-23, 2002

[57]. Vichare N., Rodgers P., Eveloy V., Pecht M. G., "Environment and Usage Monitoring of Electronic Products for Health Assessment and Product Design", Accepted for publication in Journal of Quality Technology and Quantitative Management

[58]. Harchani, N.; Jimenez, F.; Almohamed, M.; Esteve, D.; and Courvoisier, M., "Time Stress Measurement Device: System Design and Synthesis", Proceedings of the SPIE, Vol. 4051, 2000, pp. 337-48.

[59]. Rouet, V. and Foucher, B., "Development and Use of a Miniaturized Health Monitoring Device," Proceedings of the IEEE International Reliability Physics Symposium, 2004, pp. 645-6.

[60]. Searls, D.; Dishongh, T.; and Dujari, P., "A Strategy for Enabling Data Driven Product Decisions Through a Comprehensive Understanding of the Usage Environment," Proceedings of IPACK'01, Kauai, Hawaii, USA, July 8-13, 2001.

[61]. Herbst, G., "IBM's Drive Temperature Indicator Processor (Drive-TIP) Helps Ensure High Drive Reliability," IBM White Paper, http://www.hc.kz/pdf/drivetemp.pdf, viewed in September 2005.

[62]. Vichare N.; Rodgers P.; Eveloy V.; and Pecht M. G., "In-Situ Temperature Measurement of a Notebook Computer - A Case Study in Health and Usage Monitoring of Electronics," IEEE Transactions on Device and Materials Reliability, Vol. 4., No. 4, December 2004, pp. 658-663.

[63]. Bodenhoefer, K., "Environmental Life Cycle Information Management and Acquisition – First Experiences and Results from Field Trials," Proceedings of Electronics Goes Green 2004+, Berlin, September 5-8, 2004, pp. 541-546.

[64]. ELIMA Report, "D-19 Final Report on ELIMA Prospects and Wider Potential for Exploitation," April 30, 2005, www.ELIMA.org, viewed in December 2005.

[65]. Skormin, V.A.; Gorodetski, V.I.; and Popyack, L.J., "Data Mining Technology for Failure Prognostic of Avionics," IEEE Transactions on Aerospace and Electronic Systems, Vol. 38, No. 2, April 2002, pp. 388 – 403.

[66]. Mishra, S.; Ganesan, S; Pecht, M.; and Xie; J., "Life consumption monitoring for electronics prognostics," Proceedings of the IEEE Aerospace Conference,.Vol. 5, March 6-13, 2004, pp. 3455 – 3467.

[67]. Orsagh, R.; Brown, D.; Roemer, M.; Dabney, T.; and Hess, A., "Prognostic Health Management for Avionics Power Supplies," IEEE Aerospace Conference Proceedings, 2005

[68]. Goodman, D.; Vermeire, B.; Spuhler, P.; and Venkatramani, H., "Practical Application of PHM/Prognostics to COTS Power Converters," IEEE Aerospace Conference, Big Sky, Montana, USA, March 5-12, 2005.

[69]. JEP 122B, Failure Mechanisms and Models for Semiconductor Devices, JEDEC Standard, August 2003.

[70]. JEP 148, Reliability Qualification of Semiconductor Devices Based on Physics of Failure Risk and Opportunity Assessment, April, 2004.

[71]. IPC-SM-785, "Guidelines for Accelerated Reliability Testing for Surface Mount Attachments", IPC Standard, November 1992.

[72]. S. Bosworth, S.C. Hsu, and J. Polcari, "Exceptional performance from the development, qualification, and implementation of a silicone adhesive for bonding heatsinks to semiconductor packages," IEEE Transactions on Components, Packaging and Manufacturing Technology – Part A, vol. 18, no. 1, pp. 94-100, 1995.

[73]. M.F. Ben Achour, A. Bar-Cohen, "Mechanical stress reduction in heat sink bond layers – a numerical feasibility study," in Proc. Electronic Components Technology Conference (ECTC), pp. 307-315, 1999.

[74]. A. Kaisare, Z. Han, D. Agonafer, and K. Ramakrishna, "Prediction of effect of heat sink adhesive on mechanical reliability of a wire bonded plastic ball grid array package," in Proc. Eighth Intersociety Conf. on Thermal and Thermomechanical Phenomena in Electronics Systems (ITHERM 2002), pp. 926-931, 2002.

[75]. V. Eveloy, P. Rodgers, C. Hillman, and M. Pecht, "Reliability of pressure sensitive adhesive tapes for heat sink attachment in air-cooled electronic assemblies," IEEE Trans. on Device and Materials Reliability: Thermal Management for Reliability, December 2004.

[76]. Socie, D., Rainflow Cycle Counting: A Historical Perspective, pp. 3-10, The Rainflow Method in Fatigue, Butterworth-Heinemann, Oxford, 1991.

[77]. ASTM E-1049, Standard Practice for Cycle Counting in Fatigue Analysis, ASTM International Standard, 1997.

[78]. Holman, R., Liaw, P., Methodologies for Predicting Fatigue Life, Journal of Materials, July 1997, pp.46-51.

[79]. Rychlik, I., Rainflow Cycles in Gaussian Loads, Fatigue and Fracture of Engineering Materials and Structures, Vol. 15, no.1, 1992, pp. 57-72.

[80]. Anzai, H., Algorithm of Rainflow Method, The Rainflow Method in Fatigue, Butterworth-Heinmann, Oxford, pp 11-20, 1991.

[81]. Yigang, Z., Shijie, Z., Minaggo, Y., A Cycle Counting Method Considering Load Sequence, International Journal of Fatigue, Vol-15, no. 5, 1993, pp. 407-411.

[82]. Cluff, K., Barker, D., Robbins, D., and Edwards, T., "Characterizing the Commercial Avionics Thermal Environment for Field Reliability Assessment", Proceedings-Institute of Environmental Sciences, pp. 50-57, 1996.

[83]. Brown, M.W., et al., "An Analysis of Mean Stress in Multiaxial Random Fatigue", Fatigue and Fracture of Engineering Materials and Structures, Vol. 19, no. 2, pp. 323-333, 1996

[84]. Nagode, M., and Zingsheim, F., "An Online Algorithm for Temperature Influenced Fatigue Life Estimation: Strain Life Approach", International Journal of Fatigue, Vol-26, 2004, pp. 155-161

[85]. Nagode, M., and Michael, H., "An Online Algorithm for Temperature Influenced Fatigue Life Estimation: Stress Life Approach", International Journal of Fatigue, Vol-26, 2004, pp. 163-171

[86]. Mukhopadhyay, et al., Online fatigue creep monitoring system for high temperature components of power plants, International Journal of Fatigue, Vol. 23, 2001, pp. 549-560

[87]. Stubbington, C.A., and Pearson, S., "Effect of dwell on the growth of fatigue cracks in Ti-6Al-4V alloy bar", Engineering Fracture Mechanics, vol.10, no.4, 1978. p. 723-56.

[88]. Cowles, B.A., Sims, D., Warren, J., "Evaluation of the Cyclic Behavior of Aircraft Turbine Disk Alloys", NASA Report CR 159409, 1978.

[89]. Askoy S., Peng, Y., and Armstrong, H., "Thermal Fatigue Analysis of Air-Cooled Gas Turbine Nozzles", ASME Pressure Vessels and Piping Conference, San Diego, 1987

[90]. Seshadri, R., "Design and Life Prediction of Furnace Tubes in Creep Range", ASME Pressure Vessels and Piping Conference, San Diego, 1987

[91]. Goswami, T., "A New Dwell Sensitivity Damage Parameter", Materials and Design, Vol. 25, 2004, pp. 191-197.

[92]. Goswami, T., "Dwell Sensitivity: Part I – Behavior and Modeling", Mechanics of Material, Vol. 22. 1995, pp 105-130.

[93]. Wand, P., Data Based Choice of Histogram Bin Width, The American Statistician, Vol. 51, No. 1, pp.59-64, March 1997.

[94]. Izenman, A. J., Recent Developments in Non Parametric Density Estimation, Journal of American Statistical Association, Vol. 86, No. 413, pp.205-13, March 1991.

[95]. Scott, D., On Optimal and Data Based Histograms, Biometrika, Vol. 66, No. 3, pp. 605-10, 1979.

[96]. Freedman, D., P. Diaconis, On Maximum Deviation Between the Histogram and Underlying Density, Zeitschrift fur Wahrscheinlichkeitstheorie und verwandte Gebiete, 58, pp. 139-167, 1981.

[97]. He, K., G. Meeden, Selecting the Number of Bins in a Histogram a Decision Theoretic Approach, Journal of Statistical Planning and Inference, Vol. 61, No. 1, pp. 49-59, 1997.

[98]. Jones, M., J. Marron, S. Sheather, A Brief Survey of Bandwidth Selection for Density Estimation, Journal of American Statistical Association, Vol. 91, No. 433, pp.401-407, 1996.

[99]. Koyama, S., S. Shinomoto, Histogram Bin Width Selection for Time-Dependant Poisson Process, Journal of Physics A: Mathematics and General, Vol. 37, No. 29, pp. 7255-65, 2004.

[100]. Song, M., R., Haralick, Optimally Quantized and Smoothed Histograms, Proceedings of Joint Conference on Information Sciences, Computer Vision, Pattern Recognition and Image Processing, pp. 894, 2002.

[101]. Paulter, N.G., The Effect of Histogram Size on Histogram- Derived Pulse Parameters, IEEE Transactions on Instruments and Measurements, Vol. 47, No. 3, pp.609-12, 1998.

[102]. Silverman, B. W., Density Estimation for Statistics and Data Analysis, Chapman and Hall, New York, 1986.

[103]. Fadda, D., E. Slezak, A. Bijaoui, Density Estimation with Non-parametric Methods, Astronomy and Astrophysics Supplement Series, Vol. 127, pp. 335-52, January 1998.

[104]. Sheather, S., M. Jones, A Reliable Data Based Bandwidth Selection Method for Kernel Density Estimation, Journal of Royal Statistical Society, Vol. 53, No.3, pp.683-90, 1991.

[105]. Chiu, S., Bandwidth Selection for Kernel Density Estimation, Annals of Statistics, Vol. 19, No. 4, pp. 1883-1905, 1991.

[106]. Glavinovic, M., Comparison of Parzen Density and Frequency Histograms as Estimators of Probability Density Function, European Journal of Physiology, Vol. 433, No. 1-2, pp. 174-179, 1996.

[107]. Vichare, N., Rodgers, P., Pecht, M., Methods for Binning and Density Estimation of Load Parameters for Prognostics and Health Management, International Journal of Performability Engineering, Vol. 2, No. 2, April 2006, pp. 149-161.

[108]. Engel S. et al., Prognostics, The Real Issues Involved With Predicting Life Remaining, IEEE Aerospace Conference, vol.6, 2000, p. 457-69.

[109]. Ayyub, B., Uncertainty Modeling and Analysis for Civil Engineers, CRC Press, Boca Raton, 1998.

[110]. Frey, C., and Patil, S., Identification and Analysis of Sensitivity Analysis Methods, Risk Analysis, Vol. 22, No. 3, 2002.

[111]. Helton, J., and Davis, F., "Illustration of Sampling-Based Methods for Uncertainty and Sensitivity Analysis", Risk Analysis, Vol. 22, No. 3, 2002

[112]. Zimmermann, H., An Application Oriented View Of Modeling Uncertainty", European Journal of Operation Research, Vol. 122, pp. 190-198, 2000

[113]. Nilsen, T.; Aven, T, Models And Model Uncertainty In The Context Of Risk Analysis, Reliability Engineering & System Safety, Mar2003, Vol. 79 Issue 3, p309, 9.

[114]. Zio, E., Apostolakis, G.E., Two Methods For The Structured Assessment Of Model Uncertainty By Experts In Performance Assessments Of Radioactive Waste Repositories, Reliability Engineering & System Safety, v 54, n 2-3, Nov-Dec, 1996, p 225-241.

[115]. Banks, J., Carson, J., Nelson, B., and Nicol, D., Discrete Event System Simulation, 4th Edition, Prentice Hall, NJ, 2004.

[116]. Vose, D., Quantitative risk analysis: a guide to Monte Carlo simulation modeling, Chichester ; New York : Wiley, c1996.

[117]. Osterman, M., Qi, H., Explanation of First Order Thermal Fatigue Model for Solder Interconnects in Area Array Packages, CalcePWA Software Documentation, 2002.

[118]. P. Sharma, and A. Dasgupta, "Micro-mechanics of creep-fatigue damage in PB-SN solder due to thermal cycling—Part II: mechanistic insights and cyclic durability predictions from monotonic data," Transactions of the ASME, Journal of Electronic Packaging, vol. 124, no. 3, pp. 298-304, 2002.

[119]. C. Zhai, Sidharth, and R. Blish, "Board level solder reliability versus ramp rate and dwell time during temperature cycling," IEEE Transactions on Device and Materials Reliability, vol. 3, no. 4, December 2003, pp 207-212.

[120]. R. Mahajan, C.P. Chiu, and R. Prasher, "Thermal interface materials: a brief review of design characteristics and materials," Electronics Cooling, vol. 10, no. 1, 2004.